THE THERMAL CONDUCTIVITY OF POLYETHYLENE AT VERY LOW TEMPERATURES

A thesis

presented by

JOHN N. ROGERS, Bsc

to the

University of St. Andrews

in application for the Degree of

Doctor of Philosophy.

CERTIFICATE

I certify that John N. Rogers, BSc, has spent nine terms at research work in the School of Physical Sciences in the University of St. Andrews under my direction, that he has fulfilled the conditions of the Resolution of the University Court, 1967, No.1, and that he is qualified to submit the accompanying thesis in application for the Degree of Doctor of Philosophy.

D.M. Finlayson
Research Supervisor

DECLARATION

I hereby certify that this thesis has been composed by me, and is a record of work done by me, and has not previously been presented for a Higher Degree.

The research was carried out in the School of Physical Sciences in the University of St. Andrews, under the supervision of Dr. D.M. Finlayson.

John N. Rogers

ABSTRACT

Thermal conductivity measurements have been made of four polymer specimens in the temperature range 0.1 to 3K. Three of the samples were polyethylene, a semi-crystalline material, and the fourth a sample of polymethylmethacryalate (PMMA), an amorphous polymer. All four specimens had previously been measured in the temperature range 3 to 100K and the object of this work was to extend the measurements to lower temperatures.

Below 2K the extruded polyethylene specimens show a higher thermal conductivity than the isotropic polyethylene sample. This is explained in terms of a structure scattering model where the phonons are scattered by the crystalline inclusions in the polymer. The orientation of these crystalline lamellae is changed by extrusion and this is suggested as the reason for the differences in the thermal conductivities of the samples.

The amorphous PMMA specimen has been measured as a check on the accuracy of the technique and shows good agreement with previous measurements in this temperature range by other authors.

ACKNOWLEDGEMENTS

I wish to express my gratitude to the people without whom this thesis would not have been possible - Dr. D.M. Finlayson my supervisor for his unfailing guidance and patience; Dr. D. Greig for providing the polymer specimens; Professor S.B. Woods for his help in the early part of this work and a special vote of thanks to Mrs. R. Macalindin for her assistance with the dilution refrigerator and S.Q.U.I.D.s.

I would also like to thank my wife and parents for their moral and financial support which enabled me to complete this thesis.

TABLE OF CONTENTS

cont.

LIST OF FIGURES

LIST OF PLATES

CHAPTER I

INTRODUCTION

The thermal conductivity of all measured amorphous dielectrics is virtually identical below 1K (Stephens 1973). Both the thermal conductivity and specific heat in this temperature range appear to be determined by resonant two-level scattering modes (Anderson et al. 1972, Phillips 1972). Semi-crystalline polymers show greater variation in their thermal conductivity than do amorphous materials and this is generally ascribed to "structure scattering" - phonon scattering by variations in the material properties (Morgan and Smith 1974, Walton 1974). Burgess and Greig (1975) measured the conductivity of extruded and isotropic polyethylene (a semi-crystalline polymer) between 3 and 100K. They found differences in the conductivity of the specimens above 10K which they attributed to changes in the structure of the crystalline regions on extrusion. The object of this work was to extend the measurements to lower temperatures (0.1K) and see if any observed differences between samples could be related to the differences in structure or whether their thermal conductivities were similar to those of amorphous solids.

A review of the previous measurements of the thermal properties of amorphous and semi-crystalline solids is given in Chapter II together with a description of the main models proposed to describe these findings. Attention has been concentrated on the resonance two-level scattering model and the Morgan and Smith "structure scattering" model. An analysis of the specific heat is included

as this may be closely related to the thermal conductivity.

The samples were cooled in a $^3He/^4He$ dilution refrigerator. A description of the cryostat and the modifications made to it are contained in Chapter III and include an account of a typical run. The thermometry is discussed in Chapter IV with particular emphasis on the computer techniques applied to the calibration of the germanium resistance thermometers. The steady-state-heat flow method was used to measure the thermal conductivity of the specimens and is described in Chapter V. This chapter also contains details of the experimental techniques used to ensure thermal contact between the specimens and the cold finger of the refrigerator and the method used to thermally isolate the specimen leads from the cryostat.

The thermal conductivity results are presented in Chapter VI and their analysis in terms of the Morgan and Smith model is given in Chapter VII. The final chapter is a summary of the conclusions and some suggestions for further work.

CHAPTER II

THEORETICAL AND EXPERIMENTAL BACKGROUND

2.1 Introduction

The materials considered in this thesis are all dielectrics with an extremely low electrical conductivity. The electronic component of the thermal conductivity, K , can therefore be neglected and thus references to the thermal conductivity in this work are taken to refer to the lattice component of this property.

In recent years a great deal of work has been done, both theoretical and experimental, on the thermal properties of amorphous dielectrics at very low temperatures. Stephens (1973) has shown that between 0.1 and 10K the thermal conductivities of all measured amorphous solids are very similar. This would seem to indicate that the form of K is a result of these materials being in an amorphous state rather than a result of their detailed atomic structure.

Most of the work on semi-crystalline polymers has been done at higher temperatures (above 2K) but a few materials have been measured down to 0.2K. These samples show greater differences between each other than are seen for amorphous materials.

The low temperature thermal properties of amorphous solids have been explained in terms of a model assuming the tunnelling of atoms between almost equivalent equilibrium positions. This model does not explain the measured thermal conductivities of semi-crystalline polymers which are best interpreted in terms of "structure

scattering" - the scattering of phonons by changes in the material properties.

2.2 Experimental Background

2.2.1 Amorphous solids

The thermal conductivities below 10K of a wide variety of noncrystalline dielectric solids show great similarities in both magnitude and temperature dependence (Stephens 1973). Between 2 and 10K there is a plateau in the conductivity curve where K is independent of the temperature, T. Below 1K, K is proportional to T^n where n is between 1.8 and 2.2 (see Figure 2.1).

The low temperature experimental specific heat of noncrystalline solids can be described by the expression

$$C_{exp} = aT + bT^3$$

(Reese 1969, Pohl et al. 1973, Stephens 1973). The coefficient b is larger than that expected from the Debye model and is temperature dependent with a maximum at about 5K. The linear term is large enough to dominate below about 0.3K and is responsible for the large specific heat seen at very low temperatures.

The same mechanism is not necessarily responsible for the form of the thermal conductivity and the specific heat at low temperatures. From their experiments on the Brillouin scattering and Casimir boundary scattering in glass fibres, Pohl et al. (1973) deduced that Debye phonons exist at very low temperatures and that they are the main carriers of heat. These findings were confirmed by the thermal conductivity measurements in borosilicate glass fibres by Zaitlin

and Anderson (1974, 1975). They concluded that the thermal carriers between 0.1 and 10K are phonons with acoustic velocities and a Debye density of states, and that the thermal conductivity could therefore be calculated from the Debye specific heat and the phonon mean free path. Clearly however, these Debye modes cannot account for the very large specific heat seen at low temperatures.

2.2.2 Semi-crystalline solids

The thermal conductivity of semi-crystalline polymers shows a temperature dependence different from that of both amorphous and crystalline solids. The plateau in the conductivity between 2 and 10K which is characteristic of amorphous materials disappears with increasing crystallinity (Choy and Greig 1975) and the absolute value of the conductivity is lower below about 10K. In the range 0.1 to 10K, temperature dependences between T and T^3 have been observed for a number of materials (Anderson et al. 1963, Reese and Tucker 1965, Kouloch and Brown 1968, Scott et al. 1973). Particularly relevant to this work are the measurements of an uncharacterised polyethylene specimen by Scott et al. which showed $K \propto T^{1.8}$ between 1 and 4.2K and $K \propto T$ from 0.2 to 0.4K.

Results of measurements on semi-crystalline polymers between 2 and 100K show that the thermal conductivity depends on the crystallinity and, for extruded specimens, on the draw ratio and direction of measurement with respect to the extrusion direction. Below 10K a decrease in the conductivity is obtained with increasing crystallinity whilst above 20K the reverse is seen, the conductivity increasing with crystallinity (Choy and Greig 1975). Several

authors have examined the effect of extrusion on the thermal resistance (Burgess and Greig 1975, Gibson et al. 1977, Choy and Greig 1977). At high temperatures, about 100K, the conductivity in the direction of extrusion, $K_{//}$, is increased compared with an isotropic specimen, but is decreased in the direction perpendicular to it, $K_{\perp}$. At lower temperatures this anisotropy is decreased and below 20K $K_{//}$ and $K_{\perp}$ are nearly equal.

The results of Burgess and Greig (1974) are of particular importance to the work reported in this thesis. They examined the effect of varying percentages of dispersed PMMA in a continuous phase of polyol. In two of the specimens used in this experiment the plateau in the conductivity curve was smoothed out and they suggested that this was due to the dispersed regions for which the correlation length was calculated at $\lesssim 100\text{Å}$.

The specific heat of semi-crystalline materials shows an anomalous behaviour similar to that seen in amorphous materials.

Measurements of the specific heat of polyethylene above 2.5K by Tucker and Reese (1967) showed the heat capacity to have a linear dependence on the crystallinity. They extrapolated their results to obtain the values for completely crystalline and completely amorphous polyethylene. They interpreted their results in terms of a cubic temperature dependence

$$C_{exp} = bT^3$$

where for the crystalline material b was independent of temperature but for the amorphous material it showed a hump at about 5K. Thus the anomalous behaviour at high temperatures (above 2K) is clearly

associated with the amorphous regions of the semi-crystalline material (Reese 1969).

Scott et al. (1973) measured the specific heat of their single specimens of nylon and polyethylene from 4K down to 0.3K. They observed a temperature dependence below 0.8K which was lower than the T^3 expression predicted by the Debye model. Unfortunately their measurements did not extend to sufficiently low temperatures to see whether they approached the linear temperature dependence seen in amorphous materials.

2.3 Theoretical Models

2.3.1 Amorphous solids

A number of different models have been proposed to explain the thermal properties of amorphous solids. I will only consider the two main groups of theories; namely the two-level tunnelling model due to Anderson et al. (1972) and Phillips (1972) and the structure scattering model advanced in different forms by Klemens (1951), Ziman (1960), Walton (1974), Morgan and Smith (1974) and others.

(i) Two-level scattering

Resonant two-level scattering has been used to explain a variety of phenomena in amorphous solids including the temperature dependence of the dielectric constant, the ultrasonic attenuation and the specific heat. The model has also been applied to the thermal conductivity where it successfully predicts the observed T^2 dependence below 1K.

This explanation centres on the proposal that in any glass system there should be localised "tunnelling states" due to atoms which

can sit equally well in two positions. These positions for an atom can be represented as two local minima in the energy separated by a potential barrier. In general the potential well will be assymmetric and can be treated one-dimensionally by considering the coordinate connecting the two minima. The density of states of these tunnelling modes leads to a linear term in the specific heat which will dominate at low temperatures.

As reported above, acoustic phonons with a Debye density of states have been shown to be the main carriers of heat between 0.1 and 10K. Thus the thermal conductivity can be calculated from the Debye specific heat and the phonon mean free path. Resonant scattering then leads to a mean free path at very low temperatures $l \propto k^{-1}$ where k is the phonon wavevector, and hence to a thermal conductivity proportional to T^2.

The plateau between 5 and 10K is explained in terms of Rayleigh scattering ($l \propto k^{-4}$) of the phonons by vacancies associated with the atomic displacement in noncrystalline solids (Zaitlin and Anderson 1974, 1975, Morgan and Smith 1974).

(ii) Structure scattering

The structure scattering or density fluctuation model has been proposed in several different forms and in particular most recently by Walton (1974) and by Morgan and Smith (1974). The form used by Walton has the advantage of being mathematically more simple and he used it to explain the thermal conductivity curves of several amorphous solids. This simplicity however prevents it being used to explain the more complicated results found for the thermal conductivity of semi-crystalline polymers. I will therefore concentrate on the

model as proposed by Morgan and Smith (MS).

In this approach, the amorphous material is treated as an elastic continuum and the phonons are considered to be scattered by fluctuations in the density of the material. The scattering rate is derived in terms of a correlation function for the fluctuations in the material properties

$$f(r) = \exp(-r/a)$$

where a is a correlation length. It is assumed that

$$V^{-1} \int D(x)D(x+r)dx = D^2\exp(-r/a)$$

where $D^2 = V^{-1} \int D^2(x)dx$ and V is the volume of the system. The parameter D^2 gives a measure of the mean square fluctuations of the amorphous material properties from point to point. The scattering rate can then be written in terms of D(x) and the Boltzmann equation solved to find the relaxation time, T(k). MS have evaluated a "universal" relaxation curve for the relaxation rate in terms of D^2, a and the longitudinal and transverse velocities v_l and v_t.

At long wavelengths, when $ka \ll 1$, the phonon relaxation time becomes proportional to k^{-4} which leads to an infinite thermal conductivity. This anomaly is avoided by introducing boundary scattering so that the total mean free path l_T is given by

$$1/l_T = 1/l_b + 1/l_e$$

where l_b is the mean free path due to boundary scattering (i.e. from the specimen dimension) and l_e is the mean free path due to elastic scattering.

The thermal conductivity of amorphous solids can be derived by

using two values of the correlation length a. For large values of a (1000 - 3000 Å) the conductivity between 0.1 and 1.0K rises approximately as T^2. Small values of a (5 - 15 Å) produce the plateau in the conductivity seen between 1 and 10K. Thus the curve can be explained in terms of short-range and long-range order existing simultaneously and giving a total mean free path

$$1/l_T = 1/l_b + 1/l_{el} + 1/l_{es}$$

where l_{el} and l_{es} denote mean free paths for the long-range and short-range correlations respectively. This two phase approach successfully fits the conductivity curve for a variety of amorphous dielectrics.

The application of the MS theory to amorphous dielectrics assumes the existence of long-range order in all glasses. Although there is evidence of large correlation lengths from light scattering experiments in some polymers, their presence in all amorphous solids has still to be experimentally verified.

One of the main criticisms of the MS theory has been its inability to explain any of the other observed properties of amorphous materials, in particular the anomalous specific heat term. Zaitlin and Anderson, however, have shown that the carriers responsible for the thermal resistance below 10K are phonons with a Debye density of states. It is therefore possible that two distinct mechanisms are responsible for the thermal conductivity and the specific heat (Walton 1974). For example Giaquinta et al (1977) have proposed that a linear specific heat term can be deduced as a consequence of the nonapplicability of the third law of thermodynamics in amorphous materials. Therefore too much emphasis should not be placed on the ability of a particular theory to explain the conductivity and the

specific heat.

The thermal conductivity of a number of amorphous solids has been measured below 0.1K, and in particular Lasjaunias et al. (1977) extended their measurements of vitreous silica down to 25mK. All these materials show the conductivity continuing to display the T^2 dependence to the lowest temperatures measured. The MS theory predicts a decrease in the slope of the conductivity when the dominant phonon wavelength is greater than the scale of the density variations. For the long-range correlation values proposed by MS (1000 - 3000 Å), this change should be appreciable below 0.1K. The fact that no such change has been observed is strong evidence in favour of the two-level scattering interpretation of the thermal conductivity of noncrystalline solids.

2.3.2 Semi-crystalline solids

Before examining the various theories put forward to explain the thermal properties of semi-crystalline polymers it is worth considering the structure of these materials and how this is altered by extrusion.

The semi-crystalline polymer is generally thought to have a lamellar texture (Peterlin 1965, Meares 1965, Keller 1968, Billmeyer 1971). The crystalline inclusions are in the form of platelets with the long molecular chains folded back and forth perpendicular to the crystal surfaces. Some of the molecular chains extend between the lamellae and tie them together. The platelets in polyethylene are typically about 100Å thick. In the isotropic state the lamellae form spherulites with a diameter of approximately 1 - 10 μm. On crystallisation the lamellae grow out from a nucleation point to

give a twisted ribbon structure in which the molecular chains are perpendicular to the radial direction. The volume in the spherulites between the crystalline lamellae is filled with amorphous material as are the regions between the spherulites.

When the polymer is extruded this spherulite structure is first deformed and then, for higher extrusion ratios, broken up to form lamellar planes. (The extruded Hostalen polyethylene specimen used in this work had a low extrusion ratio, 3.85, and the lamellar planes were aligned at approximately 48° to the draw direction.) The molecular chains in the crystalline lamellae are folded so that the chain axes remain aligned with the extrusion. For high draw ratios the lamellae start to slip past each other until at large enough deformation ratios the folded chains in the lamellae unwind and become stretched out in the extrusion direction.

There is considerable evidence for this view of a semi-crystalline polymer including wide- and small-angle X ray diffraction, neutron diffraction and microscopic analysis. We will make use of this picture of the material composition in our attempts to explain the thermal conductivity.

The resonance scattering model depends on the existence of two-level tunnelling modes in the amorphous phase. It is assumed that there is a wide range of these modes and that their distribution is not critically dependent on the microscopic structure of the amorphous material. It is unlikely therefore that the two-level scattering model can be used to explain the differences seen in the thermal conductivity of various semi-crystalline materials. In particular, it would be expected from this model that the thermal conductivity would increase with crystallinity at low temperatures

as there are no two-level scattering centres in the crystalline inclusions. In fact the conductivity has been observed to fall with increasing crystallinity at 1K (Choy and Greig 1975). This suggests that for semi-crystalline polymers the behaviour of the thermal conductivity is best explained in terms of structure scattering. The two-level scattering model may still be useful, however, in explaining the specific heat which cannot be interpreted solely in terms of the Debye states which are assumed to be responsible for the thermal conductivity.

Structure scattering has been invoked in a number of different forms to explain the thermal conductivity results. Choy and Greig used the acoustic mismatch model of Little (1959) to interpret the changes in the thermal conductivity with crystallinity which they had observed. This theory has been applied to composites (Anderson and Rauch 1970, Garrett and Rosenberg 1972) in which inclusions of a good thermal conductor (e.g. copper) were dispersed in an amorphous matrix (e.g. grease) which was in itself a poor thermal conductor. The conductivity of the resulting composite was then lower than that of a sandwich made from alternate layers of the bulk materials. This was explained by phonon mismatch at the inclusion interfaces giving rise to strong phonon scattering. Choy and Greig performed a similar analysis for their results for polyethylene terephthalate by assuming that below 10K the phonons were scattered by changes in the elastic constants at the boundaries between crystalline lamallae and amorphous regions in the spherulites. Above 10K the boundary scattering was no longer important and the higher conductivity of the crystalline material gave an increasing conductivity with

crystallinity. Little's model is only valid when the dominant phonon wavelength is smaller than the dimension of the scattering inclusions. For polyethylene the lamallae are approximately 100Å wide and this analysis cannot therefore be used below about 2K.

The MS model uses a similar concept of phonon scattering by changes in the material properties. Burgess and Greig (1975) applied the MS theory to Hostalen polyethylene and two of their specimens have been used in the work reported here. As their analysis was on thermal conductivity data obtained between 3 and 100K, they only included a single short-range correlation length, a_s = 8Å, for the amorphous regions. The additional long-range correlation length employed by MS for amorphous materials was not expected to be of importance in this temperature range. Burgess and Greig used a correlation length, a_c = 100Å, to account for the phonon scattering by the crystallites. For the isotropic specimen, SHO, they included the additional effect of Umklapp scattering in the crystallites perpendicular to the c-axis (the direction of the molecular chains). This explained why the isotropic specimen had a lower conductivity than the extruded specimen above 10K (see Figure 2.2).

The advantage of this analysis in terms of the MS theory is that it includes the scattering in the amorphous regions and can therefore be applied below the temperature at which the dominant phonon wavelength is greater than the dimension of the crystalline inclusion (approximately 2K for polyethylene).

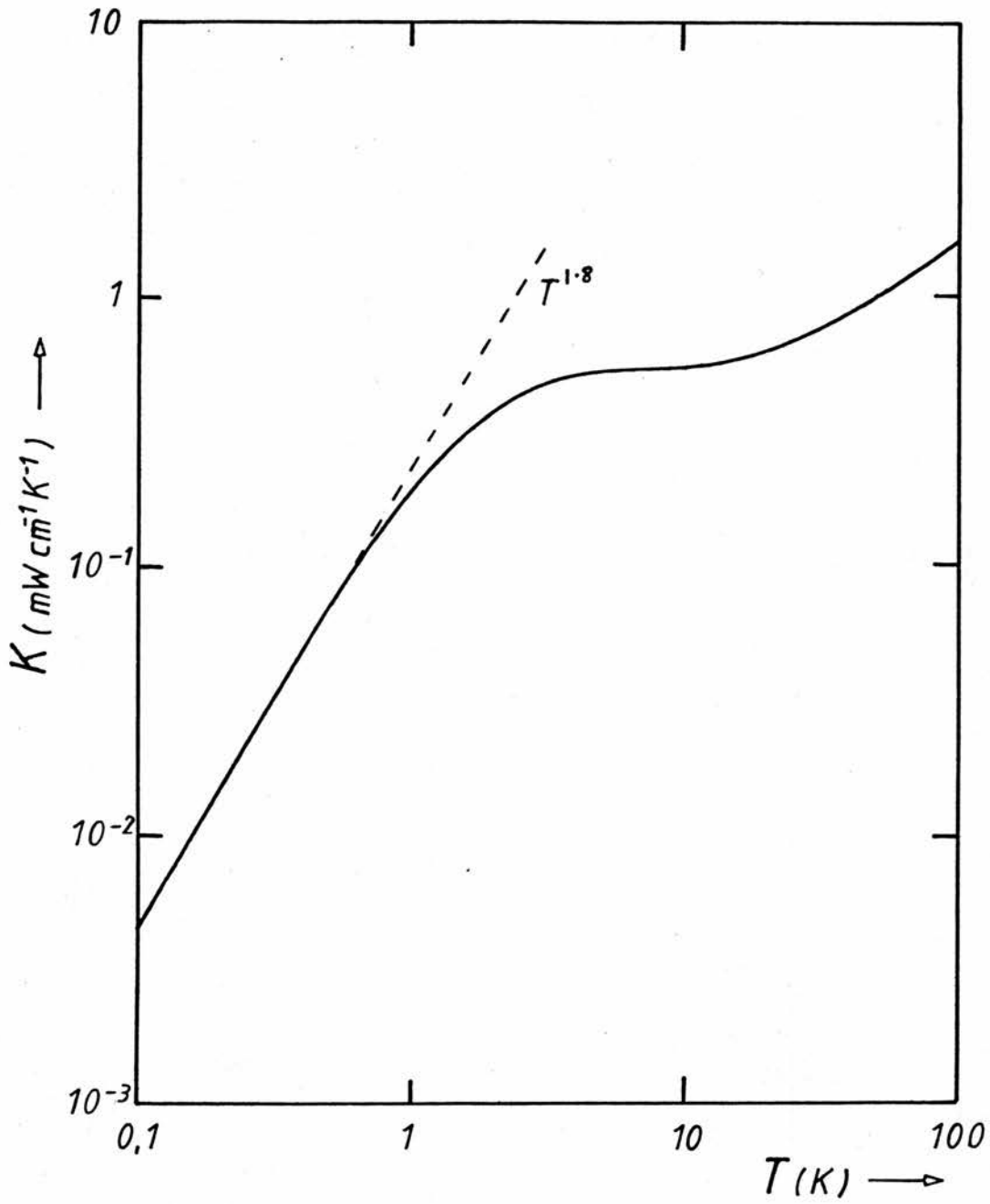

Figure 2.1. Temperature dependence of the thermal conductivity of an amorphous polymer, polymethylmethacryalate (PMMA).

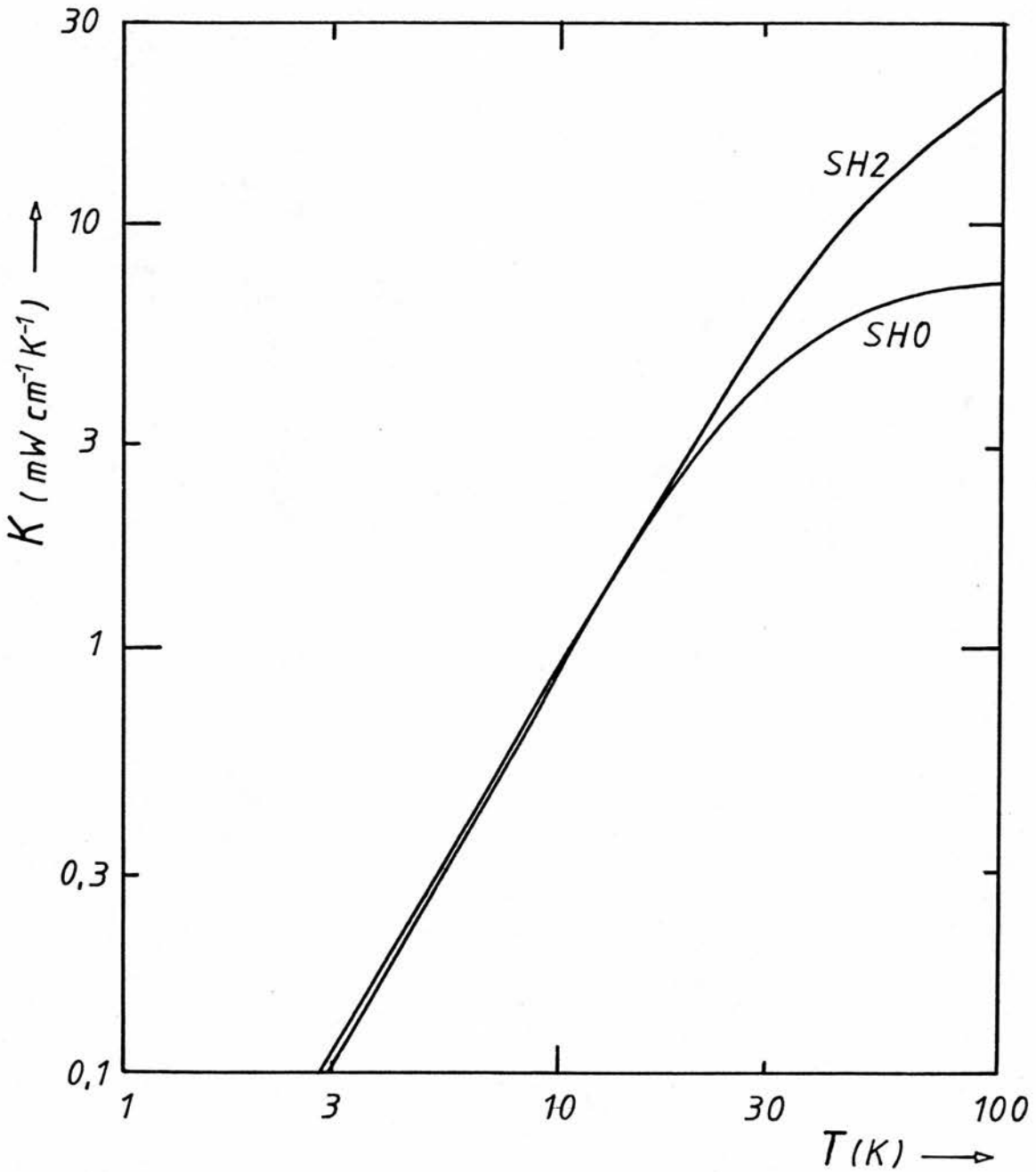

Figure 2.2. Temperature dependence of the thermal conductivity of a semi-crystalline polymer, polyethylene: SHO isotropic specimen; SH2 extruded specimen (after Burgess and Greig 1975).

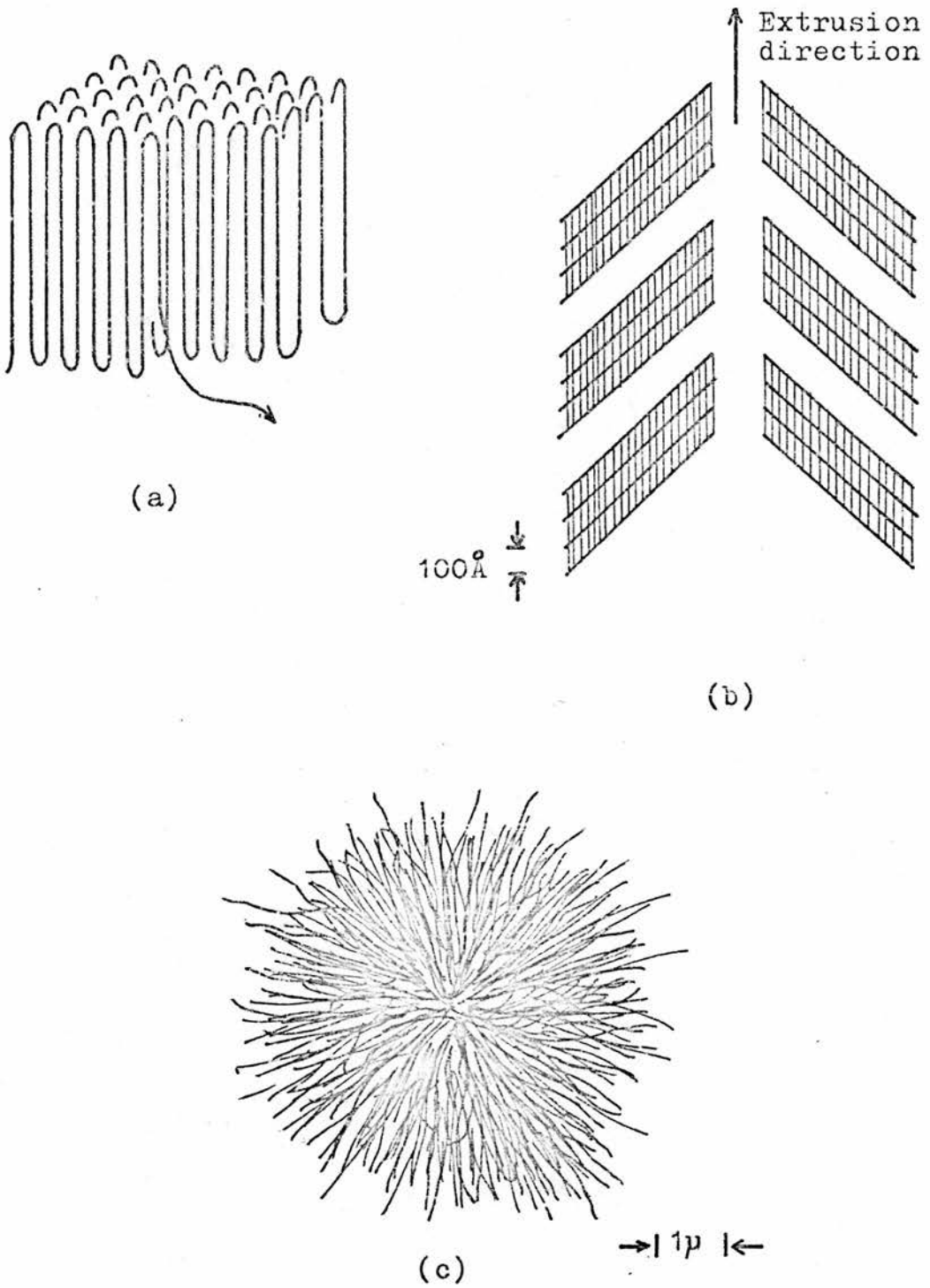

Figure 2.3. Crystallites in polyethylene. (a) Polymer chains folded in a crystalline lamellum. (b) Lamellae in extruded specimen. The polymer chains are aligned with the extrusion direction. (c) Spherulite in isotropic polyethylene - the fibrils are long narrow lamellae.

CHAPTER III

DILUTION REFRIGERATOR

The specimens were cooled in a "Harwell" 3He/4He Refrigerator Mk.III, the dilution unit of which had been replaced with a more modern version in 1971.

3.1 Description of fridge.

The general theory and design of a dilution refrigerator have been described by Wheatley et al.(1968) and by Lounasmaa (1974). This model consisted of an Outer Vacuum Can (OVC), Liquid Nitrogen Shield, Liquid Helium Container, Inner Vacuum Can (IVC), Pumped Liquid Helium Pot (1K pot) and Dilution Unit. Each of these components is described briefly below.

(1) Outer Vacuum Can (OVC). This consisted of an 11" diameter aluminium cylinder with demountable rubber O-ring seals at top and bottom flanges.

(2) Liquid Nitrogen Shield. The liquid nitrogen jacket was an annular aluminium container with a 10 litre capacity. Suspended from the bottom of the nitrogen jacket was the liquid nitrogen shield, a 10" diameter aluminium cylindrical can cooled by conduction from the jacket. Although the vacuum in the OVC was better than 10^{-5} Torr on the Penning gauge at the throat of the diffusion pump (see Figure 3.1), the jacket required filling every twelve hours, except when there was liquid helium in the cryostat when it lasted for an average of eighteen hours. It was therefore necessary during a run to go into the laboratory to top up the shield during the night and an automatic liquid nitrogen filling system was built to avoid this. The filler consisted of a sensor in the shield, a resistance

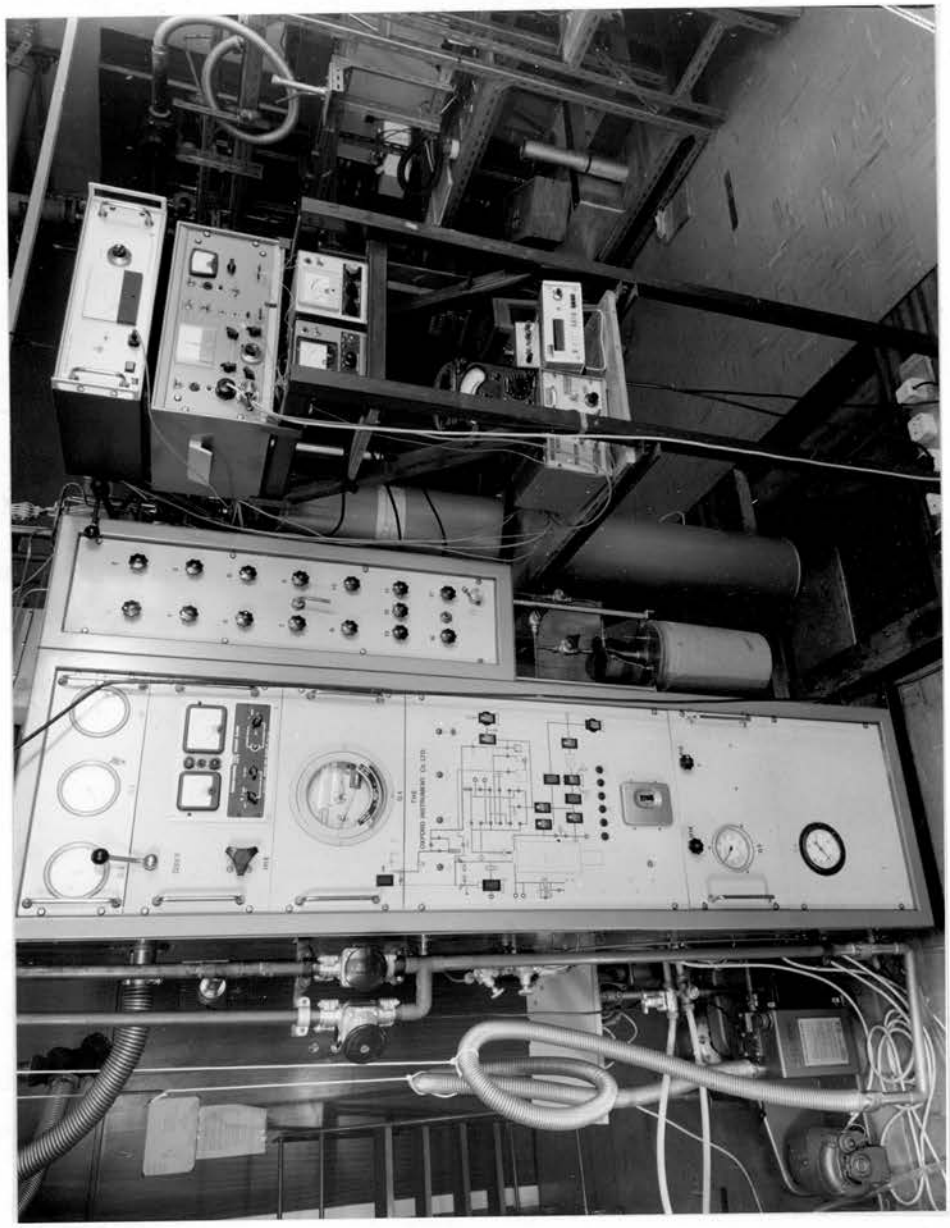

Plate 1. Front view of the dilution refrigerator.

comparator and time delay circuit and a liquid nitrogen pump. The pump fitted into the 25 litre storage dewars used in the department.

The sensor was a 2k ohm Allen Bradley carbon resistor fixed to a probe in the nitrogen shield approximately 2" from the bottom. The resistance of the sensor was monitored by a resistance comparator and time delay circuit described in the Appendix. When the liquid level in the shield dropped below the sensor, it warmed and its resistance decreased, triggering the amplifier circuit which in turn closed a mains relay starting the pump. When the level had risen to the height of the resistor the resistance returned to its original value and started the timer. After the set time had elapsed, the timer circuit opened the relay again, switching off the pump.

The pump itself consisted of a heater in the liquid nitrogen storage dewar and a solenoid valve on the boil-off line. The solenoid valve shut when the heater was on, preventing the evaporated nitrogen gas from escaping from the dewar. The resulting build up in pressure forced the liquid over into the nitrogen shield through an insulated ("Armaflex") hose (see Plate 2).

(3) Liquid Helium Container. The top can of the helium dewar was made of 7" diameter thin-walled (.016") stainless steel tubing and was suspended from the top flange. The lower can was of 9" diameter, .022" wall stainless steel with a tail of 7" diameter, .016" stainless steel. The dewar held approximately 18 litres and, with an average boil-off rate of 0.25 litres an hour, the system could be run for three days before needing refilling.

In June 1974 the upper half of the helium can was collapsed and was replaced by a similar section. The welds of this tube onto its flanges were never satisfactory, as when the can was evacuated and

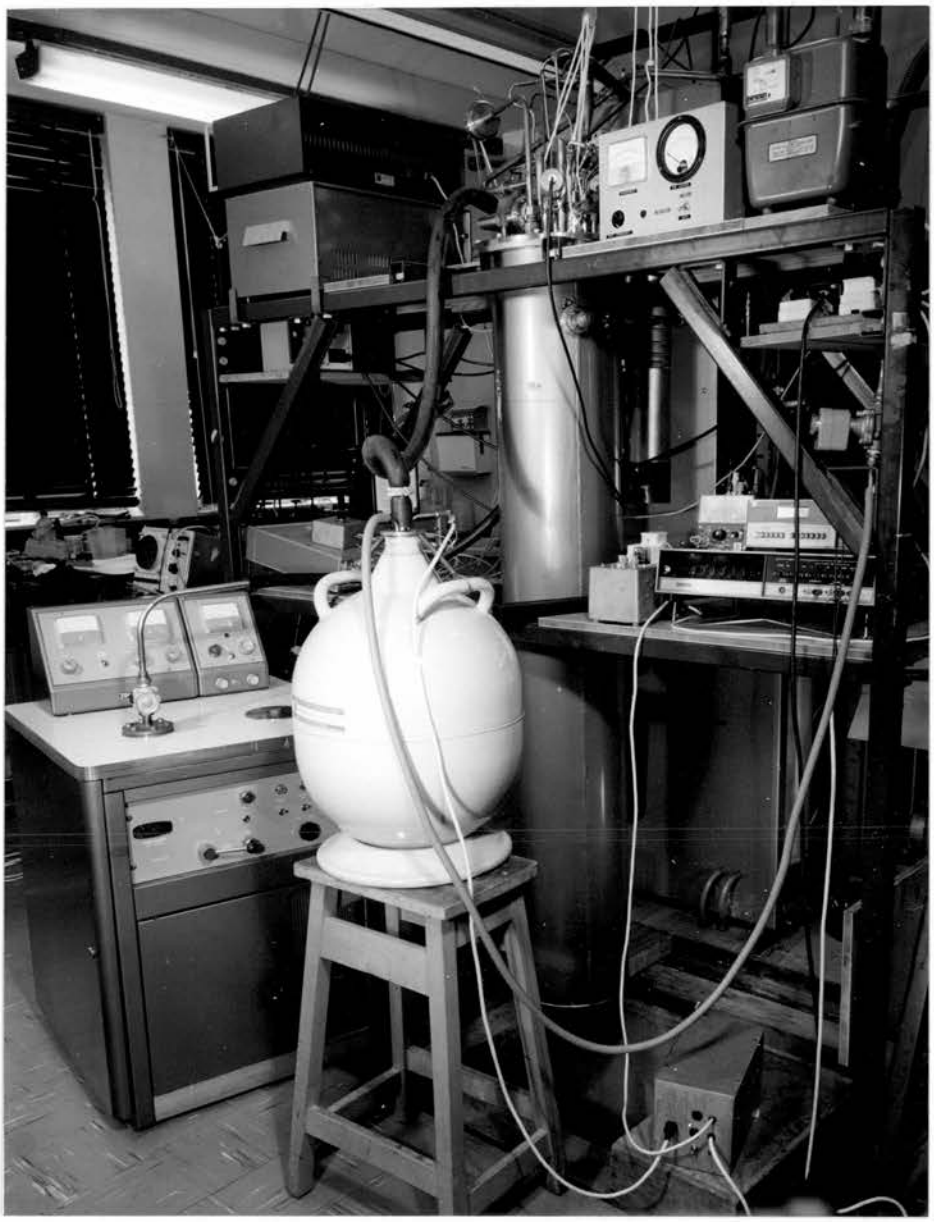

Plate 2. Side view of the refrigerator showing the nitrogen transfer system (centre) and the mass spectrometer leak detector (bottom left).

then filled with gas, the flexing of the tube walls opened small cracks at the welds giving low-temperature leaks into the OVC. This tube in turn was therefore replaced in July 1976 by a section of .028" wall tubing. This increase in the wall thickness had no noticeable effect on the boil-off rate and showed none of the problems at the welds associated with the previous can.

The lower can was sealed onto the upper one by compressing 1.6 mm. Indium wire between the flanges on the cans using 2 BA socket cap screws. With these screws it was impossible to compress the Indium sufficiently to ensure a good seal on every run without risking stripping the threads of the screws. The lower can was therefore replaced with a new design which enabled 2 BA high tensile steel nuts and bolts to be used. This can had a flange made from 1" stainless steel plate with a re-entry machined in it for the fitting of the nuts. No problems were then encountered with the Indium seal. The new can was made from 1/16" stainless steel so that it could be evacuated with an atmosphere of pressure outside and could therefore be leak tested whilst removed from the fridge.

(4) Inner Vacuum Can (IVC). This was suspended from the top flange inside the helium can by three stainless steel support tubes. The upper can, enclosing the 1K pot, was of 4" I.D. copper tube, and the tail can, enclosing the dilution unit, was of 3" I.D. copper. The two cans were sealed together by compressing 1.33 mm diameter Indium wire between their flanges. The Indium wire for this seal and that on the helium can were extruded in the laboratory using a small hydraulic press so that the Indium could be recycled. The lower half of the IVC was later replaced with a 4" I.D. can to provide more room for isolating the specimen leads from the dilution unit

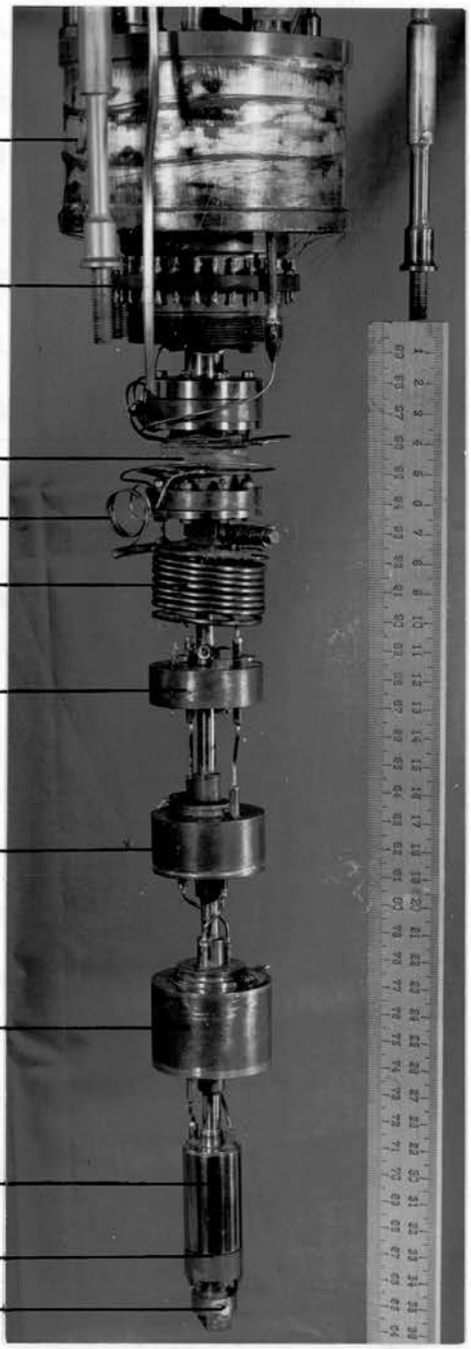

Plate 3. Dilution unit of the refrigerator.

(see Plate 4).

(5) 1K pot. The 4He pot was maintained at a temperature of approximately 1.1K during a run and had a capacity of 250 ml. (see plate 3). Initially the pot could only be pumped for six hours after filling before it was empty and the 3He/4He mixture could not, therefore, be kept condensed overnight. It was found that there was no radiation trap on the IVC pumping line. A shield from the inner wall of the IVC was positioned over the end of the pumping line and this extended the lifetime of the pot to approximately twenty four hours.

The fridge was run without a 1K radiation shield for the dilution unit as this provided more room for the mounting of the specimen and leads and this was thought to be of more importance than the fridge reaching its minimum temperature.

(6) Dilution Unit. This consisted of a condenser, still, continuous heat exchanger, three step heat exchangers and the mixing chamber to which the cold finger was attached (see Plate 3).

In normal operation the circulating 3He gas was liquefied in a condenser, a coil of 1/16" I.D. copper pipe immersed in the 1K pot. Between the 4He pot and the still there was a flow impedance of 1 mm. thin-walled stainless steel capillary tubing which ensured that the pressure of the gas in the condenser was high enough for condensation to occur and provided thermal isolation between the 1K pot and still. The incoming liquid was then cooled by passing through a 1/16" O.D. copper capillary tube would around and soldered to the still, before percolating through the flow-limiting impedance, a 0.1 mm. stainless steel capillary tube, to the heat exchangers and the mixing chamber.

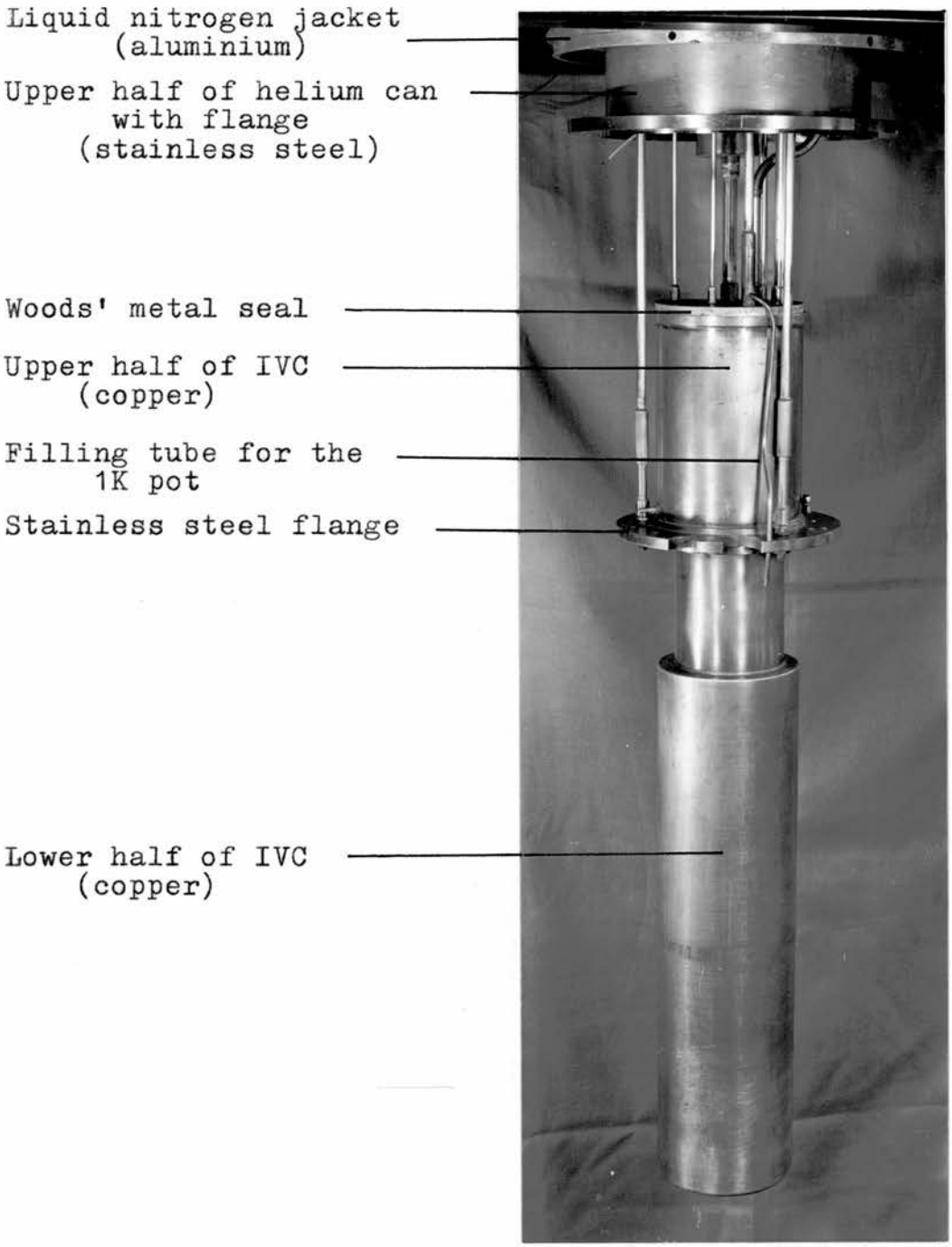

Plate 4. Side view of the refrigerator showing the concentric arrangement of the cans.

The still was maintained at 0.6K at which temperature 3He atoms were preferentially evaporated from the 3He/4He solution and removed by pumping. Removing 3He from the still created an osmotic pressure gradient which drove 3He atoms from the mixer, through the dilute superfluid phase in the heat exchangers, to the still. The circulation loop was then completed by returning the 3He which had been pumped off to the condenser after first passing it through oil and liquid nitrogen traps in the room temperature pipe work. A flow diaphragm at the neck of the still reduced 4He film flow and hence the heat load on the still.

The samples were cooled by attaching them to a copper tail on the mixing chanber. This tail was bolted onto the open bottom of the mixing chamber and was sealed with Indium wire. When thermometers required soldering into the tail block or the wiring needed renewing, this tail could be easily unbolted. A plug of sintered copper, fitted into the copper finger, protruded into the mixing chamber and was covered by the 4He in the chamber, providing good thermal contact between the liquid and the tail.

3.2 Problems with, and modifications to the fridge.

When the work described in this thesis was started in 1973, the fridge would only cool to 0.3K with the middle step heat exchanger the coldest point. The 3He circulation rate was lower than expected and it was therefore suspected that the concentration of 3He in the mixture was too low and that as a result the concentrated 3He phase in the dilution unit did not extend down to the mixing chamber. Professor Woods introduced a means by which the ratio of 3He to 4He in the dump mixture and in the vapour pumped off from the still could be measured. A "Centronics" Mass Spectrometer,

tuned for 3He and 4He, was used to obtain "leak rates" for both gases taken from a sample from a Bourdon gauge containing equal amoumts of the two gases. These readings were then compared with the "leak rates" obtained from a sample of the circulating mixture and the ratio of the 3He to 4He in the mixture calculated. This system showed that approximately 20% of the dump mixture was 3He - the recommended percentage. A sample sent to the Oxford Instrument Company was found by them to contain 19.5% and they confirmed that the total amount of mixture (1.3 moles) was correct for the fridge model.

It was still suspected, however, that the problem was either in the proportions of the two gases in the mixture or in the distribution of the constituents after the mixture had been condensed. A check was made to ensure that the mixture was not too rich in 3He. The 3He/4He gas was condensed into the dilution unit and circulation started on the rotary pump until the still was at about 0.7K. Some of the mixture (0.04 moles) was then pumped off into the dumps and the circulation continued. At this temperature the vapour pressure of 3He is very much higher than that of 4He, and as a result, most of the mixture pumped off was 3He. On restarting the circulation, the flow rate and cooling power were lower than before and it was therefore concluded that the problem was too little 3He in the mixture. 3He was gradually added to the mixture and the fridge tried after each addition. When the 3He content had been increased by 0.066 moles, the fridge cooled to 0.2K with the mixing chamber coldest. The flow rate was still low, however, and a further 0.044 moles of 3He and 0.088 moles of 4He were added before the fridge cooled properly and a minimum temperature of 80 mK was obtained.

The circulation rate in the fridge could now be held at the correct level but the mixing chamber was still not reaching the expected minimum temperature of 50mK. It appeared that the problem was no longer in the mixture and the cause was suspected to be the vibration in the dilution unit causing self-heating. With all the cans removed and the pumps on, the mixing chamber could be seen to oscillate through an arc of several millimetres. Three sources were found for this vibration. The most important of these was the cooling fan for the diffusion pump EO1 mounted in the system cabinet. It was difficult to decouple this unit from the cryostat, but the effect could be easily eliminated merely by switching the pump off when the mixing chamber was below 0.2K, the temperature at which the heating had a noticeable effect on the cooling power.

The other two main sources of vibration were the circulating rotary pump and the main pump for the 1K pot. The circulating line close to the rotary pump was a 1" copper pipe with stainless steel bellows at three points in the pipe to reduce the vibration. The 1/2m of this line closest to the rotary pump, and including the bellows, was replaced by a 4m length of 1 1/2" I.D. "flexihose" (flexible plastic tubing).

The main ^{4}He pump was situated in a room 30 yards down the corridor and connected to the cryostat by a 2" metal pumping line. The section of the line immediately in front of the system cabinet was replaced by a 4m length of 2" I.D. "flexihose". Both lengths of "flexihose" were suspended from the ceiling by sprung lines to reduce the oscillation frequency (see Plate 1).

These three changes to the system reduced the vibration to a level where it could neither be seen nor felt at the mixing chamber.

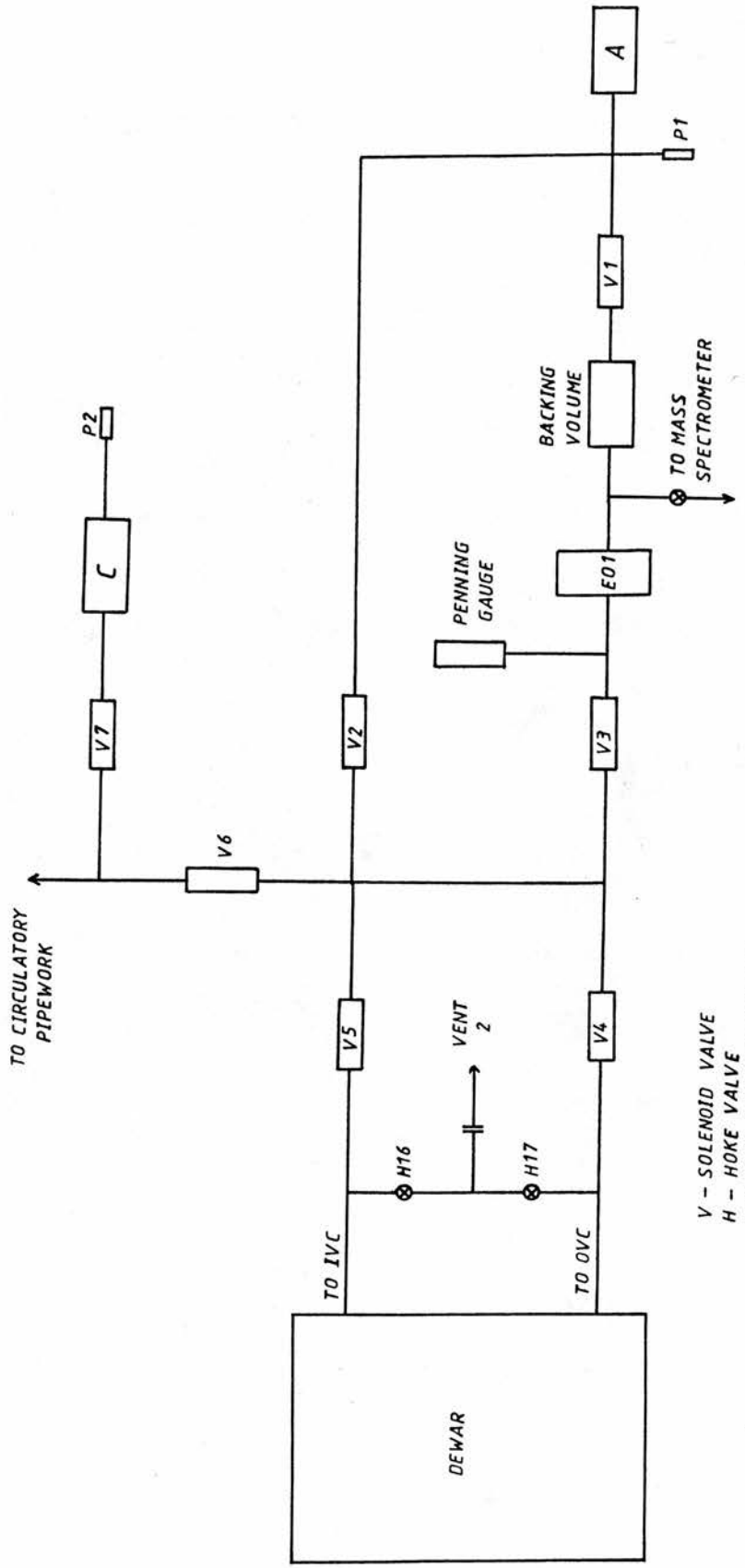

Figure 3.1. The vacuum pumping system for the dilution refrigerator.

The fridge then cooled rapidly to 65mK and then more slowly to 55mK.

The time taken to condense the mixture was four hours, and even then about a tenth of the mixture was left in the dumps when they were shut-off and circulation started. An additional line was therefore built into the room temperature piping, so that the rotary pump could be used to evacuate the dumps to ensure the use of all the mixture, and to liquefy it under a higher pressure.

A new condensing circuit was also built to by-pass the existing line during the initial condensation and reduce the time required. An 1/8" stainless steel tube was joined to the condensation line at the head of the cryostat, passed through a Hoke toggle valve, through the top flange of the helium can and down to a condenser in the 1K pot. The condenser consisted of a 1 cm. diameter, 5 cm. long copper tube with a solid brass shaft down the centre, leaving 0.025 cm. clearance between the shaft and the tube wall. The end of the tube had an interference-fitted sintered-bronze plug, 1 cm. thick, to provide a large area of contact between the gas and the liquifier. The condenser was soldered to the 1K pot with Wood's Metal to provide good thermal contact. Below the liquifier, the line was a 10 cm. length of 1 mm. thin-walled Cu-Ni capillary tubing providing thermal isolation between the 1K pot and the still. This capillary was joined to 1/16" O.D. copper tubing which was wrapped repeatedly around the still and soldered in place to ensure thermal contact between the 1K pot and the still. From the still, this copper capillary led to a copper T-piece which joined it to the bottom of the flow-limiting capillary and the top of the continuous heat exchanger. The Hoke valve at the head of the cryostat enabled this auxiliary condensing line to be isolated after the mixture had been liquified and before the circulation was started on the rotary pump.

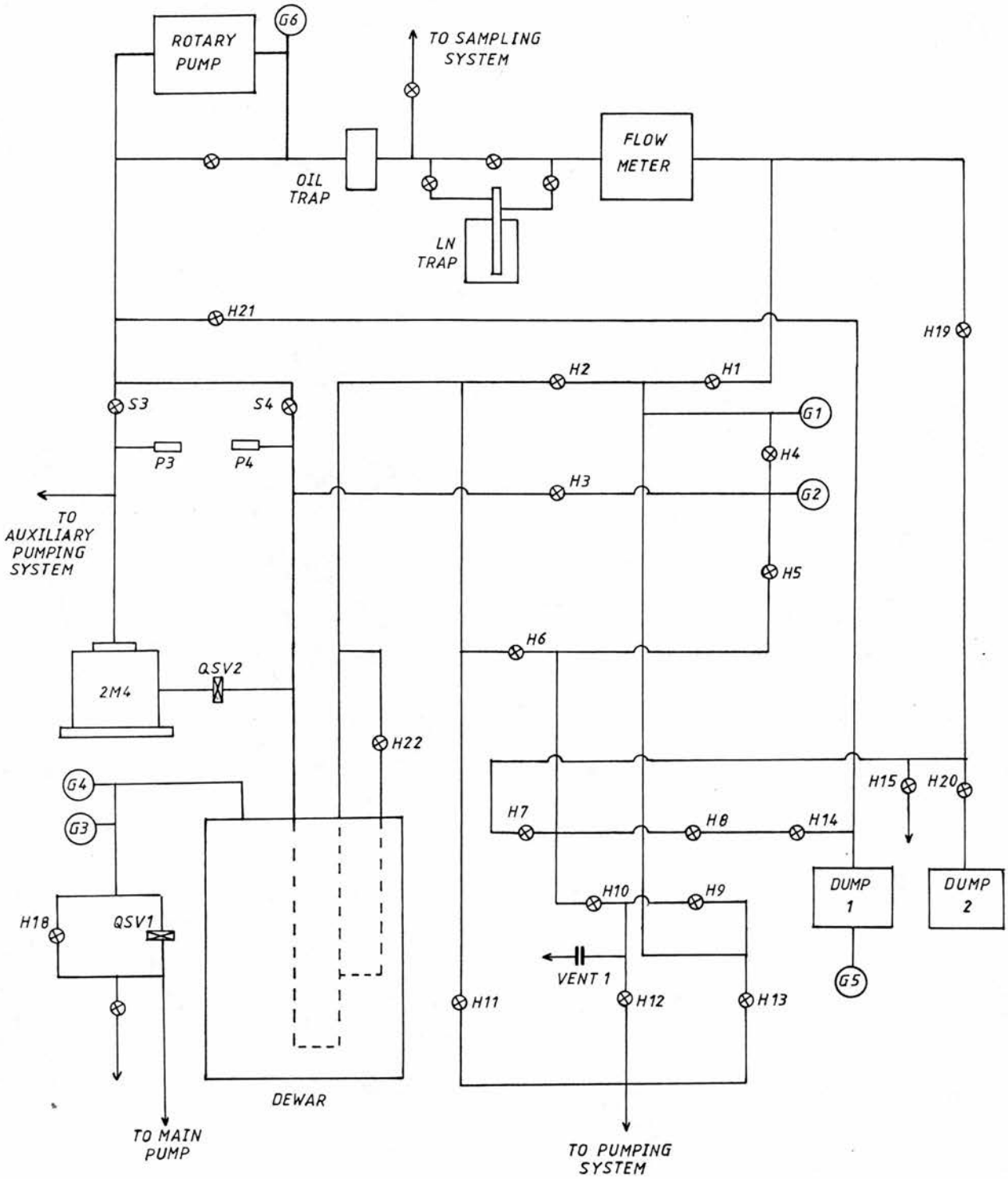

H - HOKE VALVE
S - SAUNDERS VALVE
QSV - QUARTER-SWING VALVE

P - PIRANI GAUGE
G - BOURDON GAUGE
G4 - MACLEOD GAUGE

Figure 3.2. The gas handling system for the dilution refrigerator.

Using this method the condensing time was reduced to an hour and a half and all the mixture could be used.

3.3 Description of a typical run.

The 3He/4He mixture was kept in two dumps at room temperature at a pressure of approximately 600 Torr. At the start of a run, all the isolating vacuums and the circulating piping were evacuated with the oil diffusion pump E01 (see Figure 3.1). The system was then leak tested using a 20th Century "Centronics" Mass Spectrometer backing the diffusion pump and tuned for 4He. If no leak was observed, the helium can was evacuated and filled with an atmosphere of helium gas from the return line whilst the leak rate into the IVC, OVC and circulating system was monitored. When it was clear that there was no leak at room temperature, the nitrogen shield was filled with liquid and the system allowed to precool for 24 to 36 hours. The dilution unit was cooled by allowing 0.5 Torr helium exchange gas into the IVC. Helium liquid was then transferred into the helium dewar which held approximately 18 litres. This liquid lasted for three days under normal running conditions.

The helium exchange gas in the IVC was pumped out over-night. The 3He/4He mixture was then introduced into the cryostat down the still side of the dilution unit, and used to do a flow test on the flow-limiting capillary to ensure that it was not blocked with solid air (see Figure 3.3). The rise in the pressure in the Bourdon gauge G1 was measured with a mixture pressure of 200 Torr across the capillary. When it was clear that the capillary was free, the by-pass valve to the auxiliary condensing system was opened and the mixture condensed by pumping the 1K pot and using the rotary pump to pull the mixture out of the dumps and push it into the condenser under

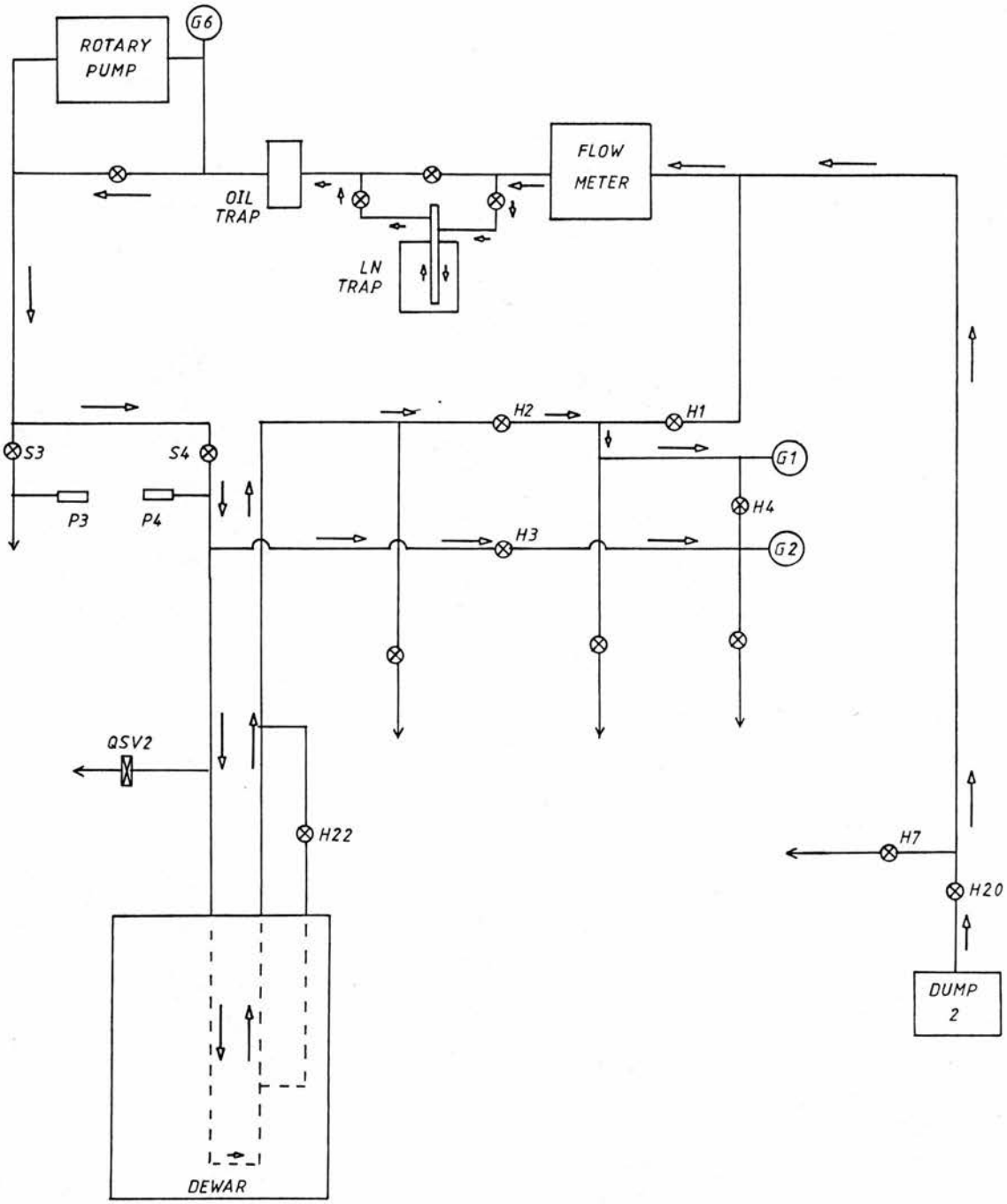

H - HOKE VALVE
S - SAUNDERS VALVE
QSV - QUARTER-SWING VALVE

P - PIRANI GAUGE
G - BOURDON GAUGE

Figure 3.3. Circulation test using the 3He/4He mixture to ensure the flow-limiting capillary was clear. The arrows indicate the path of the gas flow from the dumps.

pressure. It took approximately a quarter of an hour to empty the dumps after which the 1K pot was refilled by "cracking" the needle valve to the helium bath whilst continuing to pump the pot and condense the mixture. When the 1K pot was full its pressure rose sharply and the needle valve was shut. The pot then lasted for approximately 24 hours.

A further hour was required before the condensing pressure dropped below 30 Torr and the auxiliary condensing system was shut off and circulation started with the rotary pump (see Figure 3.2). After the vapour pressure of the liquid in the still had dropped low enough, the diffusion pump 2M4 was switched in and the still cooled to 0.5K. There was then a negative temperature gradient across the dilution unit with the still coldest and the mixing chamber warmest at 0.8K. The dilution unit cooled slowly until phase separation of the 3He and 4He occurred in the middle step exchanger causing the refrigerator to cool more rapidly. Phase separation then occurred in the lowest heat exchanger and finally in the mixing chamber. The dilution unit then quickly developed a positive temperature gradient and cooled rapidly. Approximately 0.6mW of heat was put into the still by a small electric heater to keep the temperature at about 0.6K and hence ensure a sufficiently high circulation rate.

After circulation had started, the fridge took two hours to reach 0.3K and a further hour and a half to cool to 60 mK. The circulation rate was then kept constant and the temperature stabiliser used to select and stabilise the mixing chamber temperature over the range 60 mK to 1.4K whilst data was being acquired.

After a run, the system was allowed to warm to room temperature

and the mixture returned to the dumps using a cryopump. The mixture was "scrubbed" periodically by passing it repeatedly through the nitrogen trap. The impurities frozen out in the trap were then pumped out of the system.

CHAPTER IV

THERMOMETRY

Resistance thermometers were chosen for use in the fridge as they provide fast response, high sensitivity and ease of measurement. The temperature of the still, mixer and heat exchangers of the dilution unit were measured with carbon resistors. Germanium resistance thermometers were used on the polymer specimens and the copper specimen-holder block.

4.1 Carbon Resistors.

These were Speer 220 ohm, 1/2 watt 1002 Grade resistors. They have the advantage of being inexpensive and having a simple equation fit to their resistance versus temperature curve. They have the disadvantage of non-reproducibility, and for accurate work need to be recalibrated each run.

One of the batch provided by the Oxford Instrument Company, that used on the mixing chamber, had been calibrated by them against "magnetic" temperature. This calibration was also used for the other four resistors in the batch as they showed close agreement and the relative values of the resistances from one run to the next were of more interest than the absolute temperatures they indicated. The temperature given by the carbon resistor mounted on the dilution tail was compared with that given by the germanium resistor on the specimen-holder, and was found to agree to within about 1%. This limit was probably due to variations in the thermal contact of the thermometer to the tail rather than to the reproducibility of the resistor.

In addition to the above Speer resistors, two Allen Bradley (A.B.) carbon resistors, one 10 ohm and the other 22 ohm, were used as sensors

for the temperature stabiliser. These resistors were chosen for their greater sensitivity above 0.5K and were mounted in the specimen block.

The resistance of the carbon resistors was measured with a prototype two-terminal a.c. bridge operating at a frequency of 133 Hz and supplied by Oxford Instruments with the dilution fridge. The power dissipated in a sensor monitored with this bridge is shown in Table 4.1. It was found that there was self-heating in the thermometers below about 0.2K ($R > 3k$ ohm) and the reference oscillator stage was modified to reduce the amplitude of the output waveform by half, thus reducing the power dissipated to a quarter of its former value. Although this greatly reduced the self-heating effect, it was still not negligible. Since absolute values of temperature were not required from these thermometers, however, it was decided not to reduce the output again as we did not want any further loss in the sensitivity of the bridge.

4.2 Germanium Resistors

Germanium resistance thermometers were chosen to obtain the temperature of the specimen and specimen block as they provide good sensitivity over a wide temperature range, have small sensor size and mass, and a short response time (Swartz et al.1976). They have several advantages over carbon resistors: they are highly reproducible ($\pm$0.5mK at 4.2K) and a single resistor can be used over the entire temperature range 3.2K to 50mK. Since the thermal conductivity of germanium is very much larger than that of carbon, there is less self-heating in a germanium resistor for the same power dissipation. They have the disadvantages that they are more expensive and require much more elaborate fitting procedures for their calibration curves

Table 4.1

Power dissipation in a sensor by the Oxford Instruments' resistance bridge as a function of temperature for a typical Speer 220 ohm carbon resistor.

T(K)	Resistance(ohms)	Power(watts)
0.05	30k	3×10^{-12}
0.1	7k	3×10^{-11}
0.3	2k	3×10^{-11}
0.5	1250	3×10^{-11}
1.0	900	3×10^{-10}
4.2	500	3×10^{-10}

Table 4.2

Power dissipation in a sensor by the S.H.E. conductance bridge as a function of temperature for a typical germanium resistance thermometer.

T(K)	Resistance(ohms)	Power(watts)
0.05	40k	2×10^{-14}
0.1	5k	2×10^{-13}
0.3	500	2×10^{-12}
0.5	200	5×10^{-11}
1.0	100	1×10^{-10}
4.2	30	3×10^{-10}

(Blakemore et al.1970, Martin 1975).

The germanium thermometers were commercial units supplied by Scientific Instruments and Lake Shore Crytronics, and consisted of a suitably doped germanium crystal encapsulated in a gold plated copper cylinder. The cylinder was filled with ^{3}He to transport heat from the germanium chip to the capsule wall.

A.c. techniques were used in the resistance measurement to avoid problems with thermal e.m.f.s and to obtain higher sensitivity from the measuring equipment. A four-terminal measurement was made to eliminate the lead resistances, each thermometer having separate current leads. If they are wired in series, the high resistance of the thermometers at low temperatures gives an excessive current lead resistance for the sensor being measured.

Initially a bridge was tried that had been built by Professor S.B. Woods and designed by J. Rogers, both of the University of Alberta. However, the germanium resistors used in the fridge were not suitable for use with this bridge as their resistance values were low above 0.5K (under 100 ohms) and the bridge was designed to provide large excitation currents for low values of resistance. This caused excessive self-heating in the thermometers below 0.7K. The bridge also proved to be gain sensitive below 1K with germanium resistors but not with carbon resistors of comparable resistance. This effect was thought to be due to the larger capacitance of the germanium sensors which at the comparatively high frequency of the bridge, 140 Hz, gave a capacitive component of impedance of the same order as the resistance.

A S.H.E. Potentiometric Conductance Bridge was therefore purchased. This had been specifically designed for the measurement of calibrated

germanium resistors at very low temperatures. It was a self-balancing, four-terminal a.c. conductance bridge with a 4 1/2 digit readout and a nominal accuracy of 0.1%. Four ranges were available with full scale conductances of 200μMho (5k ohms) to 200 mMho (5 ohms). The bridge provided an excitation signal of a 27.5 Hz square wave with constant selectable voltages across the voltage terminals of 10μV, 30μV, 100μV and 300μV. Four different resistors were used in the fridge and at any given temperature they had very different values of resistance. A compromise voltage level was selected so that the voltage range did not have to be changed when switching from one thermometer to another, although this could easily be done if necessary. The 100μV range was used between 4.2K and 0.3K and the 30μV range below this. Typical sensor dissipation levels are given in Table 4.2.

4.3 Noise Levels for the Germanium Thermometers

Initially problems were encountered with high noise levels in the thermometers at low temperatures. There were several sources of noise generation in the conductance measurement:

(1) Noise inherent in the conductance bridge (including Johnson noise in the sensor). Values for this were given in the bridge manual and the only significant component was the 50 Hz ripple on the excitation signal fed to the sensor. This noise current varied from 0.2nA on the 200μMho range to 200nA on the 200mMho range. Since the bridge operated at a frequency of 27.5 Hz, this noise had only a small effect on the display, but the lowest conductance range possible was always used. This prevented the noise power dissipated being larger than the excitation power and causing self-heating of the germanium thermometer at very low temperatures.

(2) 50 Hz pick-up from ambient mains fields. Shielded multicore cables were used for the room temperature thermometer leads from the bridge to the connector plate at the head of the cryostat. The four-pole switch for changing from one thermometer to another was shielded in an aluminium box. A bundle of thirty leads led from the connector plate, down the IVC pumping line to the 1K pot (see Chapter V). These leads relied on the cryostat itself for screening from the ambient fields. Ideally the leads to each thermometer should be in screened, twisted pairs and this had not been provided for when wiring the high temperature stage of the fridge (i.e. that part of the fridge which normally operated above 1K). Attempts to measure the 50 Hz pick-up signal with a C.R.O. were unsuccessful as the noise introduced into the circuit by the C.R.O. itself was too large. As with the 50 Hz signal fed in by the bridge, the main problem was one of self-heating rather than the not insignificant noise in the display. Changes of the leads, and hence presumably of the noise pick-up, showed no change in the conductance values.

(3) Piezoresistive effects in the germanium due to vibration of the dilution unit. These vibrations are known to cause noise problems with poorly mounted germanium chips. The dilution unit was suspended from the 1K pot and vibrated sufficiently to cause substantial heating of the mixing chamber itself (see Chapter III). After this vibration had been greatly reduced, no dimunition of the noise level in the bridge display was observed and it was therefore concluded that this was not a significant noise factor.

(4) "Noise" produced on the display by thermal fluctuations. Calculations of the temperature deviations corresponding to the display noise for each thermometer, showed that they were approximately the same for all the thermometers across the temperature range,

despite the large differences in conductance (greater than a factor of ten) between the highest and lowest conductance. This indicated that it was the primary source of noise. An estimate of the noise level for the calibrated thermometer, GeN, is given in the Appendix. The value of conductance was read half a dozen times over a 15 minute period and the standard deviation calculated. The scatter appeared to be random rather than due to a systematic drift in temperature.

The noise on the display on the two top conductance ranges was within the ±1 digit specification. On the two lower ranges, the 3 second time constant on the bridge was used and this reduced the display noise to less than 0.1%. This value of time constant was quite acceptable as the time for equilibrium of the specimen at the lowest temperatures could be as great as 30 minutes and a high speed of response was therefore not essential.

One thermometer, Ge2, was found to be unsuitable for use below 0.1K as its conductance was then approximately 1 μMho (1M ohm resistance) and this was comparable with the noise level on the display.

4.4 Thermal Contact to the Thermometers

During calibration runs with the fridge, all the germanium thermometers were soldered with Wood's metal into holes in the copper specimen-block. When a thermal conductivity measurement was being made the specimen thermometers were attached as described in Chapter V. Wood's metal was chosen because of its low melting point (60^{0}C) but was unfortunately superconducting in the region of interest (below 2K). The area of contact of the solder was equal to the area of the thermometer capsule, approximately 0.5 sq.cm., and with a thickness of solder of only about 0.025cm., the thermal conductivity

of the solder was high enough to provide good contact above 0.3K. Below this temperature, the efficiency of the 3He gas in the capsule as a heat exchange medium was greatly reduced and it was expected that most of the heat would be removed from the chip via the leads. The leads provided with the thermometer were coated in "teflon" and therefore not suitable for thermal anchoring. Instead they were soldered to the pins on the mixer connector ring (see Chapter V) and the Eureka wires from this ring provided the thermal contact to the dilution tail. This was found to provide insufficient thermal grounding (see Chapter V) and the thermometer leads were extended with 20 cm. lengths of #30 SWG enamelled copper wire. These were wrapped tightly around the copper tail and cemented down with Ge 7031 varnish thinned with toluene.

4.5 Calibration

It had originally been intended to calibrate the germanium thermometers against "magnetic" temperature obtained from a S.Q.U.I.D. and C.M.N. pill. Problems with the S.Q.U.I.D. led to the purchase of a germanium standard from Scientific Instruments. This primary thermometer was calibrated from 3.2K to 50mK with 25 points. The secondary thermometers were calibrated against this standard in two stages:

(i) Between 3.2K and 1.3K A simple glass 4He dewar was used and the temperature reduced from 4.2K to 1.3K by pumping over the liquid. The thermometers were immersed in the 4He bath and their conductance measured with the S.H.E. bridge. The bath temperature was stabilised using an Oxford Instruments resistance bridge with a 47 ohm Allen Bradley resistor as sensor. The off-balance signal at the 7V diode output was used to provide power to a 100 ohm heater.

The bath temperature was held steady to better than ±2mK above the lambda point and ±1mK below. The resistors were found to be mutually reproducible to within the noise level of the S.H.E. bridge (±1 digit) or the error in the temperature stabilisation, whichever was greater.

(ii) Between 1.4K and 50mK. This part of the calibration was done in the fridge. Initially there were problems with the thermal contact of the thermometers to the mixer tail (see above). This gave a lack of reproducibility from one run to the next and the resistance against temperature curves from the two calibration ranges did not coincide at the overlap region between 1.4 and 1.3K. This indicated that even at 1.5K the important factor for the thermal contact of the germanium chips was the leads and not the case and ^{3}He exchange gas as had previously been assumed. Improved thermal contact of the leads showed the thermometer reproducibility to be better than the experimental error in the conductance measurement.

Data points for the calibrations were taken at intervals of approximately T/10, where T was the absolute temperature, giving about 75 points for each thermometer.

4.6 Computer Fitting of the Calibration Curves

A table was generated for the primary thermometer of conductance against temperature at 1mK intervals between 3.2K and 50mK and used to calibrate the secondary thermometers. High accuracy for this initial table was essential as any errors led to even larger errors in the secondary thermometer resistance curves. The number of calibration points provided with the standard, 25, was insufficient for very accurate numerical analysis and, in addition, two of these points were shown to be "bad". The resulting problems with the computer fitting were the largest single source of error in the

thermal conductivity measurements.

Many different empirical formulae have been tried for fitting to the resistance versus temperature curve of germanium thermometers at low temperatures and these have been extensively reported in the literature (Blakemore et al.1970, Martin 1975). At the time of starting this work, the consensus of opinion was that the best fit was obtained using a polynomial of the form

$$y = \sum_{j=0}^{n} A_j x^j \qquad (4.1)$$

where $y = \log(R)$ and $x = \log(T)$.

A programme was written for the university's IBM 360/44 computer using the method of least squares and incorporating subroutines from the IBM Scientific Subroutine Package. These subroutines were converted to double precision form (48 binary digit numbers) and stored on magnetic tape for easy loading. Double precision was necessary to prevent roundoff errors in the matrix inversion for high order polynomials. The programme generated increasing order polynomials up to a maximum of 15th degree or until there was no improvement in the sum of squares on going from one order to the next. The best fit was not necessarily the highest order polynomial as the least squares polynomial superimposed spurious oscillations about the true log(R) versus log(T) curve.

After each polynomial had been computed a table of the values T,R,R(calc), ΔR, ΔT,dR/dT and d^2R/dT^2 at the data points was printed out, where T and R were the input values of the temperature and resistance for each data point and R(calc) the calculated resistance.

Then $\Delta R = R(calc) - R$

$dR/dT = dy/dx \times R(calc)/T$

$d^2R/dT^2 = d^2y/dx^2 \times R(calc) \times 0.4343/T$

$\Delta T = R/(dR/dT) = T - T(calc).$

The order of polynomial used, n, was selected by imposing the condition that the first derivative, dR/dT, was monotonic and the second derivative, d^2R/dT^2, smooth. Typically polynomials of about 10th order were used.

One poor data point affected not only the value of n chosen but also the regression coefficients and hence the calculated resistance values across the entire temperature range. As a check for bad points in the primary thermometer input data, plots were drawn of the deviations in temperatures from the curve, ΔT, versus the temperature, T, for each polynomial. Those for the 5th, 8th and 12th degree polynomials are shown in Figure 4.1. The oscillations due to the least squares polynomial technique show up clearly on these, as does the effect of the two bad points at 0.6K and 0.8K. A 10th order polynomial was used for the primary thermometer giving a r.m.s. scatter for ΔT of $\pm$2.5mK (excluding the two bad points) and a maximum deviation of $\pm$6mK.

After a polynomial had been selected for the primary thermometer, a second computer programme generated a table of conductance against temperature at 1mK intervals using the regression coefficients from the first programme. This table provided the calibration values for the secondary thermometers, which were then processed in an identical manner to those for the primary.

When the results of the thermal conductivity measurements of a sample of PMMA were obtained, it was found that there were

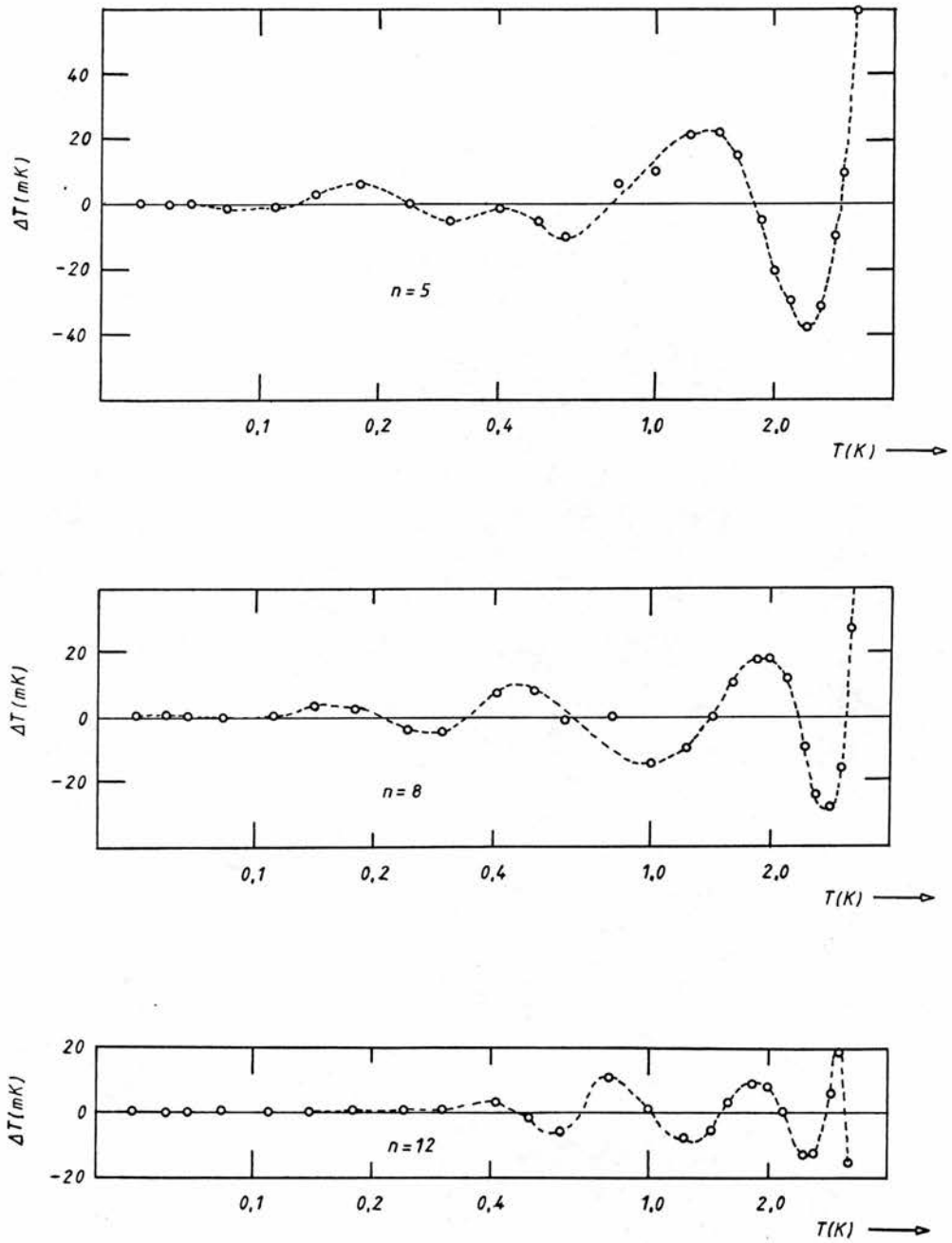

Figure 4.1. The points represent a plot of the difference between the input and least squares result for each calibration point for the standard thermometer GeN. The differences, $\Delta T = T - T(calc)$, are calculated from Equation 4.1 for the 5th, 8th and 12th degree polynomials. The oscillations imposed by the least squares technique show up clearly as does the effect of the two bad points at 0.6K and 0.8K.

oscillations about the expected log(κ) versus log(T) curve and that the amplitude of these ripples was largest, approximately 10%, at about 1K. They were thought to be due to the oscillatory behaviour of the thermometer resistance curves. Different polynomials were tried for each thermometer and the thermal conductivity calculations repeated. The new thermal conductivity curve again oscillated about the expected curve but in a different manner to that before, indicating that the problem indeed lay in the calibration of the thermometers rather than in the conductivity measurements themselves.

An improved interpolation technique due to Godratt et al.(1977) was tried. An expression of the form

$$y = \sum_{j=0}^{n} A_j x^j \qquad \text{(4.2)}$$

was again used but with y = log(T) and x = log(R). A least squares polynomial of low order, $n \approx 5$, was made to all the data points to obtain an initial temperature versus resistance curve for the primary. A plot of the deviations in temperature, ΔT, was made as before showing the same ripple of the data points about the curve, see Figure 4.2. The data was then divided into subsets of half-cycle ripples and each ripple segment individually fitted with a second polynomial of fourth degree,

$$\text{i.e.} \quad \Delta T = \sum_{k=0}^{4} B_k (\log(R))^k .$$

The segments were made overlapping so that each point was an internal point for some segment except for the two end points corresponding to highest and lowest temperature. This also gave a smooth fit where the boundaries of one polynomial gave way to another.

When a single segment contained less than six points, it and the next adjacent segment were fitted simultaneously by the same polynomial. The computer programme automatically selected the segments to be fitted.

The temperature at the input points were again calculated

$$\Delta^2 T = \Delta T - \Delta T(\text{calc})$$

The values $\Delta^2 T$ are shown versus log(T) in Figure 4.2. Therefore the final value of T4 for any value R was

$$T4 = T(\text{calc}) + \Delta T(\text{calc}) = T - \Delta^2 T.$$

The 5th degree polynomial fit to the whole curve for the primary thermometer GeN showed a r.m.s. scatter of the data points (excluding the two bad points at 0.6K and 0.8K) of $\pm$6mK with a maximum deviation of $\pm$10mK. The final r.m.s. scatter found after fitting the half-cycle ripples was $\pm$1.0mK with a maximum deviation of $\pm$2mK. Therefore when calibrating the secondary thermometers, any data point with a deviation from the calculated curve greater than $\pm$2mK was considered "bad" and discarded. This was not possible with the primary thermometer as there were insufficient points for those at 0.6K and 0.8K to be left out.

This second calibration method had the advantage that any bad points could be identified and their effect localized to the segment in which they occurred. Godratt et al. compared the values of T obtained when fitting sixth and fourth order polynomials for the first polynomial and found that the differences in the values between these two interpolation curves was a factor of two better than the scatter in the data. That is, the interpolation values were more accurate than the raw data.

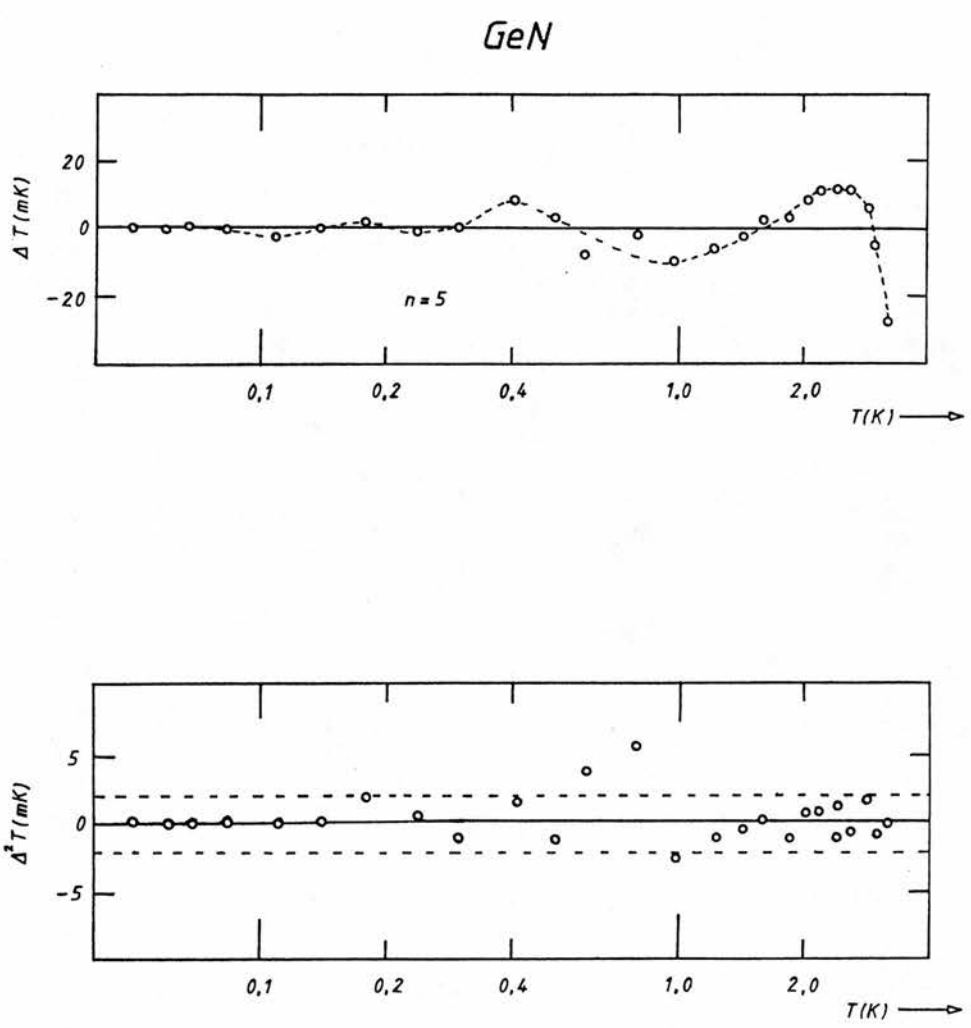

Figure 4.2. Deviation plots for the calibrated thermometer GeN using Equation 4.2. The upper plot represents the differences, $\Delta T = T - T(calc)$, between the input and least squares result at each datum point for the 5th order polynomial. The lower plot shows the second differences, $\Delta^2 T = \Delta T - \Delta T(calc)$, between the data points and the 4th order polynomials fitted to the half-ripple segments in the upper plot. The dashed lines represent scatter of $\pm$2mK. The two bad points at 0.6K and 0.8K again show up clearly.

The programmes written to apply this technique were based on the Nottingham Algorithm Group (NAG) package which was available on the computer in double precision form on a permanently mounted magnetic disc. There was therefore no need to store the subroutines on magnetic tape. This second method had the computational advantage of using only low order polynomials, thus avoiding problems with roundoff errors. It had the disadvantages that the interpolation formula was different for each segment of the curve and that the value of the conductance at any temperature could not be found by an analytical method but had to be solved iteratively when generating a table of conductance versus temperature. Since these programmes were seldom run, these disadvantages were not considered to be of great importance.

The thermal conductivity curve of the PMMA specimen was recalculated using the new calibration tables. The calculated curve then showed a much closer fit to the expected curve at higher temperatures, above 1K, but at the lowest temperatures, the amplitude of the oscillations was larger than those obtained previously. This was thought to be due to errors in the calibration below 0.1K caused by differences in the thermal contact between the secondary thermometers and the primary during the calibration run. All the recalculated thermal conductivity curves showed a "hump" at about 0.6K. This was almost certainly due to the poor calibration points on the primary at 0.6K and 0.8K. It was therefore decided to use the calibration tables obtained by the first method below 0.7K and the new tables above this temperature. The thermal conductivity curves then showed only small oscillations at low temperatures and, at the temperature at which the tables were changed (0.7K), the curves showed a smooth join for all the specimens.

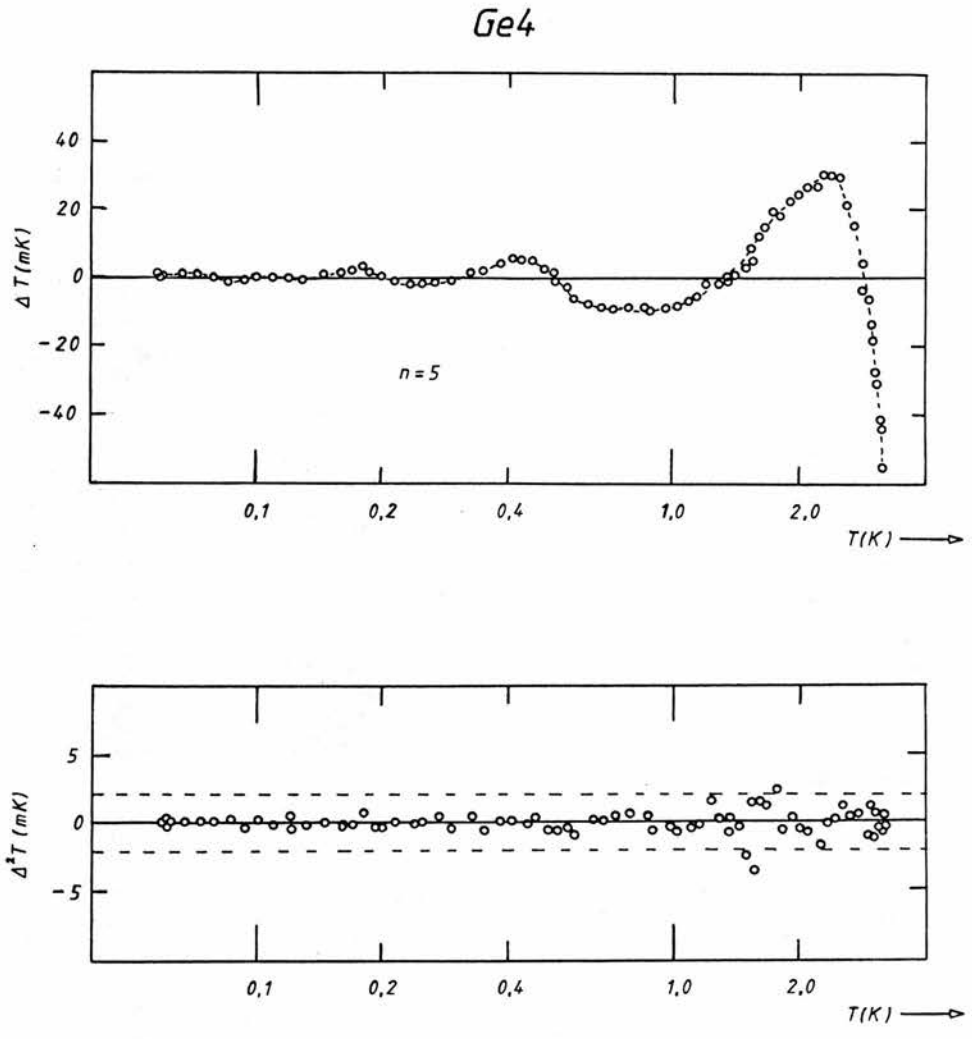

Figure 4.3. Deviation plots for the secondary thermometer Ge4 using Equation 4.2. The upper plot represents the differences, $\Delta T = T - T(calc)$, between the input and least squares result at each datum point for the 5th order polynomial. The lower plot shows the second differences, $\Delta^2 T = \Delta T - \Delta T(calc)$, between the data points and the 4th order polynomials fitted to the half-ripple segments in the upper plot. The dashed lines again represent scatter of $\pm$2mK. The largest scatter of the points is at about 1.4K, the temperature at which the calibration method was changed (see Section 4.5).

As a check on the calibration of the two secondary thermometers on the specimens, their temperature difference was noted when the specimens were in equilibrium with no heat applied (see Chapter V). Typically the r.m.s. scatter of this temperature difference in the temperature range 0.12K to 3K was $\pm$1.5mK with a maximum difference of $\pm$3mK. Below 0.12K, the temperature difference could be as large as $\pm$8mK due to the poor calibration at the lowest temperatures. This was clearly the reason for the larger scatter (about 10%) in the thermal conductivity results in this region. With better thermal contact between the thermometers in the calibration run in the fridge, the technique of Godratt et al. could be expected to give a typical difference in the temperature readings of the thermometers of less than $\pm$1mK below 1K.

CHAPTER V

EXPERIMENTAL DETAILS

5.1 Introduction

The thermal conductivity, K , of the polymer specimens was measured over the temperature range 0.1 to 3K in the 3He/4He dilution refrigerator. The steady-state-heat flow method was used. Heat was applied to the specimen through a heater wound on one end and removed through the other end which was attached to the cold finger of the fridge. The resulting temperature difference across a section of the specimen was measured with two germanium resistance thermometers.

5.2 The Specimens

Four polymer specimens were measured, all four having been provided by Leeds University Polymer Group and previously measured in the temperature range 3 to 100K (Burgess and Greig 1974, 1975, Choy and Greig 1975). They were provided in the form of cylindrical rods, 1 cm. diameter and approximately 5 cm. long. At one end of each specimen a 1k ohm heater of #46 SWG manganin wire was wound. The other end was drilled and tapped to receive a 6 BA screw to provide thermal contact to the cold finger on the mixer block of the refrigerator. Two holes were drilled through the specimens, 1.5 cm. apart along the length of the rods, for the insertion of the specimen thermometers (see Figure 5.1).

5.3 Wiring of the fridge

Thirty leads were strung from the top of the fridge to the 1K pot. They were connected to the room temperature circuitry through three ten-pin plugs at the connector plate at the head of the cryostat and were led to the 1K pot through the 1/2" stainless steel pumping

line for the IVC. The wires were thermally anchored at 4.2K to a post soldered to the IVC wall and at 1K to the 4He pot, by winding them around several turns and cementing down with Ge 7031 varnish thinned with toluene. The wires were then soldered to pins fixed in a "tufnol" ring on the 1K pot. This pin-ring was used to join the high temperature leads to those used for the low temperature stages on the dilution unit (see Plate 3).

Initially all thirty leads were of #44 SWG Eureka (copper-nickel alloy wire with silk insulation). Later those from the Oxford Instrument Co. (O.I.C.) resistance bridge to the Allen Bradley (AB) resistors and the bridge common lead were replaced by #48 SWG copper to reduce their resistance. The leads on the dilution unit were also of #44 SWG Eureka except those to the AB resistors which were of 0.002" Niomax wire (niobium-titanium core in a copper sheath). At helium temperatures, this Niomax wire was superconducting so that the total lead resistance to these two resistors was small (less than 200 ohms). Since the resistance of the AB resistors was low above 2K (less than 1K ohm), it was necessary to have a low lead resistance so that changes in the resistor values were not hidden by the lead resistance in this two-terminal measurement. The high sensitivity of the AB resistors at high temperatures could then be utilised for greater sensitivity of the temperature stabiliser. The leads were thermally anchored at each stage on the dilution unit by winding three or four turns of wire around the stage and cementing down with varnish. After anchoring the wires to the mixing chamber, the leads were soldered onto pins in a small "tufnol" ring similar to that on the 1K pot.

The still heater was wound from #44 SWG Eureka with the double silk insulation impregnated with varnish to provide good heat

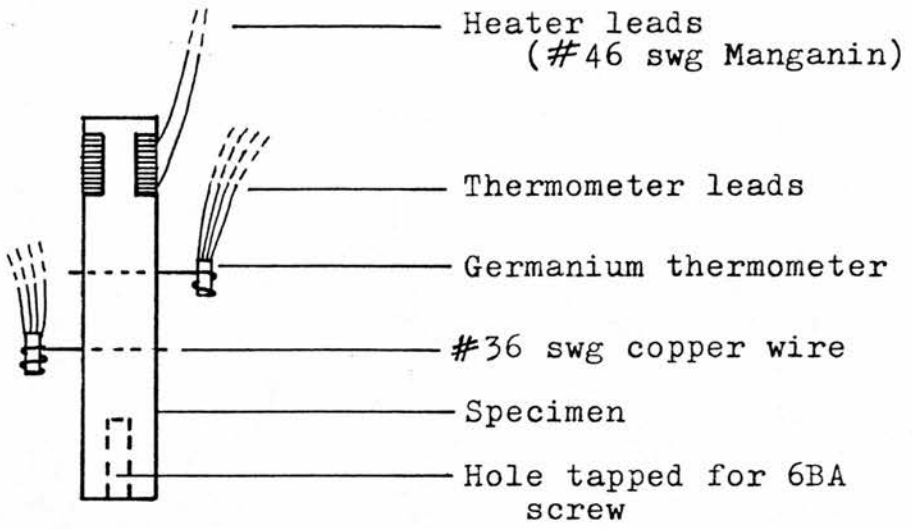

(a)

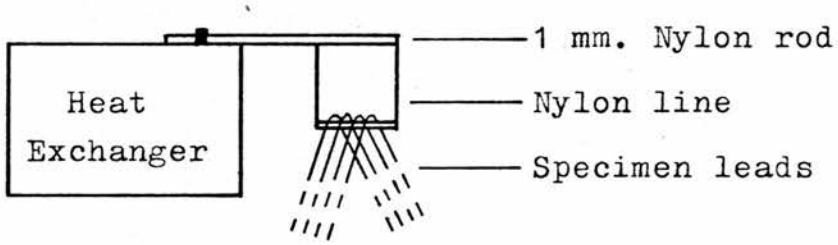

(b)

Figure 5.1. Specimen geometry and leads. (a) Specimen with two germanium thermometers mounted on it. The heat was applied through a heater wound on one end of the sample and extracted from the other end which was attached to the cold finger of the fridge. (b) Thermal isolation of the specimen heater and thermometer leads using nylon "trapezes".

conduction between the layers. The power to this heater was provided by a constant current supply incorporated in the O.I.C. resistance bridge. Typically a current of o.8mA was supplied to the 1k ohm heater, dissipating a power of approximately 0.6mW.

5.4 Thermal contact on the Mixing Chamber

The specimens were mounted on a copper block attached to the copper mixer tail (see Figure 5.2). Three distinct thermal contact problems had to be overcome:

(1) between the block and tail,

(2) between the specimen and block and

(3) between the thermometers and specimen.

5.4.1 Thermal contact between the block and mixer tail

The specimens were attached to a copper block which was fixed onto the mixer tail with two 6 BA brass bolts. The thermal contact between the block and tail was provided by the pressure between the two flat copper surfaces. These surfaces were carefully cleaned and polished, coated with a thin layer of Apiezon 'N' grease and then bolted together. The Speer 220 ohm carbon resistor used as a sensor for the temperature stabiliser was thermally anchored by its leads onto the mixer tail. The stabiliser heater, a 1.3k ohm carbon resistor, was inserted into the copper block. When calibrating the germanium thermometers, they were soldered into the specimen block (see Chapter IV) and it was found that when the stabiliser was in use, there was a slow drift in the temperature of the block. This drift was attributed to poor thermal contact between the stabiliser heater and sensor since one was in the block and the other in the tail. The copper block was therefore soldered to the mixer tail with non-superconducting (cadmium-bismuth) solder. The sensor and

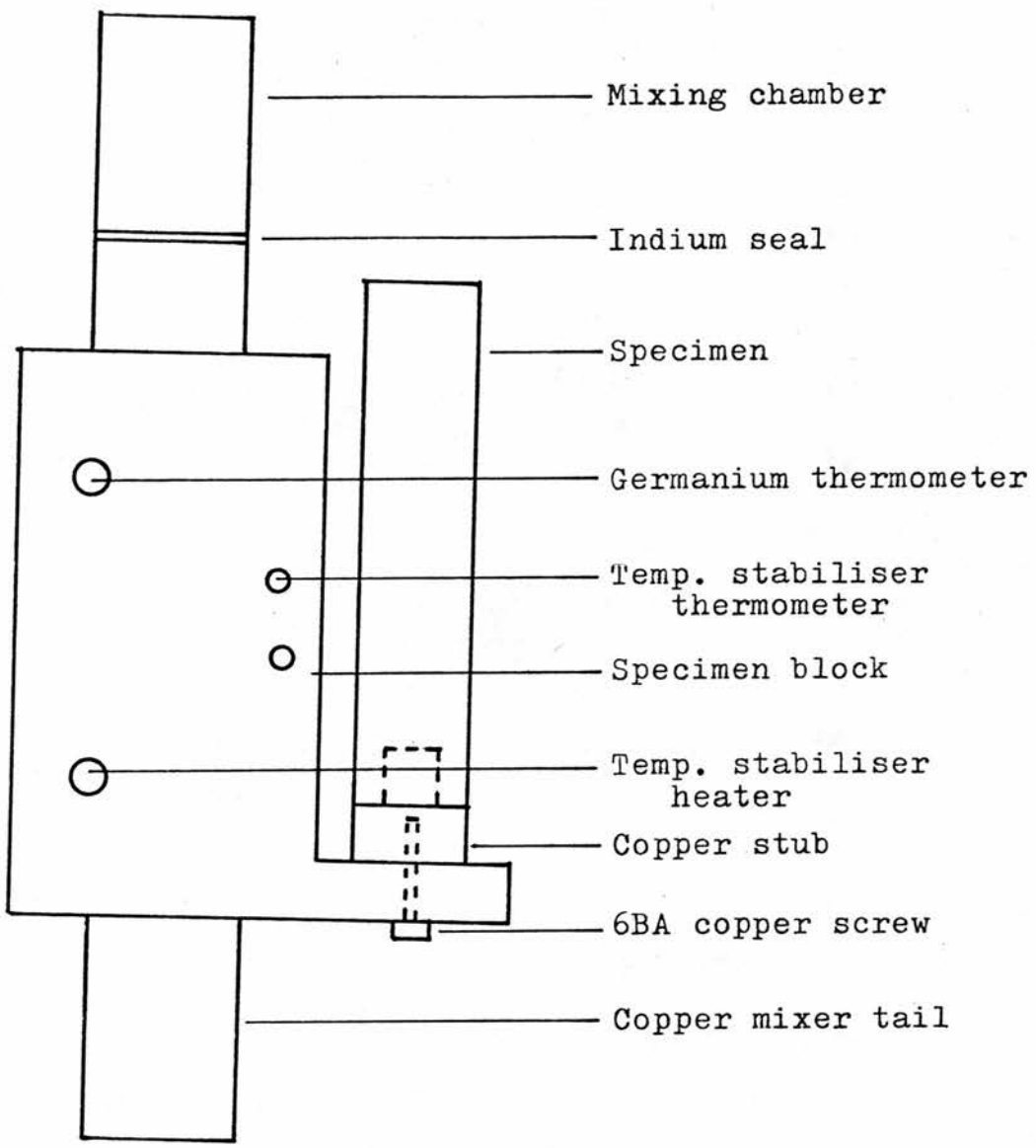

Figure 5.2. Mounting of the polymer specimen on the sample holder using a copper stud. The sample holder was soldered to the copper tail of the dilution unit.

heater leads were also more carefully thermally anchored to the tail using the technique described for the germanium thermometers in Chapter IV. This reduced the thermal drift of the block to a negligible level. When the thermometers required inserting or removing from the block however, the entire tail unit had to be unbolted from the mixing chamber at the indium seal (see Figure 5.2).

5.4.2 Thermal contact between specimen and specimen block.

The specimens were provided with one end drilled and tapped to receive a 6 BA screw. This was used to provide thermal contact to the cold finger of the block which was also tapped for a 6 BA screw. A copper screw was then used to secure the specimen to the finger giving a tight fit at room temperature. It was found that on cooling below 1K, the two specimen thermometers, although remaining in thermal contact with each other, became thermally isolated from the finger. This was thought to be due to the specimen contracting onto the screw and away from the finger, the screw itself providing only a small area of contact onto the specimen. It was therefore decided to try to measure a metal sample as it would contract much less than the polymers on cooling. A test specimen was machined from stainless steel and its thermal conductivity measured down to 0.3K (the lowest temperature to which the thermometers had then been calibrated). The thermometers were mounted on the steel sample using Ge varnish rather than Wood's metal so that they remained electrically isolated from the dilution unit. Great care had to be taken when using this varnish with the germanium thermometers as it attacked the epoxy seals on the thermometer capsules. The stainless rod could be cooled to below 0.1K and its thermal conductivity successfully measured down to 0.3K. The problem with the polymer

specimens was thus confirmed to be one of thermal contact between the block and specimen caused by the specimen contracting on cooling.

The specimens were drilled out to take a 0.5 cm diameter, 0.5 cm high, copper stud which was a tight push-fit at room temperature. The copper stud was in turn drilled and tapped to receive the 6 BA copper screw (see Figure 5.2). This provided an area of contact of approximately 1 sq. cm. between the stud and the polymer. The difference in the thermal expansivities of polythene and copper caused the specimens to contract onto the stud as they cooled, providing good thermal contact down to 60mK.

5.4.3 Thermal contact between the thermometers and the specimen

Three germanium thermometers were used. One was soldered into the copper specimen block to ensure that the temperature of the block remained constant throughout a measurement (i.e. with the specimen heater off, on and then off again). The other two thermometers were mounted on the specimen 1.5 cm apart in the direction of the flow. The teflon coat was removed from one lead of each of the thermometers, and this lead and the thermometer case soldered to a #36 SWG copper wire with Wood's metal. This solder was choosen for its low melting point (60°C) but had the disadvantage of being superconducting below 2K (see Chapter IV). The copper wire for each thermometer was smeared with a thin layer of Apiezon 'N' grease and made a good push-fit into one of the small thermometer holes drilled through the specimen (see Figure 5.1). As the polymer cooled, it contracted onto the copper wire ensuring that the contact was under pressure. Measurements of the temperature difference between the two thermometers when the specimen was in equilibrium with no heat applied, showed that they were in good agreement (and hence in

good thermal contact to the polymer) down to 0.12K (see Chapter IV). The differences below this temperature were thought to be due to errors in the thermometer calibration rather than poor thermal contact as the temperature difference changed sign on exchanging the two thermometers' positions.

5.5 Heat loss from the specimen by conduction down the leads

The ten specimen leads (four for each thermometer and two for the heater) were made long enough to ensure that the thermal resistance in parallel with the specimen was large enough to be ignored. The leads were wired in three sets, one for each thermometer and one for the heater. The thermometer leads were of #44 SWG Eureka wire and were initially 30 cm lengths wrapped around graphite posts sufficiently thin to ensure that the heat conducted down them was negligible. Separate sets of posts were used for each set of wires.

It was difficult to wind the leads on the posts within the confined space available in the IVC without them touching either the IVC, the dilution unit or each other. It was decided therefore to change the method of isolating the leads both for ease of mounting a specimen and as a check that for the results already obtained, the heat loss down the leads was indeed negligible. Leads 50 cm long were used, suspended from nylon "trapezes" on the mixer tail and the top step heat exchanger. The two bars of the "trapezes" were made from 1 mm nylon rod and the lower bar was suspended from the upper by two short lengths of nylon fishing line. The upper bar was attached to the heat exchanger and the wires looped around the lower bar (see Figure 5.1). Separate sets of "trapezes" were used for each set of leads. The heat loss through the "trapezes" themselves was negligible and they protruded far enough to prevent

the wires contacting the side of the dilution unit.

The choice of wire for the heater leads was more difficult. They had to have a low electrical resistance so that the heat generated in them was less than 1% of that generated in the heater. The specimens were provided with leads of #46 SWG manganin wire and these were cut down to 6 cm lengths - that length of wire in which approximately 1% of the heat was generated. These leads were then extended by 50 cm lengths of 0.002" lead-coated manganin which was superconducting at helium temperatures. The wires were suspended from nylon "trapezes" as with the thermometer leads. At temperatures above 0.5K, the lead, although superconducting, was still a fair thermal conductor, and the short length of manganin wire provided the required thermal isolation. Below this temperature, the thermal conductivity of the superconductor (which is proportional to T^3) was low enough to ensure that the heat loss was negligible. As a check on the heat losses through the lead-coated manganin wires, they were replaced by 1 m. lengths of 0.002" Niomax N (niobium-titanium filaments in a copper-nickel matrix).

The changes in the thermometer and heater leads and their method of suspension produced no change in the measured thermal conductivity, K, of the specimen SHO (that with the highest thermal resistance) indicating that the heat losses were indeed negligible.

5.6 Specimen heater power

The power to the heater was supplied by a S.H.E. constant current supply. The four heater leads down to the mixer tail were Eureka and at the tail pin-ring were joined in pairs to the two superconducting leads described above. The negligible electrical resistance of these leads enabled an effective four terminal

measurement of the heater power to be made. The voltage across the 1 k ohm specimen heater was measured with a digital voltmeter. The current was obtained by using a digital multimeter to measure the voltage drop across a 10k ohm standard resistor in series with the heater.

5.7 Temperature difference across the sample

The specimen was allowed to come to equilibrium by holding the block temperature constant with the temperature stabiliser. The specimen thermometers were read repeatedly until they were steady and the temperature difference noted ($\Delta T'$). Current was supplied to the heater and the thermometers scanned until the temperatures were again constant when the temperature difference was recorded ($\Delta T''$). The heat was then switched off and a check made to ensure that the temperature distribution returned to its former value.

The induced temperature difference was thus

$$\Delta T = \Delta T'' - \Delta T'.$$

The thermal conductivity was calculated from the expression

$$K = \frac{Q}{\Delta T} \times \frac{l}{A} \qquad \text{(5.1)}$$

where l was the distance between the thermometers in cm,

A the cross-sectional area of the rod in sq. cm,

Q the heat dissipated in the heater in mW and

ΔT the temperature difference in K.

The thermal conductivity was thus calculated in units of mW/cm-K.

Equation (5.1) is only an approximate solution of the heat transfer equation

$$\underline{\nabla} \cdot (K \underline{\nabla T}) + \frac{i^2}{\sigma} = 0$$

and this approximation limits the temperature difference which can be applied across the specimen without introducing noticeable error. There was no heat generated in the specimen so the second term in the equation was zero. The cylindrical symmetry of the rods allowed a 1-D solution:

$$\kappa \frac{dT}{dx} = \frac{Q}{A} \qquad \text{(5.2)}$$

$$\kappa \, dT = \frac{Q}{A} \, dx$$

$$B = \frac{Ql}{A} = \int_{T_1}^{T_2} \kappa \, dT \qquad \text{(5.3)}$$

where the thermometer temperatures were T_1 and T_2 and

$$T_2 + T_1 = 2T$$

$$T_2 - T_1 = \Delta T .$$

T was taken as the "temperature" of the sample.

Thus

$$T_2 = T + \Delta T/2$$

$$T_1 = T - \Delta T/2.$$

Suppose $\kappa = aT^n$ where a is a constant. Hence from (5.3)

$$B = \frac{aT^{n+1}}{(n+1)} \left[\left[1 + \frac{\Delta T}{2T} \right]^{n+1} - \left[1 - \frac{\Delta T}{2T} \right]^{n+1} \right] - \text{(5.4)}.$$

Consider a binomial expansion of the two terms in the square brackets. An expansion to terms of the order of $\left[\frac{\Delta T}{2T}\right]^2$ gives

$$B_1 = aT^n \Delta T$$

$$\text{i e } K_1 = \frac{Ql}{A\Delta T} \qquad \text{as per equation (5.1).}$$

At low temperatures (below 1K), $\Delta T/T$ may be large enough for higher terms in the binomial expansion to need to be considered. Equation (5.4) was therefore expanded to terms of the order of $\left[\frac{\Delta T}{2T}\right]^4$

$$B_2 = aT^n \Delta T \left[1 + \frac{n(n-1)}{6} \left[\frac{\Delta T}{2T}\right]^2 \right] .$$

Hence $$K_2 = K_1 \left[1 + \frac{n(n-1)}{6} \left[\frac{\Delta T}{2T}\right]^2 \right] .$$

Therefore the error in using equation (5.1) for the thermal conductivity is $\frac{K_2 - K_1}{K_1} = \frac{n(n-1)}{24} \left[\frac{\Delta T}{T}\right]^2$

i.e. for a 1% error, $\frac{\Delta T}{T} = 0.35$.

The specimen with the fastest varying thermal conductivity (PMMA) showed a temperature variation which can be approximated by $K = aT^2$. The largest value of $\frac{\Delta T}{T}$ used was $\Delta T = 35$mK at $T = 0.15$K, giving an error of 0.5% from this approximation.

5.8 Time constant for equilibrium

The time constant t_1 is given by (Reese 1966):

$$t_1 = (4l^2/\pi^2)(C/K). \qquad \text{(5.5)}$$

where l is the length of the rod,

C is the specific heat and

K is the thermal conductivity.

Suppose there is initially a temperature difference across the

sample ΔT_0. The time taken after the heater is switched off for this to decay to a value T is

$$t = t_1 \ln \left[\frac{\Delta T_0}{\Delta T}\right].$$

Therefore the time taken, t_2, to reach within 1% of the equilibrium value is

$$t_2 = \frac{18.4\, l^2}{\pi^2} \times \frac{C}{K} \text{ secs.} \qquad \text{——— (5.6)}$$

Assuming $K = aT^2$ and C is the Debye specific heat ($C = bT^3$),

$$t_2 = \text{const.} \times T$$

Using the measured values for C and K for SHO at 10K from Burgess and Greig (1975), t_2 = 635 secs = 10.5 mins..

Thus $t_2 = 63.5 \times T$ secs..

In practice, the time constant at low temperatures was found to be very much larger than calculated from this formula. There were probably two reasons for this:

(i) the specific heat did not obey the Debye expression at low temperatures and

(ii) an appreciable thermal contact resistance between the specimen and the mixer cold finger gave a low effective thermal conductivity.

5.9 Temperature stabilisation

The temperature stabiliser consisted of a sensor, an a.c. resistance bridge, a current amplifier and a heater (see Appendix). Three sensors were required as no single resistor had a high enough sensitivity across the entire temperature range. A Speer 220 ohm resistor was used in the range 50mK to 0.5K, a 10 ohm AB between 0.5K and 1K and a 22 ohm AB above 1K. The resistors were coated in a

thin layer of Apiezon 'N' grease and push-fitted into holes drilled in the copper specimen block. Leads of 20 cm lengths of #30 SWG enamelled copper wire were attached to the resistors and were wrapped around and cemented down to the copper tail to provide good thermal contact.

Initially an a.c. resistance bridge constructed for this purpose was used to measure the sensor resistances (see Appendix). This left the O.I.C. bridge free for monitoring the still and heat exchanger resistors so that the still heater power could be adjusted to compensate for any drift in the still temperature and hence in the 3He circulation rate. After some experience had been gained in operating the fridge, the still heater could be set when the fridge had cooled below 0.3K and did not need to be readjusted until the tail had been warmed to above 1K. The O.I.C. bridge could thus be used to check the still and exchanger temperatures as the fridge cooled and then used to measure the temperature stabiliser sensors as the tail was warmed. The d.c. off-balance signal from the bridge phase sensitive detector fed to the current amplifier.

This current amplifier was based on a design by Rochlin (1970) with an additional low-pass amplifier to give greater control of the stabiliser time constant and sensitivity. The off-balance signal from the bridge was amplified and passed to a 1.3k ohm carbon resistor in the specimen block which acted as the heater. The amplifier had two modes; MANUAL and AUTO. When on MANUAL, a preset d.c. current was fed to the heater. When the mixing chamber had reached thermal equilibrium, the resistance bridge was balanced and the amplifier switched to the AUTO mode. Any off-balance signal from the bridge resulting from a change in the tail temperature (and hence the sensor resistance value) was added algebraically to the preset current to

alter the heater power and hence return the block to its former temperature.

The temperature stabiliser could be used to control the temperature of the mixing chamber in the range 50mK to 1K without altering any of the fridging parameters and with a typical fluctuation of $\pm 50\,\mu K$ in the temperature. Above 1K the still heater power had to be reduced to prevent the dilution unit warming suddenly, and the stability was then typically $\pm 100\,\mu K$ (see Appendix).

CHAPTER VI

EXPERIMENTAL RESULTS

6.1 Polymer Specimens

The thermal conductivity of four polymer samples was measured between 0.1 and 3K. All four were supplied by Dr. D. Greig and had been measured between 3 and 100K by Dr. Greig and his co-workers.

The results are presented in Tables 6.1 to 6.5. The data from different runs for the same sample agreed very well even when the length, type and isolation of the specimen leads and the method of thermal contact had been changed between runs (see Chapter V). Selected points from these tables are plotted graphically in Figures 6.1 to 6.5.

6 2 Hostalen GUR

Two specimens of this very high molecular weight polyethylene were measured. The crystallinity, X, was calculated from the density (ρ = 0.945 g cm^{-3}) using the relation

$$\rho = \rho_x \times X + \rho_a (1-X)$$

where ρ is the bulk density, ρ_x is the crystallite density (1.00 g cm^{-3}) and ρ_a is the amorphous density (0.85 g cm^{-3}).

The thermal conductivity of the extruded specimen (SH2) was measured in the direction of the extrusion and had a draw ratio of 3.85.

(i) SHO

The results for this specimen are presented in Table 6.1 and Figure 6.1. The data fitted very well with results obtained at higher temperatures (Burgess and Greig 1974). The $T^{1.8}$ temperature dependence observed above 3K continued down to o.6K and then decreased to approximately $T^{1.1}$ below o.4K. Both the magnitude and temperature dependence of the thermal conductivity were in good agreement with the measurements of Scott et al. (1973) for their uncharacterised polyethylene specimen. There was very little scatter in the data despite the differing conditions under which the measurements were performed (see Chapter V).

(ii) SH2

The values of the thermal conductivity are presented in Table 6.2 and Figure 6.2. The measurements around 3K again agreed well with the data obtained by previous workers. Between 2 and 3K, κ continued to vary as $T^{1.8}$. Below 2K the temperature dependence was decreased to approximately $T^{1.1}$.

6.3 Polymethyl Methacrylate (PMMA)

This sample was measured as a check on the accuracy of the apparatus, in particular the thermal isolation of the thermometer and heater leads and the calibration of the germanium thermometers. The detailed results are given in Table 6.3 and Figure 6.3. Between 1.5 and 2K, the measurements were very similar to those obtained previously for this specimen. Below about 0.6K, the familiar $T^{1.8}$ temperature dependence of amorphous materials was observed. The

results agree very well with those obtained by Stephens et al. (1972) in this temperature range.

Table 6.4 shows the values obtained using a second pair of germanium thermometers. The maximum difference between the two sets of readings is approximately 15% and the average about 5%. The three secondary thermometers Ge1, Ge2 and Ge4 had been calibrated against the primary GeN (see Chapter IV).

6.4 Rigidex 50

This linear polyethylene was choosen as its lower molecular weight enabled it to be extruded to greater extrusion ratios than Hostalen GUR. Measurements of λ had been obtained for extrusion ratios between 1 and 25 from 2 to 100K (Gibson et al. (1977)). The specimen reported in this work had an extrusion ratio of 13 and was supplied in the form of a cylindrical rod so that the thermal conductivity could be obtained in the direction of extrusion (see Chapter V).

The sample was split at the end where the copper stud was inserted. This gave problems with the thermal contact to the specimen block, particularly below 0.3K, and the results obtained for this sample are therefore suspect.

The measurements are presented in Table 6.5 and Figure 6.4. Although the values around 2K agreed well with the results of Gibson et al., there was a sharp change in slope from their conductivity curve. This may not be an indication of poor measurement, however, as it is at this temperature that the sharp change in temperature dependence was observed in the other extruded polyethylene sample, SH2.

Table 6.1a

Summary of the properties of the four polymer specimens.

	SH2	SHO	PMMA	Rigidex 50
Density ($g\ cm^{-3}$)	0.94	0.94	1.18	0.966
Crystallinity X	0.6	0.6	0	0.77
Mol. Wt. $\overline{M}_w$	3.5×10^6	3.5×10^6	2×10^6	1×10^5
Extrusion ratio	3.85	-	-	13

Below 0.2K, the temperature dependence seemed to increase again from the linear behaviour seen between 0.2 and 2K.

6.5 Accuracy of Thermal Conductivity Results

The largest source of error in the measurements was in the calibration of the secondary thermometers (see Chapter IV). There were two main reasons for this:

(i) The small number and poor quality of the calibration points supplied with the primary thermometer.

(ii) The poor thermal contact between the thermometers below 0.1K during the thermometer calibration runs.

The first source of error lead to the oscillation of the observed W curve about the expected curve. The effect of this was decreased above 0.6K by using calibration tables calculated using the technique of Godratt et al. (1977). The oscillations in the curves could still be seen below this temperature and gave about a 5% error around 0.5K where they were worst (see Figure 6.2, the thermal conductivity curve for SH2).

The second cause of error in the thermometry lead to a scatter of the results below 0.2K and this was not improved by applying Godratt's technique. The scatter was about 10% between 0.1K and 0.2K. This could be greatly reduced by improved thermal contact between the thermometers during calibration.

The thermometry introduced an error of typically 1 to 5mK in the measurement of the temperature drop across the specimen (i.e. 5% above 0.2K and about 10% below this).

In addition to these errors there is approximately 2% error in

the measurement of the geometrical factor for the specimens. This would obviously only change the absolute value of the measurements and not their scatter or the shape of the conductivity curve.

The only other significant source of error in the experiment was in the thermal contact of the thermometers to the sample and of the sample to the copper block on the mixer tail. For the first three specimens measured (SH0, SH2 and PMMA) these were clearly insignificant. It is not clear however what error they introduced into the readings for the Rigidex 50 sample.

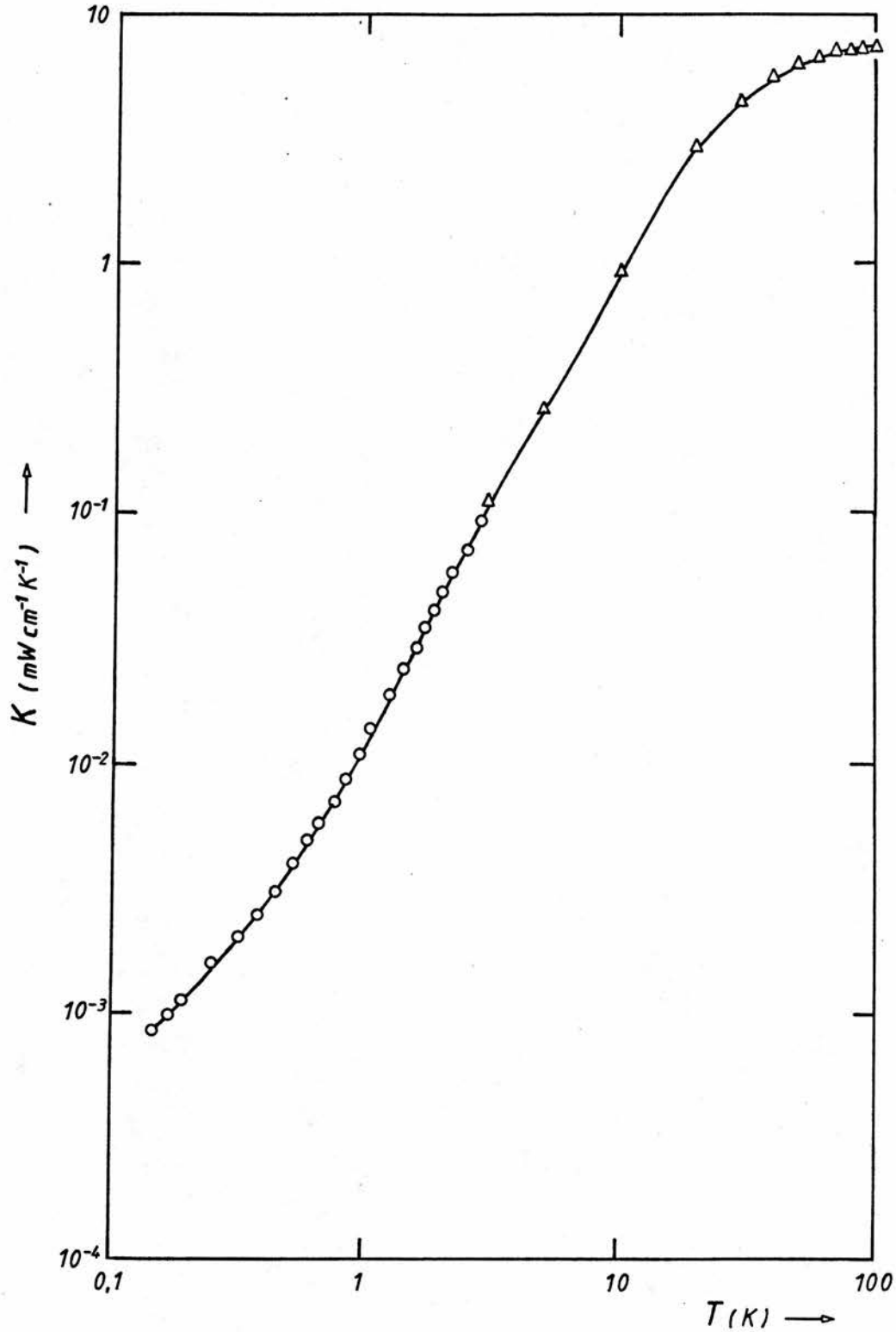

Figure 6.1. Thermal conductivity as a function of temperature of the isotropic Hostalen GUR specimen SHO. The circles are selected points from the present work, the triangles are after Burgess and Greig (1975).

TABLE 6.1

Thermal conductivity in mW cm^{-1} K^{-1} as a function of temperature T in degrees K for the isotropic Hostalen GUR specimen SHO.

T	K		
2.865	9.37×10^{-2}	1.724	3.51×10^{-2}
2.746	8.68×10^{-2}	1.639	3.11×10^{-2}
2.687	8.31×10^{-2}	1.601	2.90×10^{-2}
2 657	7.81×10^{-2}	1.529	2.74×10^{-2}
2.579	7.79×10^{-2}	1.504	2.60×10^{-2}
2.574	7.61×10^{-2}	1.427	2.42×10^{-2}
2.518	7.11×10^{-2}	1.422	2.48×10^{-2}
2.502	7.25×10^{-2}	1.409	2.43×10^{-2}
2.499	7.19×10^{-2}	1.347	2.23×10^{-2}
2.469	6.88×10^{-2}	1.342	2.18×10^{-2}
2.417	6.57×10^{-2}	1.310	2.09×10^{-2}
2.369	6.30×10^{-2}	1.247	1.91×10^{-2}
2.282	6.15×10^{-2}	1.206	1.75×10^{-2}
2.247	5.71×10^{-2}	1.180	1.70×10^{-2}
2.201	5.77×10^{-2}	1.162	1.63×10^{-2}
2.199	5.51×10^{-2}	1.131	1.61×10^{-2}
2.096	5.33×10^{-2}	1.114	1.59×10^{-2}
2.024	4.81×10^{-2}	1.070	1.40×10^{-2}
1.961	4.55×10^{-2}	1.064	1.41×10^{-2}
1.957	4.53×10^{-2}	1.031	1.36×10^{-2}
1.928	4.39×10^{-2}	0.999	1.27×10^{-2}
1.853	4.08×10^{-2}	0.957	1.14×10^{-2}

TABLE 6.1 (cont)

T	K	T	K
0.931	1.10×10^{-2}	0.376	2.44×10^{-3}
0.919	1.07×10^{-2}	0.374	2.61×10^{-3}
0.879	9.63×10^{-3}	0.352	2.31×10^{-3}
0.839	8.89×10^{-3}	0.350	2.38×10^{-3}
0.819	8.47×10^{-3}	0.345	2.40×10^{-3}
0.782	8.06×10^{-3}	0.316	2.06×10^{-3}
0.769	7.97×10^{-3}	0.282	1.83×10^{-3}
0.749	7.18×10^{-3}	0.246	1.59×10^{-3}
0.708	6.85×10^{-3}	0.184	1.13×10^{-3}
0.688	6.44×10^{-3}	0.178	1.06×10^{-3}
0.699	6.23×10^{-3}	0.164	1.00×10^{-3}
0.648	5.86×10^{-3}	0.164	9.83×10^{-4}
0.617	5.51×10^{-3}	0.142	8.52×10^{-4}
0.594	5.14×10^{-3}		
0.591	4.60×10^{-3}		
0.576	4.97×10^{-3}		
0.568	4.28×10^{-3}		
0.565	4.80×10^{-3}		
0.539	4.14×10^{-3}		
0.515	4.14×10^{-3}		
0.489	3.61×10^{-3}		
0.455	3.12×10^{-3}		
0.440	3.15×10^{-3}		
0.418	3.01×10^{-3}		
0.409	2.75×10^{-3}		
0.397	2.76×10^{-3}		

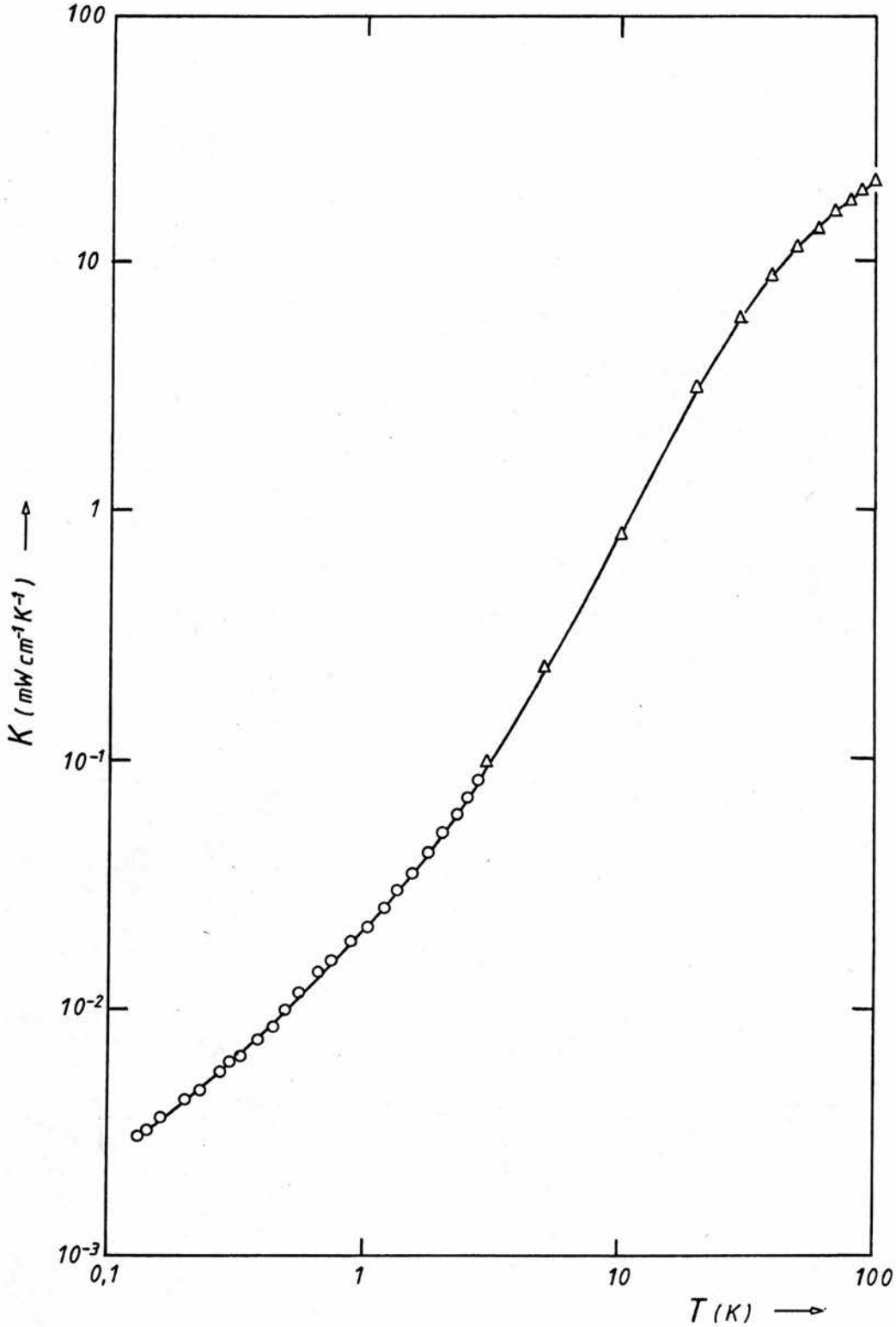

Figure 6.2. Thermal conductivity as a function of temperature of the extruded Hostalen GUR specimen SH2. The circles are selected points from the present work, the triangles are after Burgess and Greig (1975).

TABLE 6.2

Thermal conductivity in mW cm^{-1} K^{-1} as a function of temperature T in degrees K for the extruded Hostalen GUR specimen SH2.

T	K	T	K
2.747	8.53×10^{-2}	1.775	4.43×10^{-2}
2.656	7.95×10^{-2}	1.750	4.41×10^{-2}
2.579	7.52×10^{-2}	1.671	4.22×10^{-2}
2.511	7.19×10^{-2}	1.632	3.90×10^{-2}
2.488	6.86×10^{-2}	1.630	3.78×10^{-2}
2.448	6.83×10^{-2}	1.578	3.58×10^{-2}
2.388	6.57×10^{-2}	1.546	3.60×10^{-2}
2.375	6.56×10^{-2}	1.500	3.50×10^{-2}
2.344	6.38×10^{-2}	1.435	3.33×10^{-2}
2.301	6.22×10^{-2}	1.414	3.22×10^{-2}
2.252	6.01×10^{-2}	1.354	3.05×10^{-2}
2 231	5.92×10^{-2}	1.339	3.04×10^{-2}
2 223	5.95×10^{-2}	1.296	2.86×10^{-2}
2.169	5.67×10^{-2}	1.219	2.67×10^{-2}
2.144	5.49×10^{-2}	1.202	2.63×10^{-2}
2.108	5.53×10^{-2}	1.125	2.42×10^{-2}
2.010	5.25×10^{-2}	1.055	2.28×10^{-2}
2.003	5.16×10^{-2}	1.029	2.21×10^{-2}
1.972	5.01×10^{-2}	0.980	2.09×10^{-2}
1.943	4.88×10^{-2}	0.887	1.89×10^{-2}
1.911	4.88×10^{-2}	0.861	1.83×10^{-2}
1.829	4.61×10^{-2}	0.767	1.65×10^{-2}
1.800	4.72×10^{-2}	0.738	1.61×10^{-2}

TABLE 6.2 (cont.)

T	K	T	K
0.687	1.48×10^{-2}	0.229	4.73×10^{-3}
0.666	1.46×10^{-2}	0.218	4.38×10^{-3}
0.647	1.39×10^{-2}	0.197	4.33×10^{-3}
0.635	1.38×10^{-2}	0.192	4.06×10^{-3}
0.579	1.24×10^{-2}	0.170	3.28×10^{-3}
0.552	1.18×10^{-2}	0.169	3.57×10^{-3}
0.527	1.10×10^{-2}	0.159	3.65×10^{-3}
0.504	1.04×10^{-2}	0.159	3.30×10^{-3}
0.492	1.00×10^{-2}	0.150	3.45×10^{-3}
0.469	9.46×10^{-3}	0.143	3.27×10^{-3}
0.460	9.13×10^{-3}	0.130	3.08×10^{-3}
0.437	8.62×10^{-3}	0.129	3.02×10^{-3}
0.413	8.10×10^{-3}		
0.389	7.57×10^{-3}		
0.359	6.95×10^{-3}		
0.343	6.72×10^{-3}		
0.333	6.54×10^{-3}		
0.329	6.46×10^{-3}		
0.304	6.17×10^{-3}		
0.302	6.07×10^{-3}		
0.277	5.63×10^{-3}		
0.258	5.20×10^{-3}		
0.256	5.33×10^{-3}		
0.242	5.02×10^{-3}		
0.234	4.40×10^{-3}		

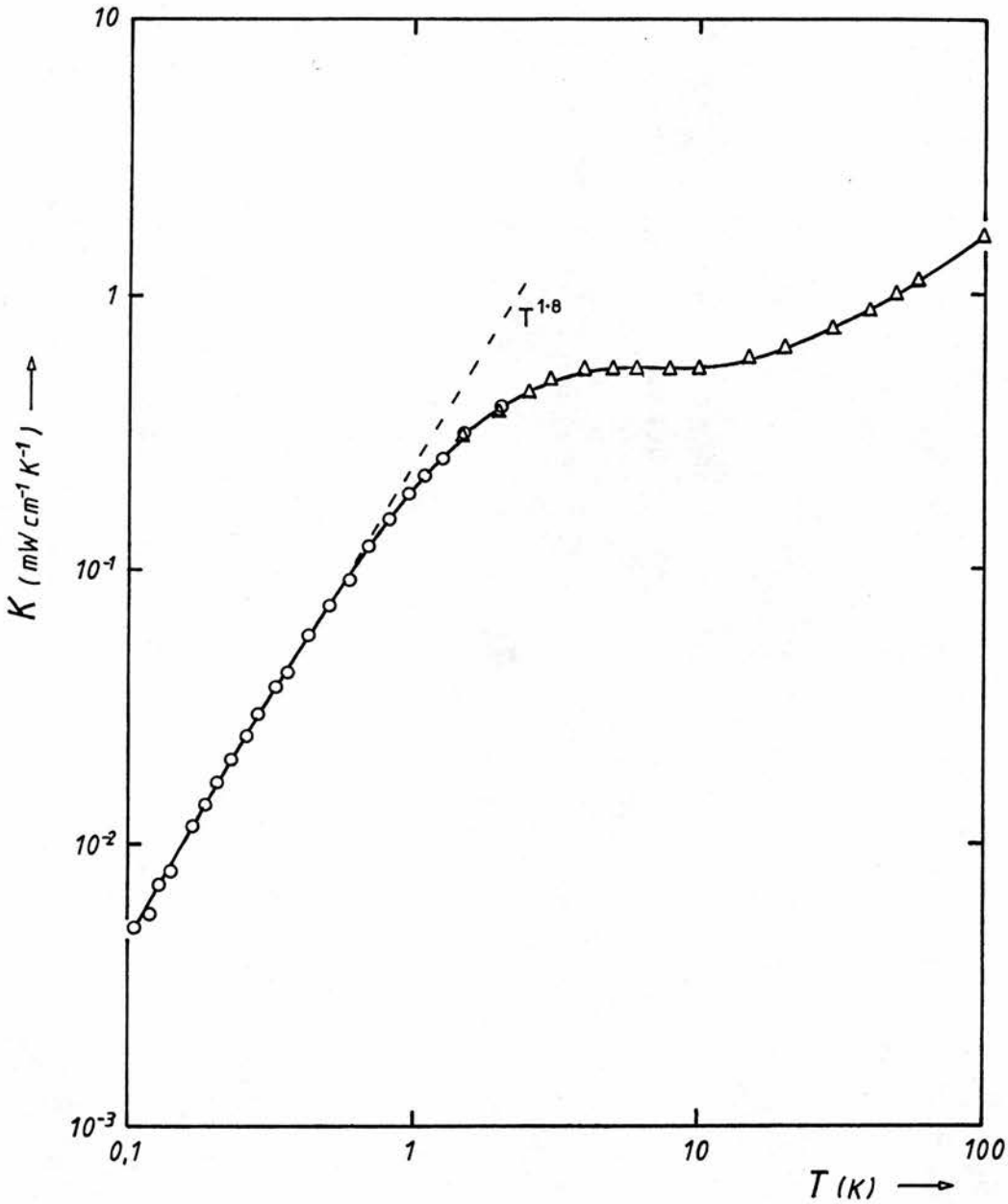

Figure 6.3. Thermal conductivity as a function of temperature of the amorphous polymer polymethylmethacryalate (PMMA). The circles are selected points from the present work, the triangles are after Burgess and Greig (1974). The thermal conductivity varies as $T^{1.8}$ below 0.8K and shows the characteristic plateau at higher temperatures. The results are in good agreement with those of Stephens et al. (1972).

TABLE 6.3

Thermal conductivity in mW cm^{-1} K^{-1} as a function of temperature T in degrees K for the polymethylmethacrylate (PMMA) specimen using thermometers Ge1 and Ge2.

T	K	T	K
2.023	4.21×10^{-1}	0.478	6.55×10^{-2}
1.896	4.05×10^{-1}	0.450	5.89×10^{-2}
1.860	4.00×10^{-1}	0.418	5.70×10^{-2}
1.749	3.57×10^{-1}	0.387	5.09×10^{-2}
1.644	3.24×10^{-1}	0.367	4.63×10^{-2}
1.538	3.10×10^{-1}	0.337	4.01×10^{-2}
1.426	3.07×10^{-1}	0.328	3.91×10^{-2}
1.321	2.88×10^{-1}	0.307	3.31×10^{-2}
1.205	2.57×10^{-1}	0.288	3.18×10^{-2}
1.106	2.33×10^{-1}	0.270	2.86×10^{-2}
1.030	2.11×10^{-1}	0.259	2.62×10^{-2}
0.965	1.95×10^{-1}	0.234	2.21×10^{-2}
0.883	1.73×10^{-1}	0.220	1.94×10^{-2}
0.832	1.55×10^{-1}	0.210	1.88×10^{-2}
0.767	1.39×10^{-1}	0.199	1.61×10^{-2}
0.728	1.31×10^{-1}	0.186	1.50×10^{-2}
0.687	1.21×10^{-1}	0.175	1.33×10^{-2}
0.671	1.19×10^{-1}	0.165	1.20×10^{-2}
0.655	1.13×10^{-1}	0.156	9.96×10^{-3}
0.613	1.06×10^{-1}	0.154	1.07×10^{-2}
0.590	9.30×10^{-2}	0.147	7.96×10^{-3}
0.550	9.25×10^{-2}	0.144	8.38×10^{-3}
0.533	7.62×10^{-2}	0.134	7.02×10^{-3}
0.517	7.33×10^{-2}	0.133	7.61×10^{-3}

TABLE 6.3 (cont.)

T	K
0.126	6.28×10^{-3}
0.123	6.60×10^{-3}
0.115	5.10×10^{-3}
0.109	4.74×10^{-3}
0.106	4.63×10^{-3}

TABLE 6.4

Thermal conductivity in mW cm^{-1} K^{-1} as a function of temperature T in degrees K for the polymethylmethacrylate (PMMA) specimen using thermometers GeN and Ge4.

T	K	T	K
2.031	4.07×10^{-1}	0.231	2.06×10^{-2}
1.902	3.86×10^{-1}	0.206	1.71×10^{-2}
1.483	3.17×10^{-1}	0.185	1.39×10^{-2}
1.392	2.98×10^{-1}	0.184	1.41×10^{-2}
1.256	2.60×10^{-1}	0.167	1.16×10^{-2}
1.174	2.35×10^{-1}	0.162	1.08×10^{-2}
1.105	2.23×10^{-1}	0.139	8.15×10^{-3}
1.031	2.04×10^{-1}	0.138	7.98×10^{-3}
0.962	1.90×10^{-1}	0.127	7.36×10^{-3}
0.818	1.55×10^{-1}	0.118	5.75×10^{-3}
0.762	1.44×10^{-1}	0.106	5.18×10^{-3}
0.689	1.22×10^{-1}		
0.652	1.14×10^{-1}		
0.593	9.39×10^{-2}		
0.562	8.72×10^{-2}		
0.509	7.61×10^{-2}		
0.474	6.59×10^{-2}		
0.430	5.82×10^{-2}		
0.390	4.97×10^{-2}		
0.362	4.31×10^{-2}		
0.331	3.81×10^{-2}		
0.305	3.31×10^{-2}		
0.283	2.87×10^{-2}		
0.258	2.47×10^{-2}		

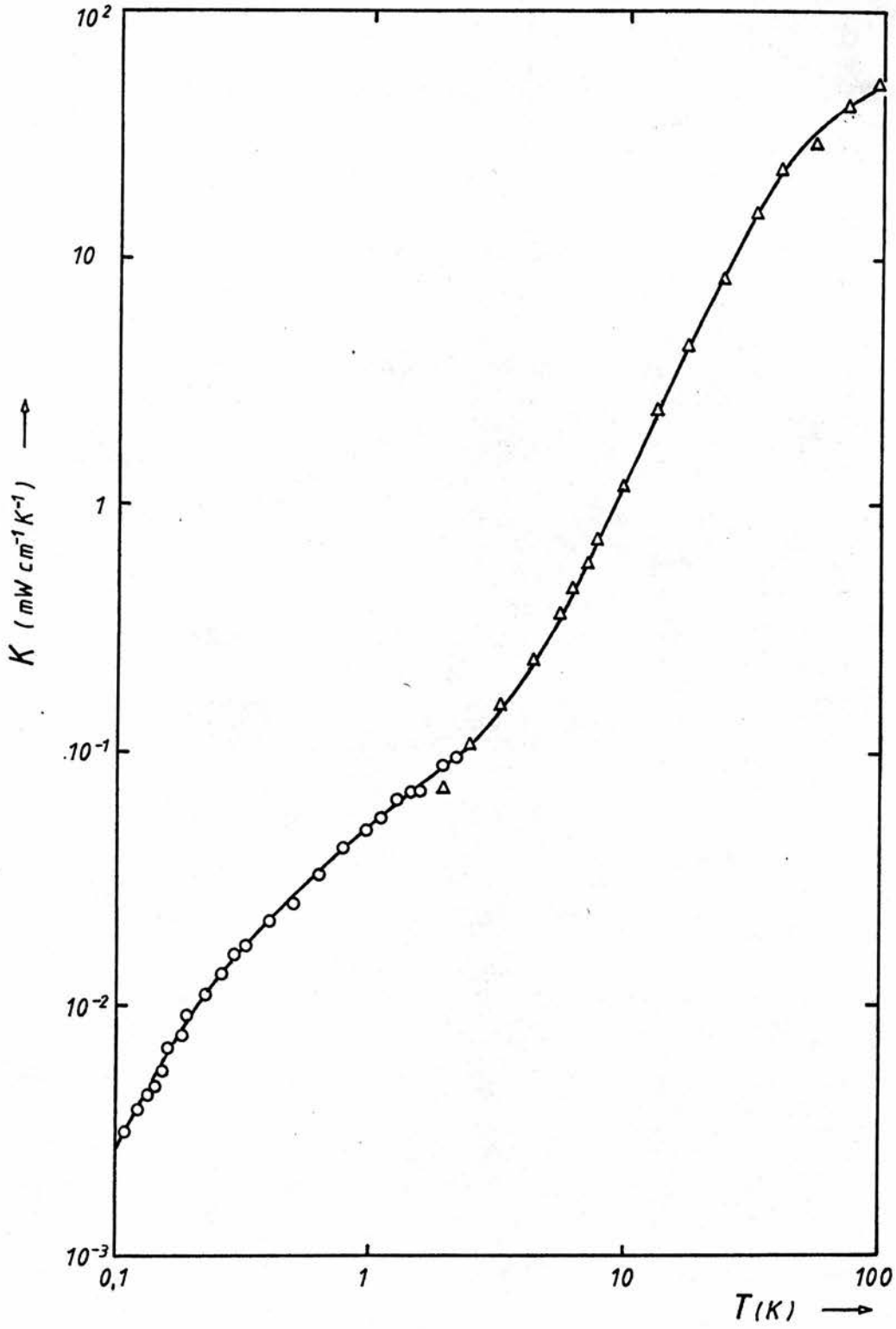

Figure 6.4. Thermal conductivity as a function of temperature of the Rigidex 50 polyethylene specimen. The circles are selected points from the present work, the triangles are after Gibson et al. (1977).

TABLE 6.5

Thermal conductivity in mW cm^{-1} K^{-1} as a function of temperature T in degrees K for the extruded Rigidex 50 specimen.

T	K	T	K
2.157	9.77×10^{-2}	0.595	2.98×10^{-2}
2.114	9.70×10^{-2}	0.581	2.94×10^{-2}
2.027	9.26×10^{-2}	0.549	2.78×10^{-2}
1.961	9.06×10^{-2}	0.506	2.50×10^{-2}
1.890	8.83×10^{-2}	0.495	2.45×10^{-2}
1.599	7.03×10^{-2}	0.493	2.53×10^{-2}
1.458	6.99×10^{-2}	0.471	2.41×10^{-2}
1.300	6.41×10^{-2}	0.467	2.31×10^{-2}
1.241	6.21×10^{-2}	0.440	2.30×10^{-2}
1.105	5.56×10^{-2}	0.434	2.27×10^{-2}
1.046	5.50×10^{-2}	0.407	2.14×10^{-2}
0.973	4.89×10^{-2}	0.407	2.08×10^{-2}
0.928	4.71×10^{-2}	0.371	1.97×10^{-2}
0.908	4.66×10^{-2}	0.369	1.90×10^{-2}
0.881	4.45×10^{-2}	0.361	1.90×10^{-2}
0.836	4.33×10^{-2}	0.325	1.72×10^{-2}
0.793	4.15×10^{-2}	0.302	1.38×10^{-2}
0.762	3.95×10^{-2}	0.299	1.50×10^{-2}
0.723	3.94×10^{-2}	0.293	1.56×10^{-2}
0.704	3.57×10^{-2}	0.268	1.18×10^{-2}
0.664	3.54×10^{-2}	0.266	1.33×10^{-2}
0.628	3.23×10^{-2}	0.263	1.29×10^{-2}
0.619	3.18×10^{-2}	0.238	9.95×10^{-3}

TABLE 6.5 (cont.)

T	K
0.230	1.08×10^{-2}
0.228	1.08×10^{-2}
0.207	9.36×10^{-3}
0.192	9.07×10^{-3}
0.188	7.37×10^{-3}
0.188	5.87×10^{-3}
0.180	7.73×10^{-3}
0.171	5.68×10^{-3}
0.166	5.97×10^{-3}
0.162	6.82×10^{-3}
0.162	6.65×10^{-3}
0.154	5.51×10^{-3}
0.150	4.87×10^{-3}
0.144	4.81×10^{-3}
0.142	4.36×10^{-3}
0.134	4.43×10^{-3}
0.125	3.84×10^{-3}
0.120	3.62×10^{-3}
0.111	3.13×10^{-3}

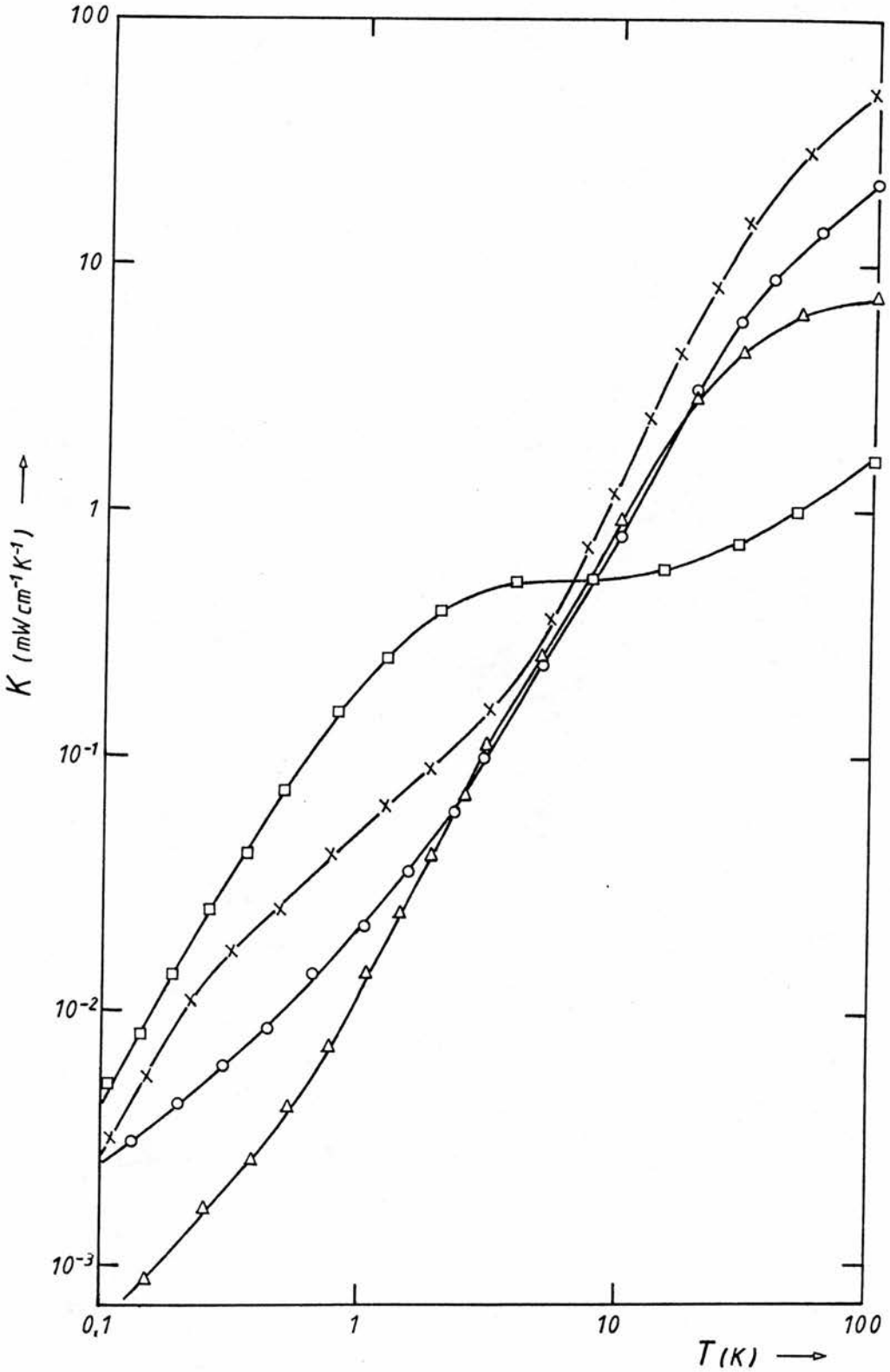

Figure 6.5. Thermal conductivity as a function of temperature of all four polymer specimens. The points represent experimental values: Δ isotropic Hostalen polyethylene; O extruded Hostalen polyethylene; X extruded Rigidex 50 polyethylene; □ amorphous PMMA.

CHAPTER VII

Application of Theory to the Experimental Results

7.1 Introduction

The most interesting feature which emerges from the thermal conductivity measurements is the difference in the temperature dependence of the extruded and isotropic Hostalen polyethylene specimens below 2K. The $T^{1.8}$ variation seen at higher temperatures changes to a linear dependence, but whilst this change occurs at about 2K for the drawn specimen, it occurs at approximately 0.4K for the undrawn specimen. Neither this difference between the samples nor the linear temperature dependence can be explained by "two-level" scattering, and it appears likely that the results for semi-crystalline polymers are best explained in terms of "structure" scattering.

7.2 Structure Scattering

The structure scattering models assume the thermal conductivity to be dominated by phonons being scattered by changes in the material properties. In their application to semi-crystalline polymers, these models assume the phonon scattering to result from changes in the density and elastic constants at the boundaries between amorphous and crystalline regions. The form of the scattering is expected to alter when the dominant phonon wavelength becomes larger than the size of scattering region and this is expected to give a change in the slope of the conductivity curve. We can thus explain the difference in the thermal conductivity between the drawn

and isotropic specimens by the change in the orientation of the crystalline lamellae on extrusion. This alters the dimension of the crystalline inclusions in the direction of measurement.

Little's acoustic mismatch theory (1959) has already been successfully applied to a semi-crystalline polymer by Choy and Greig (1975). They measured the thermal conductivity of isotropic polyethylene terephthalate and considered the phonons to be scattered as they passed through the alternate amorphous and crystalline regions in the spherulites (see Chapter II). Choy and Greig observed a decreasing conductivity with increasing crystallinity below 10K. They attributed this to the larger number of amorphous - crystalline boundaries in the more highly crystalline specimens.

Little's model is only applicable whilst the dominant phonon wavelength is smaller than the dimension of the crystalline inclusions from which they are scattered. For polyethylene it was assumed that the transverse phonon velocity, v_t, was 2×10^3 ms^{-1}. Thus the dominant phonon wavelength was given by

$$\lambda_d \approx \frac{hv_t}{4.3k_BT} \approx \frac{200}{T} \text{ Å} .$$

The crystalline lamellae were assumed to be approximately 100A thick. Little's model can therefore not be applied to explain the thermal conductivity of polyethylene below about 2K.

The Morgan and Smith (MS) structure scattering theory has been used by Burgess and Greig (1975) to explain the conductivity curves above 3K of the two Hostalen GUR specimens used in this work. The MS model can be applied to the density changes within the amorphous regions themselves and can therefore be used down to very low temperatures

(0.1K). It was therefore decided to interpret our results in terms of the MS theory.

7.3 Application of the MS model of structure scattering

The thermal conductivity was calculated from the MS theory using the expression

$$K(T) = \int_0^{k_D} \left[2/3\ v_t^2\ t_t(ka)\ C_D(k,T)_t + 1/3\ v_l^2\ t_l(ka)\ C_D(k,T)_l \right] dk$$

where v_t and v_l were the transverse and longitudinal velocities respectively, k_D the Debye cut-off wavevector and t_t and t_l the relaxation times for transverse and longitudinal mode phonons respectively. The specific heat, C, was found from the Debye expression

$$C = \int_0^{k_D} C_D(k,T)dk$$

where $C_D(k,T) = 2/((2\pi)^2 k_B T^2) \left[\frac{2(\hbar v_t)^2 k^4 \exp(y)}{(\exp(y) - 1)^2} + \frac{(\hbar v_l)^2 k^4 \exp(z)}{(\exp(z) - 1)^2} \right]$

with $y = \hbar v_t k/k_B T$ and $z = \hbar v_l k/k_B T$.

The phonon relaxation times, t_t and t_l, were obtained from the Universal Relaxation curve of MS as a function of phonon wavevector. This curve was normalised in terms of the three parameters v_n, a and D^2 where v_n was a normalising velocity equal to 4×10^3 ms^{-1}, a the appropriate correlation length and D^2 a measure of the mean square

fluctuations of the material properties from point to point. The total phonon mean free path for each mode was calculated from the relation

$$\frac{1}{l_T} = \frac{1}{l_b} + \frac{X}{l_c(k)} + \frac{(1-X)}{l_{as}(k)} + \frac{(1-X)}{l_{al}(k)} \qquad \text{7.1}$$

where X was the crystallinity, l_b the mean free path due to boundary scattering, $l_c(k)$ that due to the crystalline inclusions and $l_{as}(k)$ and $l_{al}(k)$ those due respectively to short-range and long-range order in the amorphous regions.

The relaxation times corresponding to each of the mean free paths was found from $t = l/v$. The total relaxation time for each mode was thus given by

$$t(ak) = l_b t_c t_{as} t_{al}/(v t_c t_{as} t_{al} + X l_b t_{as} t_{al} + (1-X) l_b t_{as} t_c + (1-X) l_b t_{as} t_c).$$

Fourth order polynomials were fitted to the two relaxation curves of MS for ease of calculation in the computer program. The thermal conductivity was then calculated by performing a numerical integration in a thousand steps of the phonon wavevector, k. Burgess and Greig assumed a value of 2×10^3 ms^{-1} for the transverse phonon velocity, v_t, for polyethylene and this was used for all the specimens. The parameters a and D^2 were adjusted within reasonable bounds until a good fit had been obtained to the measured conductivity curve.

As a check on the accuracy of this technique, the thermal conductivity curves for Selenium and Pyrex were calculated using the values of a and D^2 used by MS. The computed thermal conductivity between o.1 and 10K showed good agreement with their calculated curves.

7.4 Assumptions used in the application of the MS theory

The assumptions made previously in the application of the MS theory to polyethylene have been detailed by Burgess and Greig (1975). These, together with the additional assumptions required for the application at low temperatures, are discussed below.

(1) The MS theory developed for isotropic materials can be applied to these anisotropic polymers.

(2) The MS Universal Relaxation curve is valid for short as well as long correlation lengths. This assumption has been justified by MS in their paper.

(3) There is a single cut-off wavevector, k_D, for both phonon modes estimated as 10^{10} m^{-1} by Burgess and Greig from their specific heat data for polyethylene. At low temperatures (below 10K) the dominant phonon wavevector is small and the calculated thermal conductivity is insensitive to the value of k_D.

(4) The Debye expression for the density of phonon states is valid. This assumption is supported by the work of Pohl et al.(1973) and of Zaitlin and Anderson (1974, 1975). They demonstrated that the thermal carriers in the amorphous material between 0.1 and 10K are phonons with acoustic velocities and a Debye density of states and that the thermal conductivity could therefore be calculated from the Debye specific heat and the mean free path (see Chapter II).

(5) Anharmonic effects are negligible. Morgan and Smith calculated the anharmonic scattering in amorphous solids and concluded that although it was larger than in comparable crystalline solids, it was too weak to have a significant effect on the low temperature thermal conductivity. In the isotropic polyethylene specimen the thermal conductivity at high temperatures is dominated by Umklapp

scattering of phonons in the crystallites perpendicular to the c-axis, but this contribution is negligible below 10K.

(6) Equation 7.1 is still valid when the total mean free path is smaller than the long correlation length. The conductivity above 2K is only marginally affected by the introduction of a long correlation length for the amorphous regions of the semi-crystalline materials. Thus equation 7.1 appears to give a good estimate of the mean free path even when one of the terms has no real meaning for most of the phonons at that temperature.

(7) The longitudinal velocity of sound is double the transverse velocity. Athougies et al.(1972) have shown that this ratio appears to be generally true for polymers.

(8) The phonon velocity has negligible dispersion and the transverse velocity of sound has a value of 2×10^3 ms^{-1} for all our specimens. In view of the other assumptions made, particularly in using a Debye density of states, it would be unreasonable to use a more complex relationship for the phonon velocity.

(9) The results presented here were obtained at lower temperatures than the work done by Burgess and Greig and an additional assumption is therefore required, namely that the long correlation length used by MS to explain the low temperature conductivity of amorphous solids has to be included for semi-crystalline polymers. Thus three correlation lengths are required for the semi-crystalline samples, two for the amorphous regions and one for the crystalline inclusions.

7.5 Analysis of the results using the MS theory

7.5.1 The extruded Hostalen GUR specimen (SH2)

The values for the parameters a and D^2 used by Burgess and

Greig (1975) were employed again here

$$\text{i.e} \qquad a_{as} = 8\text{Å}, \quad D^2_{as} = 0.25$$

$$a_c = 100\text{Å}, \quad D^2_c = 0.08.$$

In addition a third correlation length, $a_{al} = 3000$Å, was introduced to represent the long-range order in the amorphous regions. This was expected to be important below 1K. A good fit was obtained to the experimental curve with $D^2_{al} = 0.0055$ (see Figure 7.1).

The effect of the "crystalline" correlation length was calculated by computing the three thermal conductivity curves obtained when only two of the three correlation lengths were used. It was then found that the thermal conductivity was dominated by scattering from the lamellae between 0.2 and 8K with a maximum at about 1K. Obviously the temperature region over which this effect dominates depends on the values of the parameters used for the amorphous regions. For example, if a smaller value of a_{as} (say 5Å) is used to describe the short-range order in the amorphous regions, then the maximum effect of the "crystalline" correlation length will occur at about 2K and it will dominate up to approximately 10K. The dominant phonon wavelength is given by

$$\lambda_d \approx \frac{200\text{Å}}{T} \qquad \text{(see above)}$$

and this is equal to the lamellae width at about 2K. The change in slope of the thermal conductivity curve of this specimen occurs at 2K.

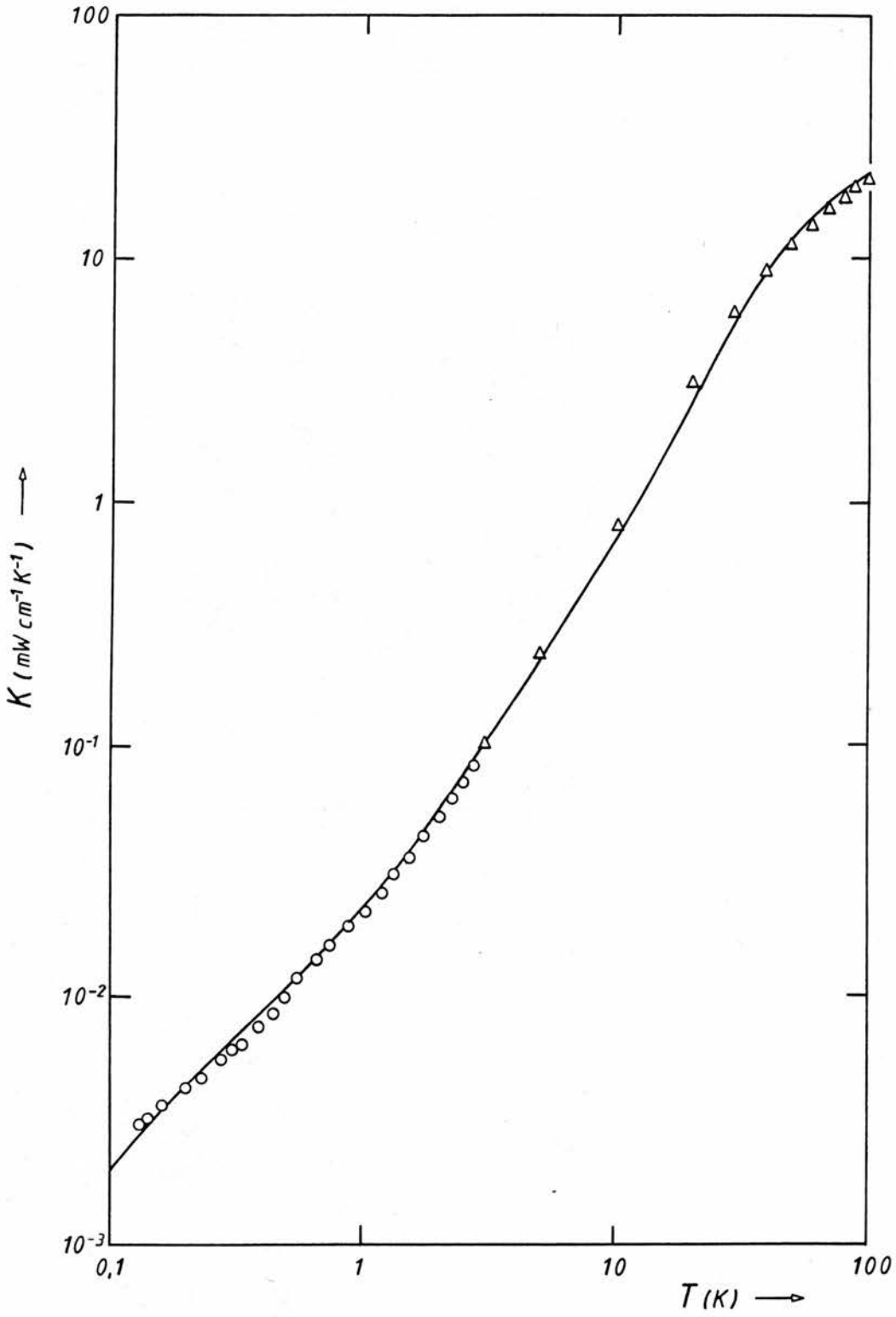

Figure 7.1. Theoretical curve of the thermal conductivity of the extruded Hostalen GUR specimen SH2 from the MS theory with a_{as} = 8A, a_c = 100A and a_{al} = 3000A. The points represent experimental values: the circles are selected points from the present work, the triangles are after Burgess and Greig (1975).

7.5.2 The isotropic Hostalen GUR specimen (SHO)

The same values of a and D^2 were used for the amorphous regions of this specimen as had been used for SH2 since it was argued that these regions were not significantly altered by the extrusion. However a different approach was adopted for the crystalline regions of the two samples. In the extruded specimen the lamellae were aligned with respect to the extrusion (and measurement) direction so that the path length of a phonon through a lamellum was approximately 100Å. In the isotropic specimen, the crystalline inclusions were in the form of spherulites composed of twisted ribbons of lamellae which were randomly oriented with respect to the measurement direction (see Chapter II).

Clearly the width of a crystalline lamellum transversed by a phonon could vary from 100Å to 10,000Å depending on the orientation of the lamellum with respect to the direction of the measurement. An average phonon path length, x, was calculated by treating the lamellae as discs 100Å thick with radii 10,000Å. The average value of x was then given by

$$x_{av} = \int_0^{\pi/2} \min\left[\frac{b}{\cos\theta}, (a^2 + b^2)^{1/2}\right] \sin\theta \, d\theta$$

$$= b\left[1 + \log\left[\frac{(a^2 + b^2)^{1/2}}{b}\right]\right]$$

where a is the disc radius and b its thickness. For a = 10,000Å and b = 100Å, the average path length x_{av} = 300Å. This value of 300Å was used for the correlation length, a_c, pertaining to the crystalline regions. This is obviously a very approximate approach as there will be a large range of phonon path lengths about this one average value.

A good fit was obtained to the experimental results by using $D_c^2 = 0.10$ (see Figure 7.2).

The region over which the scattering from crystallites will dominate the conductivity was again calculated by plotting the three curves obtained when only two of the three correlation lengths were used. The "crystalline" correlation length was found to dominate between 0.1 and 6K with a maximum effect at about 0.6K. The dominant phonon wavelength is equal to the average lamellae width traversed by a phonon (300Å) at approximately 0.7K. The change in slope of the thermal conductivity occurs at 0.5K.

The difference between the thermal conductivity of the extruded and isotropic specimens is thus explained by a decrease on drawing in the effective crystalline region width in the direction of measurement. Below 0.1K, the long-range order in the amorphous regions is expected to dominate the thermal conductivity and below 0.1K the MS theory would predict that the conductivity of the SH2 and SHO specimens would converge and would be the same below 10mK. It is possible however that at very low temperatures where the dominant phonon wavelengths are long, the spherulites as a whole will start to scatter the phonons. The conductivity curve of the SHO specimen will then again drop below that of the SH2 specimen. These polyethylene samples are highly crystalline and the spherulites are closely packed and intertwined and hence poorly defined. It is unlikely therefore that they will be sufficiently clearly demarcated to act as scattering regions.

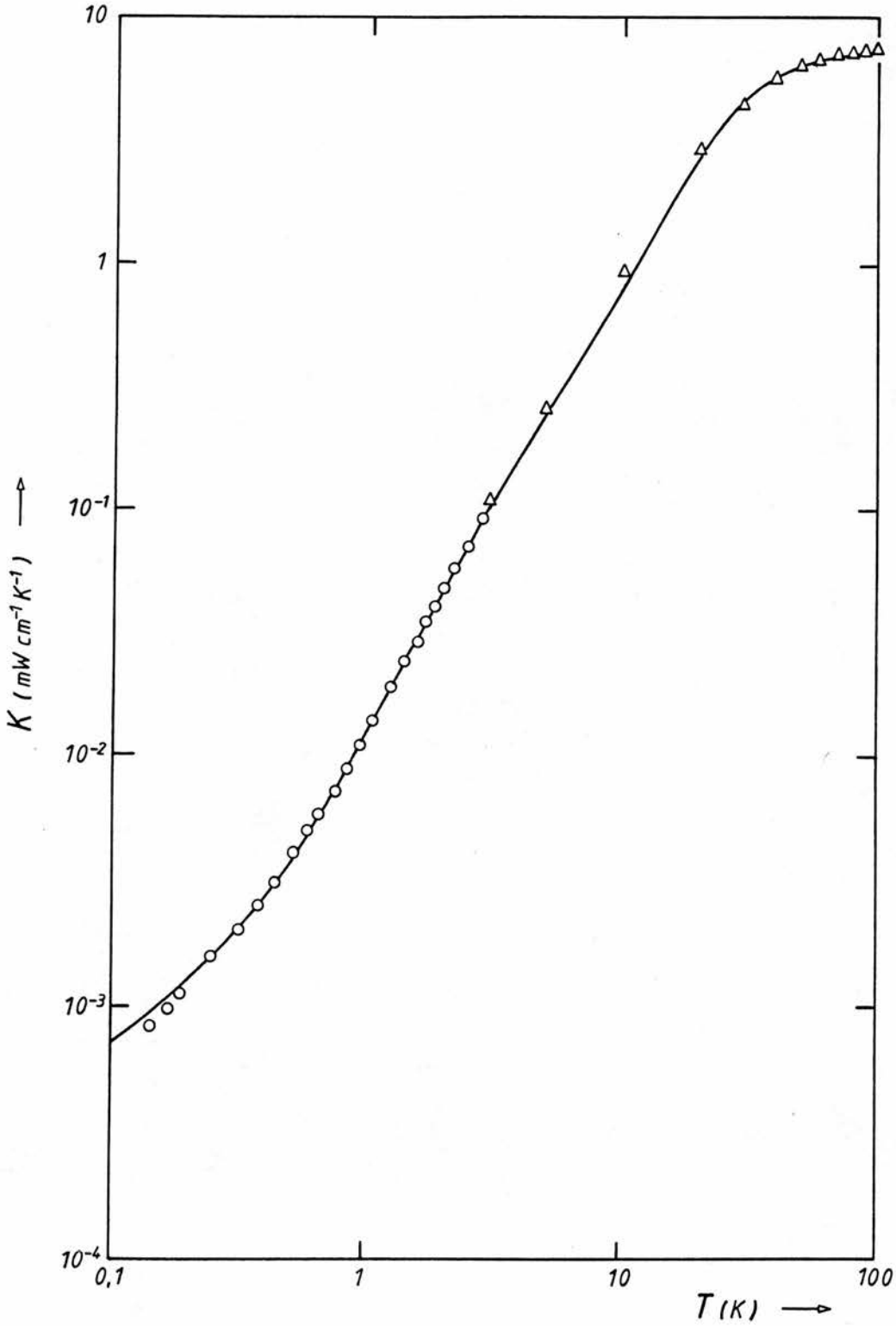

Figure 7.2. Theoretical curve of the thermal conductivity of the isotropic Hostalen GUR specimen SHO from the MS theory with a_{as} = 8A, a_c = 300A and a_{al} = 3000A. The points represent experimental values: the circles are selected points from the present work, the triangles are after Burgess and Greig (1975).

7.5.3 The Rigidex 50 polyethylene specimen

As mentioned previously, this sample was cracked and the results were therefore suspect at low temperatures where it was difficult to obtain good thermal contact.

Three correlation lengths were used in the application of the MS theory with a value of 100Å taken for the correlation length relating to the crystalline regions. It was difficult to obtain a good fit below 2K but the best curve was obtained with

$$a_{as} = 15\text{Å}, \qquad D^2_{as} = 0.22$$

$$a_{c} = 100\text{Å}, \qquad D^2_{c} = 0.03$$

$$a_{al} = 3000\text{Å}, \qquad D^2_{al} = 0.004$$

(see Figure 7.3).

A better fit could be obtained by using a smaller value for a_c. It would be difficult to justify this however as we have assumed a minimum dimension of 100Å for the crystalline lamellae. The simple view of lamellae orientation used for the extruded Hostalen specimen is not valid for this sample with its large draw ratio of 13. There is insufficient information on the detailed structure of highly extruded polyethylene for a more exact determination of the probable crystalline order.

7.5.4 The amorphous PMMA (Perspex) specimen

The thermal conductivity of amorphous dielectrics is probably best explained in terms of "two-level" scattering rather than "structure" scattering. However it was decided to try fitting the results for this specimen with the MS theory for completeness.

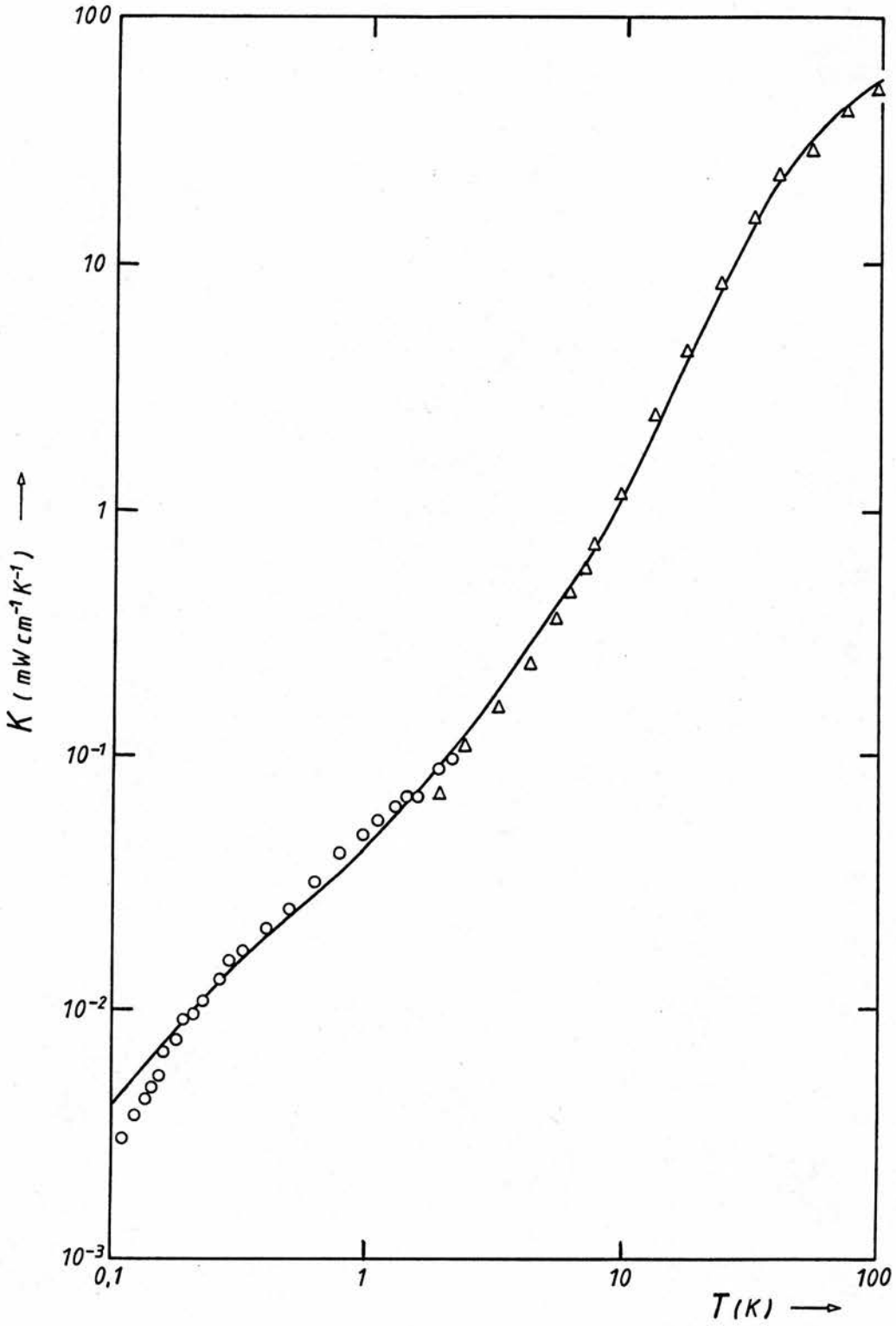

Figure 7.3. Theoretical curve of the thermal conductivity of the Rigidex 50 polyethylene specimen from the MS theory with a_{as} = 15A, a_c = 100A and a_{al} = 3000A. The points represent experimental values: the circles are selected points from the present work, the triangles are after Gibson et al. (1977).

The PMMA sample was treated in the same manner as the amorphous materials Selenium and Pyrex considered by MS with only two "amorphous" correlation lengths used. A close fit was obtained below 5K but the agreement was poor above this temperature. A similar problem had been encountered by MS in computer fitting the results for their amorphous solids. The agreement could be improved by reducing the value of a_{as} below 5Å but this would clearly be stretching the model too far.

The values used for Perspex were

$$a_{as} = 5\text{Å}, \qquad D^2_{as} = 0.7$$

$$a_{al} = 1000\text{Å}, \qquad D^2_{al} = 0.002$$

(see Figure 7.4).

7.6 Summary

The difference between the thermal conductivity of the amorphous and semi-crystalline polymers is a maximum at about 1K where the disparity is of an order of magnitude (see Figure 6.5). At this temperature the dominant phonon wavelength is approximately equal to the expected size of the crystalline inclusions. The conductivity between 0.1 and 3K of the semi-crystalline polymers therefore seems to be dominated by "structure" scattering from the crystalline lamellae.

There is good agreement between the experimental results and the conductivity curves calculated using the MS theory. The model uses two parameters (a and D^2) to describe each of the scattering regions and this allows considerable flexibility in fitting the thermal conductivity. Therefore too much emphasis should not be placed on

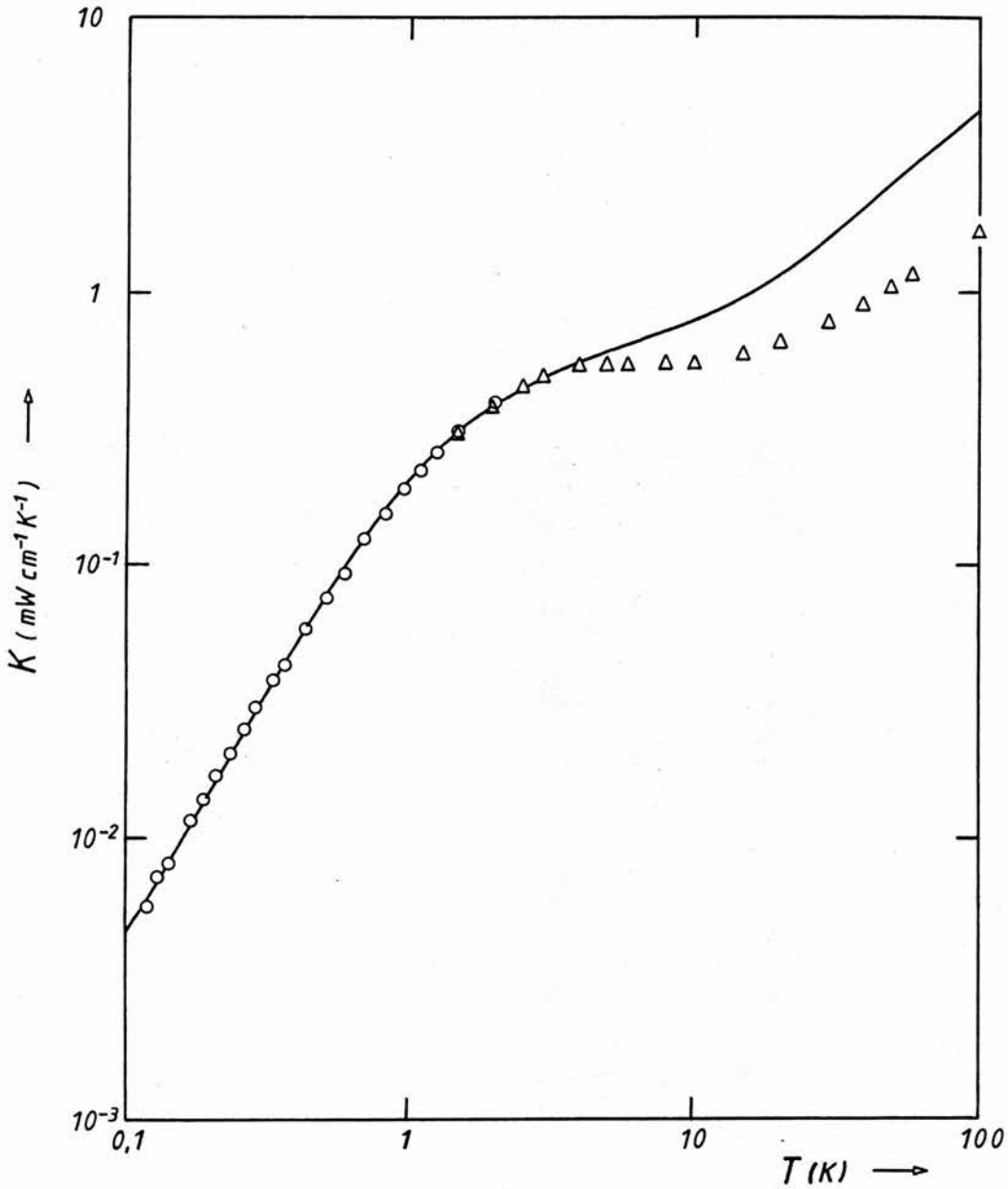

Figure 7.4. Theoretical curve of the thermal conductivity of the polymethylmethacryalate (PMMA) specimen from the MS theory with a_{as} = 5A and a_{al} = 1000A. Since this specimen is amorphous, the third correlation length (a_c) used to describe the phonon scattering by crystalline inclusions, is not required. The points represent experimental values: the circles are selected points from the present work, the triangles are after Burgess and Greig (1974).

the good numerical agreement with the measurements. However the theory appears successful in interpreting the difference observed between the drawn and isotropic polyethylene specimens. This is explained by the change in orientation of the crystalline lamellae on extrusion giving a shorter phonon path length through the crystalline regions.

The MS theory has been applied to the amorphous polyethylene regions as well as to the crystalline inclusions. The available evidence suggests that the thermal conductivity in the amorphous material is best explained in terms of "two-level" scattering. Therefore no single theory can probably explain the thermal conductivity of these dielectrics below 10K.

The summary of the parameters used in the application of the MS theory is given in Table 7.1.

Table 7.1

Summary of the values of the parameters used in the application of the MS theory to the four polymer specimens.

	SH2	SHO	PMMA	Rigidex 50
X	0.6	0.6	0	0.765
a_{as}(Å)	8	8	5	15
a_c(Å)	100	300	-	100
a_{al}(Å)	3000	3000	1000	3000
D^2_{as}	0.25	0.25	0.7	0.22
D^2_c	0.08	0.10	-	0.03
D^2_{al}	0.0055	0.0055	0.002	0.004

CHAPTER VIII

CONCLUSION

The thermal conductivity of four polymer samples has been measured in the temperature range 0.1 to 3K. The results for all four specimens are in excellent agreement with the measurements at higher temperatures. The results of the Hoestalen polyethylene samples show differences between the isotropic and extruded specimens. The isotropic sample displays a continuation of the $T^{1.8}$ temperature dependence down to 0.5K below which the conductivity varies approximately linearly with temperature. This behaviour is very similar to that observed by Scott et al. for their uncharacterised polyethylene specimen. For the extruded sample the change in slope occurs at about 2K. The difference in the conductivity of the two specimens has been related to the change in the orientation of the crystalline lamellae on extrusion. The Morgan and Smith structure scattering theory gives a good fit to the thermal conductivity curves when reasonable estimates are taken for the dimensions of the crystalline inclusions.

The thermal conductivity of the amorphous polymer specimen (PMMA) showed good agreement with the previous measurements in this temperature range by Stephens et al.. The fit with the Morgan and Smith theory is good below 5K although it is suggested that resonance scattering is the probable mechanism responsible for the behaviour of the thermal properties below 1K.

It would be interesting to extend these measurements to lower temperatures (below 0.1K) to see whether, as expected, the difference

in the thermal conductivity between the two Hostalen specimens decreases and disappears below about 20mK. The MS theory would predict an approximately $T^{1.3}$ variation at these temperatures whilst the "two-level" scattering theory would predict a T^2 dependence. In the explanation of our results we have assumed that the extrusion of the polyethylene only produces changes in the orientation of the crystalline lamellae and for low extrusion ratios produces no effective change in the amorphous regions. Since this work was completed, Phil Mason has measured the specific heat of the two Hostalen specimens below 1K and found no difference between them (Finlayson et al. 1980). This supports the assumption that the amorphous regions are not significantly altered by the extrusion. It also indicates that two different mechanisms are probably responsible for the specific heat and thermal conductivity. Mason's preliminary measurements of the specific heat show the T^3 temperature dependence seen above 1K decreasing to an approximately linear behaviour below 0.25K as predicted by the "two-level" scattering theory.

Choy and Greig (1975) have measured the effect on the thermal crystallinity above 2K of increasing the crystallinity in a semi-crystalline polymer, polyethylene terephthalate. It would be very informative to measure the thermal conductivity and specific heat of these polymer specimens below 2K to determine the effect of crystallinity on the thermal properties. It would for example demonstrate whether the linear specific heat term seen in amorphous solids is linearly dependent on the crystallinity as might be expected from the resonance scattering model. This theory would also predict an increase in the thermal conductivity with increasing

crystallinity at very low temperatures where the scattering from crystalline inclusions is no longer dominant.

BIBLIOGRAPHY

Anderson A.C., Reese W. and Wheatley J.C. (1963), Rev. Sci. Instr. 34, 1386.

Anderson A.C. and Rauch R.B. (1970), J. Appl. Phys. 41, 3648.

Anderson P.W., Halperin B.I. and Varma C.M. (1972), Phil. Mag. 25, 1.

Althougies A.D., Peterson B.T., Salinger G.L. and Swartz C.P. (1972), Cryogenics 12, 125.

Berman R. (1951), Proc. Roy. Soc. A208, 90.

Billmeyer F.W. (1971), Textbook of Polymer Science (John Wiley and Sons, Second Edition).

Blakemore J.S., Winstel J. and Edwards R.V. (1970), Rev. Sci. Instr. 41, 835.

Burgess S. and Greig D. (1974), J. Phys. D 7, 2051.

Burgess S. and Greig D. (1975), J. Phys. C 8, 1637.

Choy C.L. and Greig D. (1975), J. Phys. C 8, 3121.

Choy C.L. and Greig D. (1977), J. Phys. C 10, 169.

Dainton F.S., Evans D.M., Hoare F.E. and Melia T.P. (1962), Polymer 3, 277.

Finlayson D.M., Greig D., Mason P. and Rogers J. (1980), to be published.

Frost W. (1975), Heat Transfer at Low Temperatures (Plenum Press).

Garrett K.W. and Rosenberg H.M. (1972), Proc. 4th Int. Cryogenic Engineering Conference, 267.

Giaquinta P.V., March N.H., Parinello M. and Tosi M.P. (1977), Phys. Rev. Letts. 39, 41.

Gibson A.G., Greig D., Sahota M., Ward I.M. and Choy C.L. (1977), J. Polym. Sic., Polym. Phys. Ed. 15, 183.

Godratt E., Greenfield A.J. and Schlesinger Y. (1977), Cryogenics 17, 81.

Keller A. (1968), Rep. Prog. Phys. 31, 623.

Klemens P.G. (1951), Proc. Roy. Soc. A208, 108.

Kouloch R.J. and Brown R.G. (1968), J. Appl. Phys. 39, 3999.

Lasjaunias J.C., Picot B., Ravex A., Thoulouze D. and Vandorpe M. (1977), Cryogenics 17, 111.

Little W.A. (1959), Can. J. Phys. 37, 334.

Lounasmaa O.V. (1974), Experimental Principles and Methods below 1K (Academic Press).

Martin D.L. (1975), Rev. Sci. Instr. 46, 657.

Meares P. (1965), Polymers: Structure and Bulk Properties (D. Van Nostrand Co.).

Morgan G.J. and Smith D. (1974), J. Phys. C 7, 649.

Peterlin A. (1965), J. Polym. Sci. C 9, 61.

Phillips W.A. (1972), J. Low Temp. Phys. 7, 351.

Pohl R.O., Love W.F. and Stephens R.B. (1973), 5th Int. Conf. on Amorphous and Liquid Semiconductors, 1121 (Edited by Stuke and Brenig).

Reese W. (1966), J. Appl. Phys. 37, 864.

Reese W. (1969), J. Macromol. Sci. - Chem. A3, 1257.

Reese W. and Tucker J.E. (1965), J. Chem. Phys. 43, 105.

Rochlin G.I. (1970), Rev. Sci. Instr. 41, 73.

Rosenberg H.M. (1963), Low Temperature Solid State Physics (Clarendon).

Scott T.A., de Bruin J., Giles M.M. and Terry C. (1973), J. Appl. Phys. 44, 1212.

Stephens R.B. (1973), Phys. Rev. B 8, 2896.

Stephens R.B., Cieloszyk G.S. and Salinger G.L. (1972), Phys. Letts. 38A, 215.

Swartz J.M., Clark C.F., Johns D.A. and Swartz D.L. (1976), Proc. 6th Int. Cryogenic Engineering Conference.

Tucker J.E. amd Reese W. (1967), J. Chem. Phys. 46, 1388.

Walton D. (1974), Solid State Commun. 14, 335.

Wheatley J.C., Vilches O.E. and Abel W.R. (1968), Physics 4, 1.

Zaitlin M.P. and Anderson A.C. (1974), Phys. Rev. Letts. 33, 1158.

Zaitlin M.P. and Anderson A.C. (1975), Phys. Rev. B 12, 4475.

Zeller R.C. and Pohl R.O. (1971), Phys. Rev. B 4, 2029.

Ziman J.M. (1960), Electrons and Phonons (Oxford).

APPENDIX

ELECTRONICS

(A) Temperature Stabiliser

During a measurement of the polymer thermal conductivity, it was necessary to hold the specimen block temperature constant (i.e. steady during the time taken by the specimen to come to thermal equilibrium with no heat applied, then with the heater on and again with no heat applied). The time for measurement ranged from about 15 minutes at the highest temperatures to about 2 hours at the lowest. The temperature difference set up between the thermometers varied from 10 mK to 200 mK according to the temperature of the specimen. For the drift in the mixer block temperature to be negligible at higher temperatures (around 2K), it must be held steady to $\pm$1mK over approximately 15 minutes. At the lowest temperatures (around 50mK), this drift must be reduced to less than 0.1mK over 2 hours. A temperature controller was built to meet these requirements.

The stabiliser was constructed in two modules. The first was a two-terminal resistance bridge suitable for measuring carbon resistance thermometers at low temperatures. The second module contained a low-pass amplifier and a heater amplifier circuit (based on the design by Rochlin 1970).

(1) Carbon Resistance Bridge

The bridge was designed to use very low thermometer dissipation powers and provide high amplification and noise rejection. The design was not ideal as, for economy, a circuit board was incorporated in the module, from the germanium resistance bridge built by

Professor S.B. Woods and designed by J. Rogers. This board contained a preamplifier, main amplifier with gain control, an oscillator operating at a frequency of 144Hz and a phase-sensitive detector. The basic circuit blocks are shown in Figure 1A.

The resistance of the sensors was obtained by balancing an A.C. Wheatstone Bridge consisting of a linear 100K ohm helipot, a 33k ohm constant resistor, and one of four resistors ranging from 33k ohms to 33 ohms which provided the range selection (see Figure 3A). These values of resistance ensured that the heat dissipated in the sensor R on any range was approximately constant across that range. The excitation signal to the bridge from the oscillator was provided through a 7.5:1 transformer to isolate the oscillator common rail from that of the amplifier stages.

The off-balance signal from the bridge was fed to the pre-amplifier which was built around a FET 741 IC to ensure that the input impedance of the amplifier was very high. The output from this stage was passed through an active 50 Hz notch filter to remove the mains ripple and to a low-pass amplifier (f_o = 200 Hz) to produce additional gain and remove the high frequency (RF) noise. The signal was then amplified by the main amplifier which provided most of the gain control and hence passed to the phase-sensitive detector and meter driving circuit. This gave a D.C. offset to the $\pm 50 \mu A$ meter and which could also be used for the temperature controller.

The sensitivity and power dissipation compared favourable with the O.I.C. resistance bridge, but the time constant of the meter driving circuit was found to be too long for general use (10 to 15 seconds). This was not reduced, as doing so increased the meter noise, and the bridge was generally used with the temperature

controller with a stabiliser time constant of 30 seconds. The sensor power dissipations used by the bridge are given in Table 1A.

(2) Temperature Controller

The temperature controller module was designed so that the off-balance signal from any of the available resistance bridges could be used to drive it.

The module consisted of two stages. The first was a low-pass amplifier to provide additional gain if required and to reduce the noise (particularly the effects of transients) on the D.C. signal. The resistance and capacitance in the amplifier gain control could be choosen independently and the capacitors enabled the time constant to be varied between 0.3 and 90 seconds. A short time constant gave greater sensitivity to rapid changes in temperature but transients in the mains, the sensor leads or in the fridging power, then caused the system to become unstable and oscillate with increasing amplitude. The stabiliser was therefore used with a long time constant (30 or 90 seconds) and the loss in sensitivity compensated by setting the gain to a maximum. This length of time constant was quite satisfactory as the time for thermal equilibrium of the sample was generally very much longer.

The second stage of the module was a heater current amplifier based on the design of Rochlin (1970) (see Figure 5A) and is described in his paper.

The carbon resistance bridge and temperature controller modules were powered by Coutant Electronic Ltd. O.A.2 Operational Amplifier Power Supply Module, providing $\pm$15V and OV rails. When the bridge was used with the stabiliser, it could be run from the same supply.

A description of the use of the stabiliser and the sensors used with it are given in Chapter IV.

The temperature stability obtained with the controller was estimated from readings of the calibrated thermometer Ge N during two calibration runs (on the 6/12/76 and 10/6/77). During these runs the four germanium thermometers were soldered into the specimen block on the dilution tail as described in Chapter IV. The stabiliser was used to keep the block temperature constant whilst each unknown thermometer was measured twice, the value of Ge N being usually noted between each reading. Thus Ge N was read at least three or four times over a 15 minute period and its values were used to find a "standard deviation" (S.D.). The scatter in these readings included the drift in the stabiliser and the noise in the thermometer reading, and therefore gave an upper limit for the controller stability. Table 2A gives the calculated drifts and shows that the stabiliser met the specified requirements (see above) except in the temperature range 1.2K to 1.4K where the 3HE/4He mixture was very unstable and the fridge difficult to control.

(B) Automatic liquid nitrogen filling system

This consisted of a sensor in the liquid nitrogen jacket of the fridge, a resistance measuring and time delay circuit, and a pump which fitted into the 25 litre liquid nitrogen storage dewars. The system is described in Chapter III and shown in Figure 6A. The level detector and delay operator circuits were designed and built by the Electronics Department (see Figure 7A). The IM 311 IC was biased such that when the nitrogen level in the jacket dropped below the sensor producing a decrease in its resistance, the amplifier closed the mains relay and started the pump. When the nitrogen level rose to the sensor again, returning it to its original resistance, the 555 timer was started and after the preset time had

elapsed, the relay was opened stopping the pump. The timer could be set for 5, 10 or 15 minute delays.

The mains relay operated a solenoid valve and the pump power supply. The power supply was a mains transformer supplying 48 watts to the 13 ohm heater in the nitrogen storage dewar. The solenoid valve was in the dewar boil-off line and when the heater was on the valve was closed causing a build up in pressure in the dewar and hence forcing the liquid over into the fridge jacket through an Armaflex hose (see Plate 2). The time constant of the delay operator was selected so that the jacket was nearly filled when the circuit was triggered by the sensor resistance drop. After the preset time had elapsed, the relay was opened, switching off the heater and opening the solenoid valve to let the excess pressure escape.

When this system had been put into use, the dilution fridge could be kept cool whilst being left unattended for 36 hours.

Table 1A

Power dissipated in a carbon resistance thermometer by the resistance bridge.

Oscillator level	Range (ohms)	Power diss. (watts).
4	10k - 100k	1.6×10^{-12}
	1k - 10k	1.6×10^{-11}
	100 - 1k	1.6×10^{-10}
	10 - 100	1.6×10^{-9}
3	10k - 100k	4.5×10^{-12}
	1k - 10k	4.5×10^{-11}
	100 - 1k	4.5×10^{-10}
	10 - 100	4.5×10^{-9}
2	1k - 10k	2×10^{-10}
	100 - 1k	2×10^{-9}
	10 - 100	2×10^{-8}
1	100 - 1k	8×10^{-9}
	10 - 100	8×10^{-8}

Table 2A

The temperature drift of the sample holder with the temperature stabiliser operating is given for different temperature ranges. The drift is defined as the standard deviation of the readings of the calibrated germanium thermometer whilst a thermal conductivity measurement was being taken.

Temperature Range (K)	S.D. of Temperature (μK)
50mK - 0.1	± 20
0.1 - 0.2	± 50
0.2 - 0.3	± 70
0.3 - 0.5	± 80
0.5 - 1.0	± 50
1.0 - 1.2	± 55
1.2 - 1.4	±170

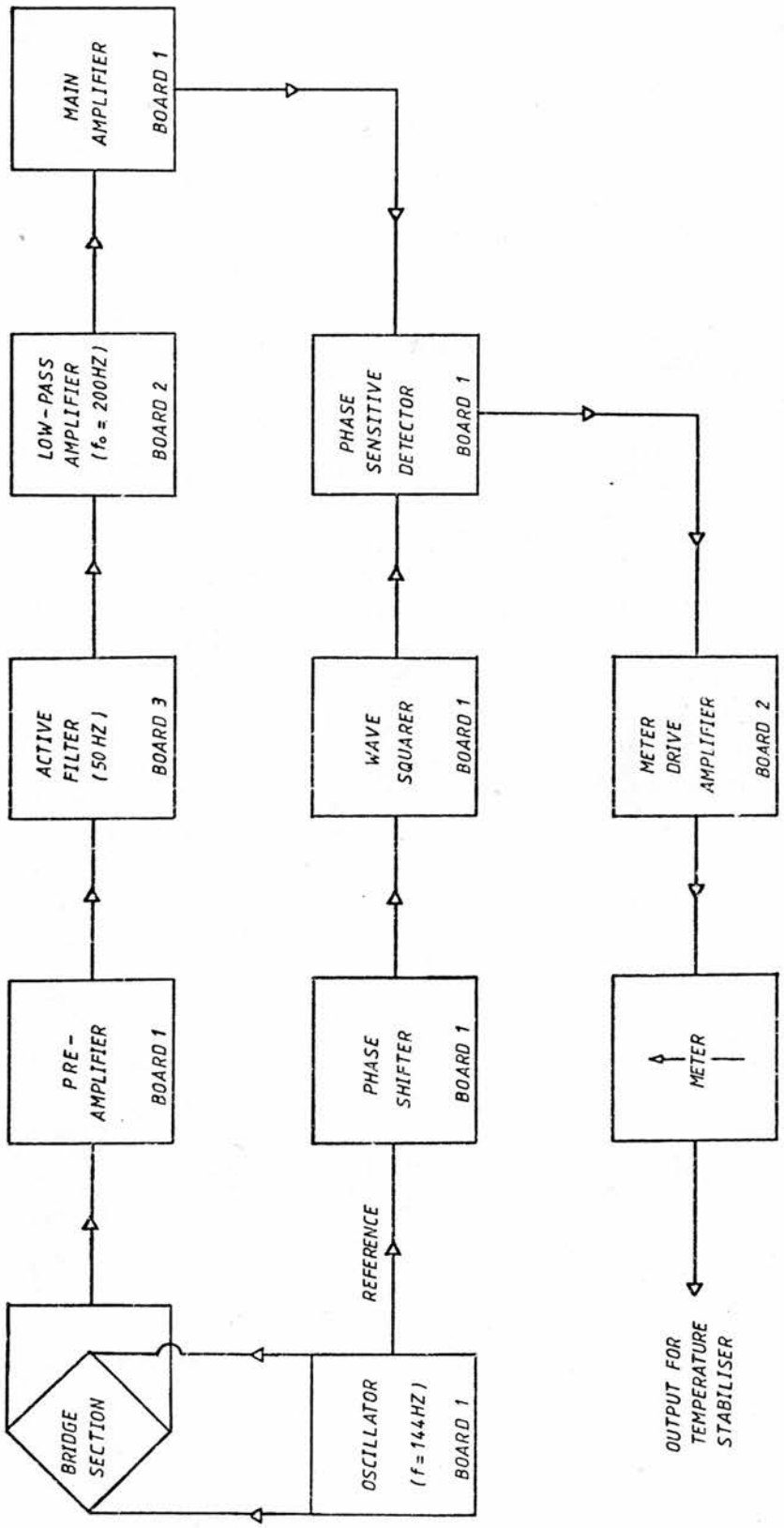

FIGURE 1A RESISTANCE BRIDGE BLOCK DIAGRAM

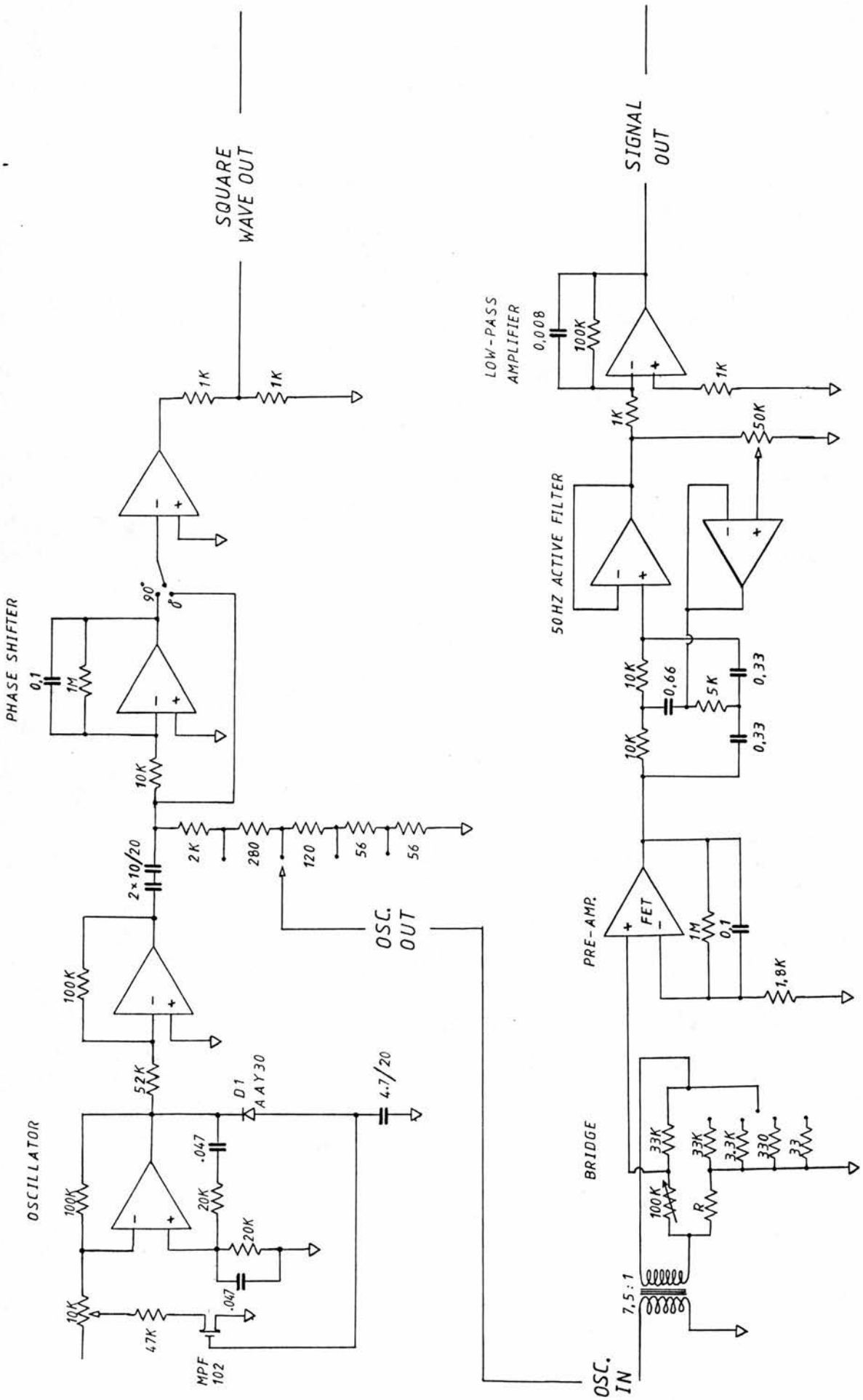

FIGURE 2A. RESISTANCE BRIDGE 1

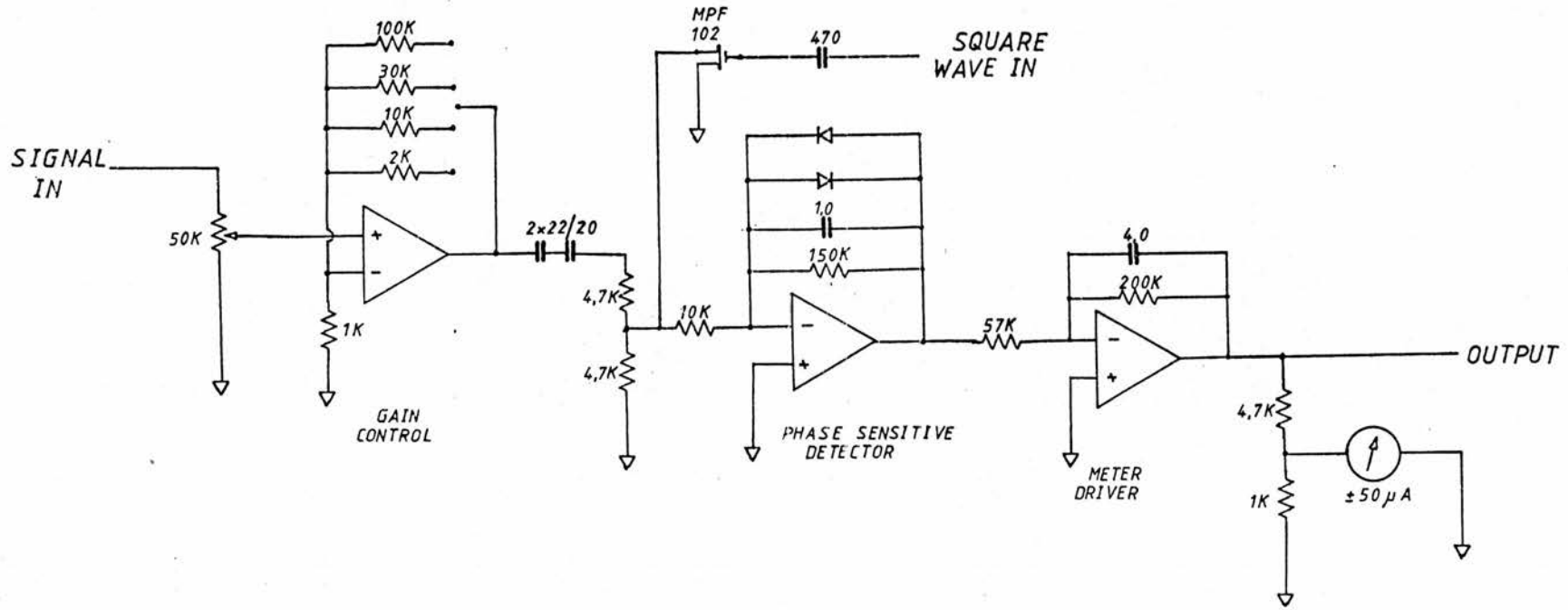

±15.0V PROVIDED BY O.A.2 POWER SUPPLY MODULE.
SMOOTHING FILTERS ON ALL ±15V RAILS

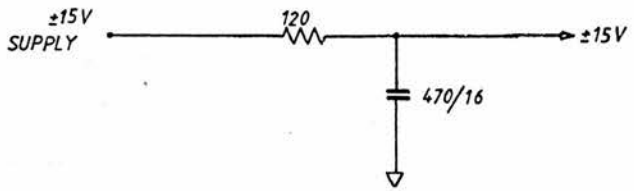

ALL OP-AMPS. AD 741 KN
or AD 741 CN

FIGURE 3A RESISTANCE BRIDGE 2

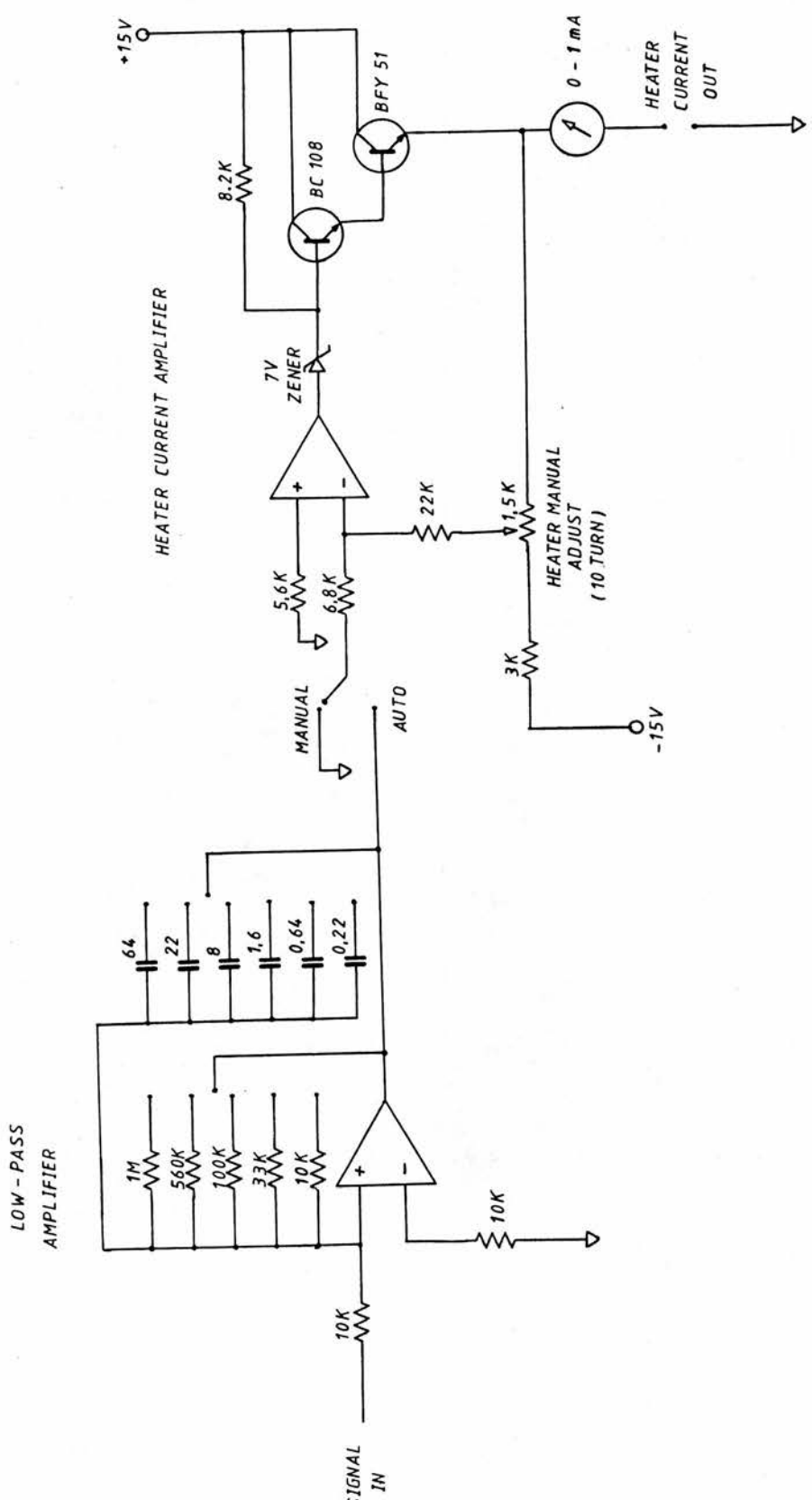

FIGURE 4A TEMPERATURE STABILISER

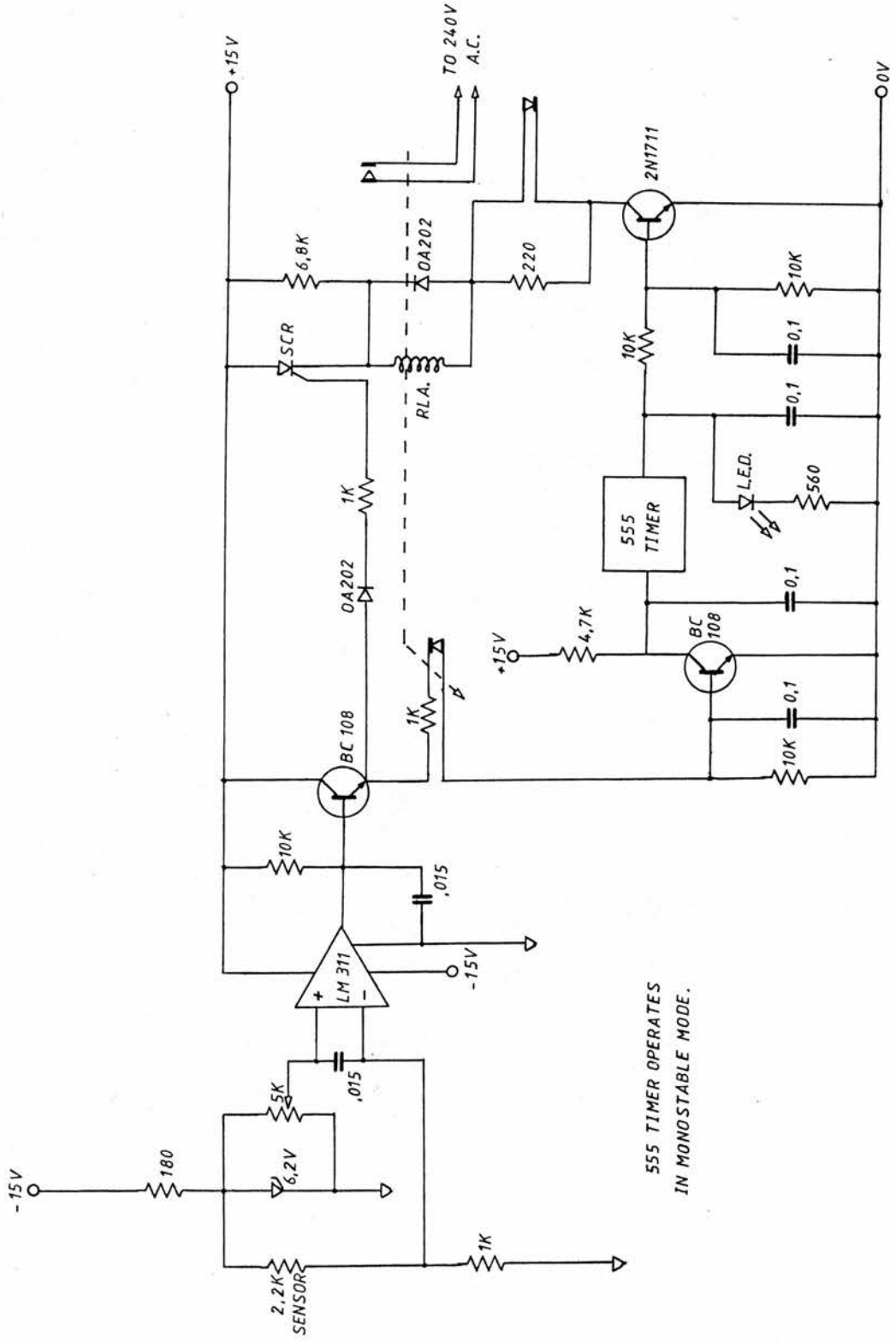

FIGURE 5A LIQUID NITROGEN LEVEL DETECTOR AND DELAY OPERATOR.